MULTIDISCIPLINARY CENTER FOR EARTHQUAKE ENGINEERING RESEARCH
A National Center of Excellence in Advanced Technology Applications

ISSN 1520-295X

Experimental Evaluation of Seismic Performance of Bridge Restrainers

by

Anastasios G. Vlassis, E. Manos Maragakis and M. Saiid Saiidi
University of Nevada, Reno
Civil Engineering Department
Reno, Nevada, 89557

Technical Report MCEER-00-0012

December 30, 2000

This research was conducted at the University of Nevada, Reno and was supported by the Federal Highway Administration under contract number DTFH61-92-C-00106.

NOTICE

This report was prepared by the University of Nevada, Reno as a result of research sponsored by the Multidisciplinary Center for Earthquake Engineering Research (MCEER) through a contract from the Federal Highway Administration. Neither MCEER, associates of MCEER, its sponsors, the University of Nevada, Reno, nor any person acting on their behalf:

a. makes any warranty, express or implied, with respect to the use of any information, apparatus, method, or process disclosed in this report or that such use may not infringe upon privately owned rights; or

b. assumes any liabilities of whatsoever kind with respect to the use of, or the damage resulting from the use of, any information, apparatus, method, or process disclosed in this report.

Any opinions, findings, and conclusions or recommendations expressed in this publication are those of the author(s) and do not necessarily reflect the views of MCEER or the Federal Highway Administration.

MULTIDISCIPLINARY CENTER FOR EARTHQUAKE ENGINEERING RESEARCH
A National Center of Excellence in Advanced Technology Applications

Experimental Evaluation of Seismic Performance of Bridge Restrainers

by

Anastasios G. Vlassis[1], E. Manos Maragakis[2] and M. Saiid Saiidi[3]

Publication Date: December 30, 2000
Submittal Date: July 18, 2000

Technical Report MCEER-00-0012

Task Number 106-F-3.2

FHWA Contract Number DTFH61-92-C-00106

1 Graduate Research Assistant, Department of Civil Engineering, University of Nevada, Reno
2 Professor and Chair, Department of Civil Engineering, University of Nevada, Reno
3 Professor, Department of Civil Engineering, University of Nevada, Reno

MULTIDISCIPLINARY CENTER FOR EARTHQUAKE ENGINEERING RESEARCH
University at Buffalo, State University of New York
Red Jacket Quadrangle, Buffalo, NY 14261

Preface

The Multidisciplinary Center for Earthquake Engineering Research (MCEER) is a national center of excellence in advanced technology applications that is dedicated to the reduction of earthquake losses nationwide. Headquartered at the University at Buffalo, State University of New York, the Center was originally established by the National Science Foundation in 1986, as the National Center for Earthquake Engineering Research (NCEER).

Comprising a consortium of researchers from numerous disciplines and institutions throughout the United States, the Center's mission is to reduce earthquake losses through research and the application of advanced technologies that improve engineering, pre-earthquake planning and post-earthquake recovery strategies. Toward this end, the Center coordinates a nationwide program of multidisciplinary team research, education and outreach activities.

MCEER's research is conducted under the sponsorship of two major federal agencies, the National Science Foundation (NSF) and the Federal Highway Administration (FHWA), and the State of New York. Significant support is also derived from the Federal Emergency Management Agency (FEMA), other state governments, academic institutions, foreign governments and private industry.

The Center's FHWA-sponsored Highway Project develops retrofit and evaluation methodologies for existing bridges and other highway structures (including tunnels, retaining structures, slopes, culverts, and pavements), and improved seismic design criteria and procedures for bridges and other highway structures. Specifically, tasks are being conducted to:

- assess the vulnerability of highway systems, structures and components;
- develop concepts for retrofitting vulnerable highway structures and components;
- develop improved design and analysis methodologies for bridges, tunnels, and retaining structures, which include consideration of soil-structure interaction mechanisms and their influence on structural response;
- review and recommend improved seismic design and performance criteria for new highway systems and structures.

Highway Project research focuses on two distinct areas: the development of improved design criteria and philosophies for new or future highway construction, and the development of improved analysis and retrofitting methodologies for existing highway systems and structures. The research discussed in this report is a result of work conducted under the existing highway structures project, and was performed within Task 106-F-3.2, "Shake Table Tests of Hinge Restrainers" of that project as shown in the flowchart on the following page.

The overall objective of this task was to conduct shake table tests to evaluate the seismic performance of bridges that have been retrofitted with hinge restrainers between simply supported adjacent spans. This experimental study investigates the impact between adjacent bridge spans at in-span hinges, evaluates the efficacy of restrainers in reducing relative displacement across the hinges and examines the effects of restrainer stiffness and gap on the

response of the hinge-restrainer system. Experimental results indicated that impacts between the adjacent frames produce acceleration levels significantly higher than what is typically assumed in design. Restrainers were capable of reducing hinge relative displacements and preventing span unseating. However, restrainer yielding occurred under strong input motions, especially when the restrainer gap was set to zero. Only pounding at the hinge location was included in this study, while pounding elsewhere in the superstructure as well as the detailed response behavior of substructure elements were neglected.

SEISMIC VULNERABILITY OF EXISTING HIGHWAY CONSTRUCTION
FHWA Contract DTFH61-92-C-00106

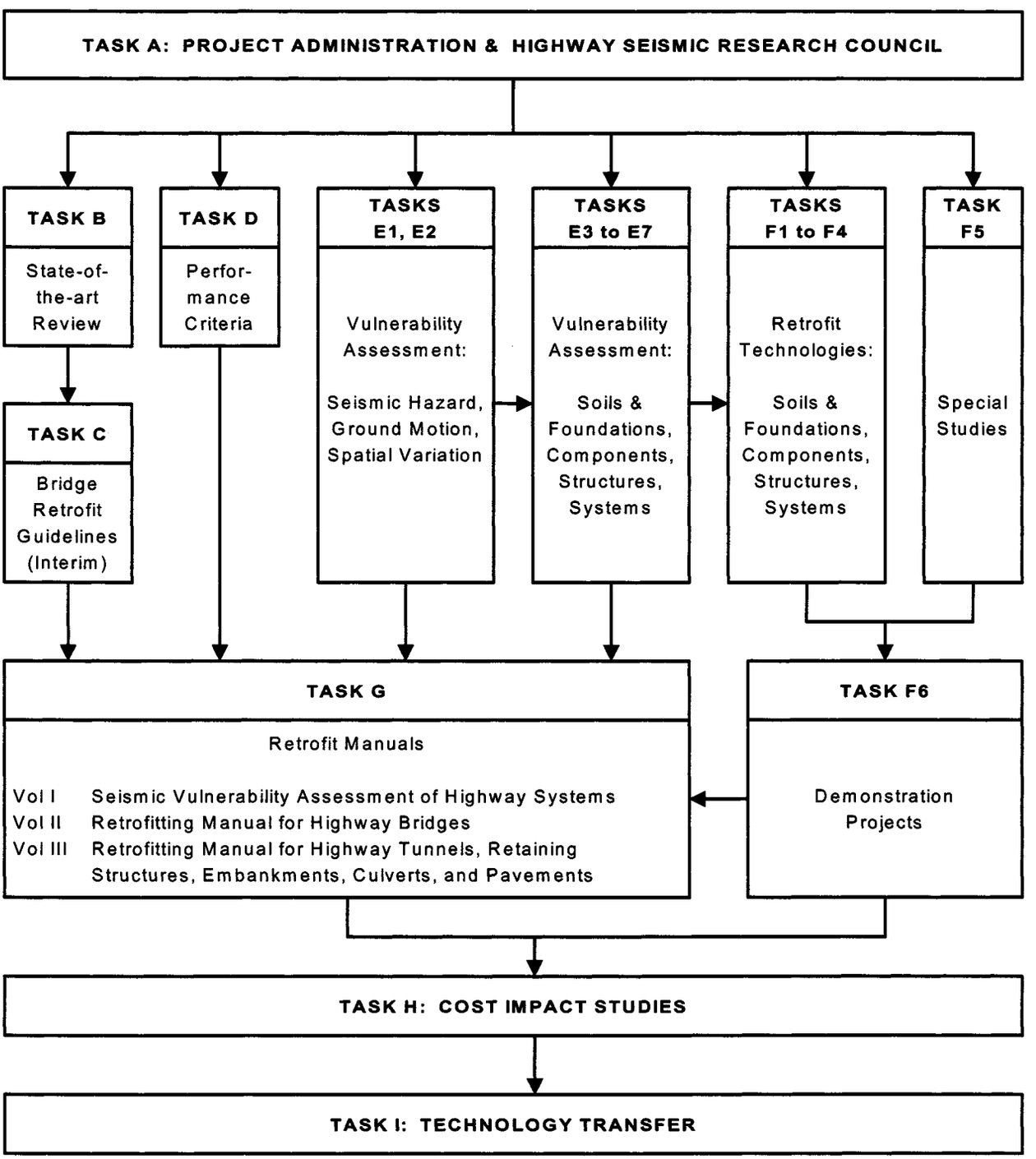

ABSTRACT

The 1971 San Fernando Earthquake showed that many highway bridges are vulnerable to collapse due to excessive longitudinal movements at expansion joints and supports. The California Department of Transportation (CALTRANS) has since initiated a retrofit scheme, which includes tying bridge spans together with restrainers at their hinges. This experimental study investigates the impact between adjacent bridge spans at in-span hinges, evaluates the efficacy of restrainers in reducing relative displacements across the hinges and examines the effects of restrainer stiffness and gap on the response of the hinge-restrainer system. A specimen consisting of two box girder reinforced concrete blocks representing the adjacent spans of a reference bridge at in-span hinge was constructed and tested under incrementally increasing worst case scenario input excitation. The blocks were supported by elastomeric bearings simulating the stiffness of the substructure. Cable restrainers were used to connect the two blocks, the number and gap of which were varied during the experiments. Experimental results indicated that impacts between the adjacent frames produce acceleration levels significantly higher than what is typically assumed in design. Restrainers were capable of reducing hinge relative displacements and prevent span unseating. However, restrainer yielding occurred under strong input motions, especially when the restrainer gap was set to zero. Only pounding at the hinge location was included in this study, while pounding elsewhere in the superstructure as well as the detailed response behavior of substructure elements were neglected.

ACKNOWLEDGMENTS

This experimental study was funded by the Federal Highway Administration (FHWA) under Task No. 106-F3.2 of the National Center for Earthquake Engineering (NCEER) Highway Project. Additional funding was provided by the California Department of Transportation (CALTRANS). Their financial aid is gratefully acknowledged.

The first author is especially grateful to Dr. Emmanuel "Manos" Maragakis for his continuous encouragement and support. Dr. Mehdi "Saiid" Saiidi is also thanked for his constructive comments and guidance.

TABLE OF CONTENTS

TABLE OF CONTENTS (cont'd)

LIST OF ILLUSTRATIONS

LIST OF ILLUSTRATIONS (cont'd)

LIST OF ILLUSTRATIONS (cont'd)

LIST OF ILLUSTRATIONS (cont'd)

LIST OF TABLES

SECTION 1
INTRODUCTION

1.1 Background

During an earthquake, adjacent bridge segments can vibrate out-of-phase due to their different dynamic characteristics and variations in the ground motions. The out-of-phase motion results in two main problems. First, when the displacement between the bridge segments exceeds the available seat width, the supported span can unseat. Many cases of bridge collapse that occurred in recent earthquakes were attributed to this phenomenon (Saiidi et al., 1993, Moehle, 1995). Second, when the segments move toward each other, pounding can occur. The significant impact forces, which are developed, can result in local damage and crushing of concrete. Furthermore, impact can increase displacements in segments beyond what is typically assumed in design. Pounding of frames produces large impact forces that can increase hinge opening at simply supported spans or at in-span hinges, resulting in a greater possibility of unseating.

The 1971 San Fernando Earthquake in California showed that many highway bridges are vulnerable to collapse due to excessive longitudinal movements at expansion joints and supports (Jennings, 1971). In order to prevent unseating, the California Department of Transportation (CALTRANS) initiated a retrofit scheme, which consisted of tying bridge spans together with restrainers at their hinges. Since then, seismic restrainers have been extensively used in the U.S. mainly in California. Under the CALTRANS Phase I retrofit program approximately 1400 bridges were retrofitted using restrainers (Yashinsky et al., 1995).

A bridge restrainer is any type of device used to inhibit relative displacements, prevent unseating and transfer longitudinal seismic forces between adjacent bridge spans. Restrainers can be in the form of plates, rods or cables. The most common type of restrainer in the U.S. is the cable restrainer. Cable restrainers used in California typically use high-strength steel cables anchored to the diaphragms or webs of concrete bridges (figure 1-1) or to the bottom flange of steel girders (figure 1-2). A variety of restrainer types are also used in Japan, including chains, rigid links and knee-joint links, which provide limited displacement before locking up (Priestley et al., 1992). Hinge restrainers are installed with a gap to allow for thermal movements of the bridge. In extreme cold conditions, this gap may be reduced to zero. At the same time the expansion joint gap increases, leaving a smaller seat width.

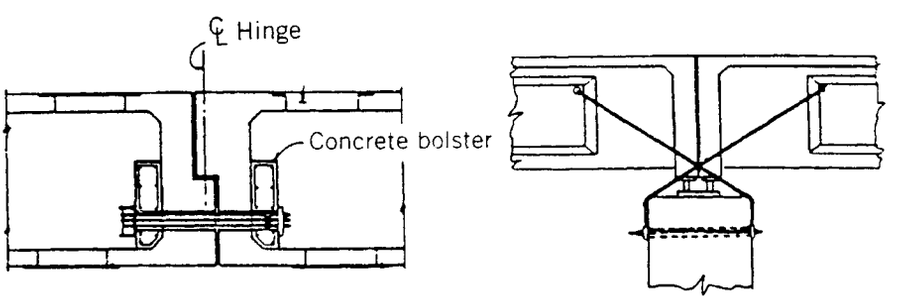

FIGURE 1-1 Cable restrainers for concrete superstructure movement joints (a) Box-girder bridges, (b) I-girder bridges

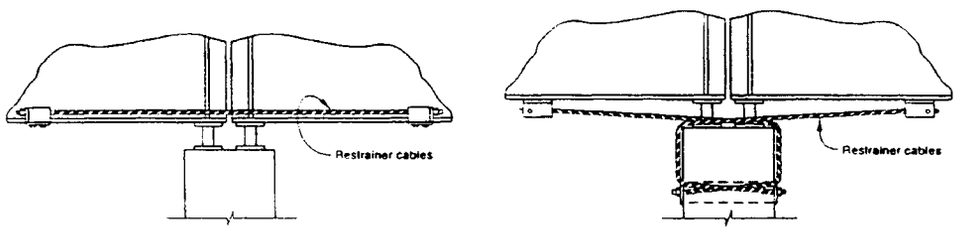

(a) Straight Cables (b) Cables Looped over Bent-Cap

FIGURE 1-2 Cable restrainers for steel superstructure movement joints

Recent earthquakes such as the 1987 Whittier Narrows Earthquake, the 1989 Loma Prieta Earthquake, the 1994 Northridge Earthquake and the 1995 Kobe Earthquake have provided a good opportunity to study the performance of bridge restrainers in bridges subjected to strong ground excitations. Reconnaissance reports following the 1989 Loma Prieta Earthquake found a few cases where restrainers failed (Saiidi et al., 1993). During the 1994 Northridge Earthquake, several bridges which had been retrofitted with cable restrainers collapsed due to unseating at the hinges (Moehle, 1995). Unseating was mainly attributed to column failure, which caused excessive movements of the adjacent spans. As a consequence, restrainers experienced very high forces and eventually failed. During the 1995 Kobe Earthquake, over 60 percent of all bridge structures in the Kobe area were damaged, costing approximately 10 billion U.S. dollars to repair (Comartin et al., 1995). In general, modern bridges performed better than older ones. However, a major problem was excessive movement at the hinges due to bearing and restrainer failures.

1.2 Existing Restrainer Design Methods

Two procedures are currently used to design restrainers in the U.S.. CALTRANS and AASHTO (American Association of State Highway and Transportation Officials), each have methods to design restrainers for bridges with the potential to become unseated in an earthquake. The main features of these two methods are presented in the following paragraphs:

1.2.1 The CALTRANS Method

CALTRANS uses an equivalent static procedure, which may be performed by hand, to determine the required number of restrainers to limit the hinge displacements to a prescribed value. The method can be applied to both simply supported spans and in-span hinges (CALTRANS, 1989).

The general procedure is as follows:

1. Calculate the restrainer length based on the hinge dimensions, assume one restrainer, compute the maximum permissible restrainer deflection and limit deflection to the available hinge seat width.
2. Compute the maximum longitudinal earthquake displacement on both sides of the superstructure joint under consideration. For curved bridges, compute the joint opening resulting from a lateral earthquake.

3. Compare the deflections from steps 1 and 2 and determine the governing case.
4. Determine the number of restrainers required.
5. Check the deflections of the restrained system and revise the restrainer and/or column stiffness assumptions if necessary. Repeat steps 1-5 if needed.

For in-span hinges, the procedure considers only the frame on either side of the intermediate hinge that has the smallest displacement. Restrainers are provided until the frame displacement is less than a prescribed value for a given design load. For simple spans on bearings, CALTRANS assumes that the bearings always fail in a strong earthquake. Further, the CALTRANS restrainer design method does not address specifically the case of skew bridges.

1.2.2 The AASHTO Method

Rather than specifying a detailed procedure, the AASHTO code defines a method to determine the longitudinal linkage force that a set of restrainers must withstand. The force is defined as the site acceleration coefficient times the weight of the lighter of the two adjoining spans or parts of the structure (AASHTO, 1996). Restrainers designed for a simply supported bridge would resist the force generated from the span weight.

The AASHTO procedure is as follows:

1. Determine the longitudinal linkage force as the product of the acceleration coefficient at the bridge site (in terms of g) and the weight of the span under consideration.
2. Determine the number of restrainers by dividing the area of the restrainers required by the area of one restrainer.

AASHTO requires that all bridges in seismic zones C and D have restrainers and satisfy seat width requirements, while bridges in zones A and B must satisfy seat width requirements only.

1.3 Literature Review on Previous Studies

A thorough review on the most important previous work related to the application of seismic restrainers for the prevention of unseating of bridge spans during major earthquakes is presented in the following paragraphs. Several previous studies have investigated the dynamic performance of restrainers in both the cases of simply supported spans and in-span hinges. These studies included skew and non-skew highway bridges with narrow and wide seats, subjected to coherent and incoherent ground motions that were acting in several directions with respect to the bridge axis. Most of these bridges were modeled and analyzed using a variety of computer programs. Field performance tests have also been conducted by some of the researchers. Furthermore, in most of the studies the adequacy of current restrainer design methods has been evaluated and several new design procedures have been developed.

1.3.1 UCLA Full Scale Structure Experimental Test (Selna et al., 1989)

In 1989 researchers at the University of California at Los Angeles (UCLA) performed a full-scale structure experimental test, whose purpose was to determine the strength, stiffness and

cyclic load-deflection behavior of box girder in-span hinge bridges that were retrofitted with longitudinal cable restrainers. The measured capacity of the retrofitted system was slightly greater than the design yield force of the restrainers. Furthermore, the failure occurred in the reinforced concrete hinge diaphragm due to deterioration resulting from combined bending and punching shear. The pull-out failure near the middle of the diaphragm did not reduce substantially the vertical load carrying capacity of the hinge because the seat in the web or stem regions of the box girder remained intact. However, if the horizontal displacement after the diaphragm failure exceeds the existing seat width, it can cause span unseating in hinges having narrow seats.

1.3.2 UNR Evaluation of the CALTRANS Design Method (Saiidi et al., 1992)

Researchers at the University of Nevada, Reno (UNR) evaluated the effects of changing the cross-sectional area of the restrainers and the restrainer gap on the non-linear response of a representative bridge with several hinges. A four-frame bridge similar to the one described in the CALTRANS design method example was chosen. The difference between the two models was the type of the abutment on the right side of the bridge. The CALTRANS example had a seat-type abutment, while the UNR model had a diaphragm-type abutment. Further, the CALTRANS example did not specify all of the dimensions and properties of the example bridge. Therefore, in order to perform a non-linear analysis of the modified CALTRANS model, the UNR researchers made several additional assumptions regarding dimensions and properties of the example bridge. The bridge was modeled using NEABS-86 and subjected to the 1940 El Centro Earthquake, North-South component, the 1954 Eureka Earthquake, North-South component and the 1989 Loma Prieta Earthquake, East-West component. Only cable type restrainers were considered. Two different gaps of 19 mm and 0 mm were chosen to represent temperature change. The parametric study indicated that the number of restrainers became more influential when the restrainer gap was reduced. A reduction in the number of cables generally increased the magnitude of stresses. To determine the most critical abutment forces it was necessary to analyze the bridge for both the extreme low and the extreme high ambient temperatures. Furthermore, abutment forces were sensitive to the ground motion. The study concluded that the extreme low ambient temperature should be considered to determine the critical restrainer stresses and that the maximum relative displacements may occur for the case of zero or non-zero restrainer gap depending on the number of restrainers. In addition, the current CALTRANS design procedure was shown to be inaccurate, since it did not produce results consistent with results of non-linear analysis. This was attributed to its lack of consideration of: (1) the cross-sectional area of the restrainers, (2) the restrainer slack, and, (3) the interaction between the restrainers and the ambient temperatures.

1.3.3 UNR Case Studies (Saiidi et al., 1993)

Prior to the 1989 Loma Prieta Earthquake very little research had been done on hinge restrainers. This can be mainly attributed to the fact that restrainers are relatively simple systems with seemingly predictable behavior. The Loma Prieta Earthquake gave researchers a very good opportunity to study the response of in-span hinge restrainers that had been subjected to an actual earthquake. The primary objectives of this study conducted at the University of Nevada, Reno (UNR) were: (1) to review the actual performance of bridge hinge restrainers during the

earthquake, (2) to develop the analytical models of selected bridges and study their earthquake response, (3) to carry out a parametric study of these bridges in order to determine the effect of stronger earthquakes and the effect of changes on the restrainer gaps, and, (4) to review current restrainer design procedures. The field study of several bridges revealed that the restrainers were activated and, in most of the cases, they performed well. It was also determined that restrainers should be analyzed as systems consisting of three components: (1) restrainer, (2) connecting hardware and diaphragms, and, (3) the superstructure adjacent to the hinge. The weak point in this assembly can be predicted based on the available seat width of the bridge. In old bridges, which are characterized by inadequate seat widths, yielding should not be allowed in any of the components of a restrainer assembly during a major earthquake because excessive movements would result in collapse. In new bridges, yielding is acceptable because seats are usually wide and cables can be easily replaced. The analytical study showed that restrainers indeed reduce hinge displacements and prevent collapse of the superstructure. Therefore, they should be used to maintain the overall integrity of the bridge structure even if analysis indicates that they are not needed. Furthermore, bridges with relatively soft substructure and high ratio of number of hinges to number of spans may be more vulnerable to unseating. Restrainer forces were far more critical when the restrainer gap was reduced to zero. As a conclusion, it was recommended that non-linear analysis should be used for restrainer design, because current restrainer design methods do not adequately approximate the response of the restrainers.

1.3.4 UCB Case Studies (Singh and Fenves, 1994, Fenves and Desroches, 1994)

The damage and collapse of two-level viaducts in the Loma Prieta Earthquake prompted researchers at the University of California, Berkeley (UCB) to study their response (Singh and Fenves, 1994) using linear and non-linear finite element analysis. It was found that cable restrainers limited the out-of-phase motion between adjacent spans. The number of restrainers required by the CALTRANS method was found to be overconservative. It was also shown that relative displacements at hinges were larger when the input ground motions were incoherent instead of coherent.

When the 1992 Landers and Big Bear Earthquakes occurred, the response of the Northwest Connector bridge in southern California was measured (Fenves and Desroches, 1994). The study indicated that non-linear models were adequate for estimating the response of the bridge and were recommended over linear hinge models.

1.3.5 UCSD Analytical Parametric Study (Yang et al., 1994)

In 1994 researchers at the University of California, San Diego (UCSD) conducted a parametric study of a two-frame bridge with an in-span hinge in order to investigate the influence of different bridge properties on the relative longitudinal displacements of hinges. The study considered the following parameters: (1) adjacent bridge frame stiffness, (2) restrainer stiffness, (3) earthquake intensity, and, (4) sliding friction and gap at the expansion joint. It was concluded that, in some of the cases, the CALTRANS method was extremely conservative, while in others it underestimated the relative hinge displacement. This study also showed that both the expansion joint gap and the Coulomb friction had a small impact on the relative displacement between adjacent frames. Greater earthquake intensity increased frame displacements. The

maximum relative hinge displacement also increased when the frames remained elastic. However, when non-linear behavior dominated the response, relative displacements did not change significantly with increasing earthquake intensity.

1.3.6 UW Evaluation of Current Design Practices and Development of New Procedure (Trochalakis et al., 1995)

In order to evaluate the AASHTO and CALTRANS restrainer design methods for in-span hinges, mandated by the AASHTO and CALTRANS, researchers at the University of Washington (UW) modeled a two-frame bridge with an in-span hinge. The non-linear response of the bridge was studied to determine the maximum opening experienced at the in-span hinge and the maximum relative displacements at the abutments. The most important parameters in predicting the maximum relative hinge displacement were found to be: (1) restrainer stiffness, (2) restrainer gap, (3) frame period, and, (4) frame stiffness ratio. Furthermore, the parametric study identified the following three variables as the most important in predicting the maximum relative abutment displacement: (1) abutment stiffness and strength, (2) sum of frame stiffnesses, and, (3) sum of frame weights. The AASHTO empirical seat width equation and the CALTRANS restrainer design method were compared with the results of non-linear response history analyses. The empirical seat width equation produced conservative results, even for very strong earthquakes. However, the AASHTO restrainer design procedure ignores variables that were shown to be very important in the parametric study. The CALTRANS method produced inconsistent results with a large amount of scatter. Using the results of the parametric study, the UW researchers developed a new restrainer design method based on the single-degree-of-freedom response of the two adjacent frames using an equivalent stiffness. The mean response of both frames is determined and used in an empirical equation to determine the mean relative hinge displacement, which must be smaller than the available seat width.

1.3.7 UCB Evaluation of Current Design Practices and Development of New Procedure (Fenves and Desroches, 1996)

In 1996 researchers at the University of California, Berkeley (UCB) also evaluated the CALTRANS and AASHTO restrainer design procedures and developed a new method for restrainers at in-span hinges. A non-linear numerical model was used to represent the longitudinal earthquake response of two frames connected at a hinge. The model included non-linear force-displacement relationships for the frames, while non-linear elements accounted for tension-only restrainers and Coulomb friction. A parametric study showed that the hinge response is governed by the period ratio of the two frames adjacent to the hinge, the target ductility demand of the frames and the stiffness of the hinge restrainers. A multi-step design procedure based on a linearized numerical method was developed. Parametric studies indicated that the procedure works well in limiting the relative hinge displacement for a wide range of parameters. The required number of restrainers decreases as the frame period ratio and the frame target ductility increase. A simplified single-step design procedure was also developed based on a non-dimensional value of the restrainer stiffness, which is determined by performing a large parametric study. Comparisons with current restrainer design procedures showed that the new multi-step and single-step procedures are more accurate than current procedures for designing hinge restrainers. The study also concluded that pounding of frames and engaging of restrainers

produce forces and displacements that are significantly different than what is typically assumed in design. Pounding typically increases the demand in stiffer frames and decreases the demand in flexible frames. Another conclusion drawn was that frames with higher ductility levels exhibit in-phase motion. Frames moving in-phase will experience smaller relative displacements and, thus, they will require fewer restrainers.

1.3.8 UW Study of Unseating in Simply Supported Spans (Trochalakis et al., 1996)

A study to investigate unseating in simply supported spans was conducted by researchers at the University of Washington (UW). A set of 68 non-linear time history analyses was performed to determine the effects of varying six parameters including pier heights, abutment stiffness and strength, earthquake record and intensity, compression gap, bearing factor, and, restrainer stiffness. Restrainers were included in 16 analyses. The study concluded that bearing pad friction, earthquake record and intensity, as well as compression gap are the most significant parameters affecting the maximum relative displacement at a bearing support and that the maximum relative abutment displacement mainly depends on the bearing pad friction resistance and earthquake record and intensity. The study also found that restrainers were ineffective in reducing relative displacements of the simply supported bridges considered in the study. However, in this study restrainers attached adjacent girders instead of attaching the girder to the bent cap, which is not a common restrainer configuration and is not typically used by CALTRANS.

1.3.9 UW Design of Restrainers Considering Spatial Variation of Ground Motions (Hudgings et al., 1997)

In 1998 researchers at the University of Washington (UW) performed a study in order to examine the effects of spatially varying ground motions on the behavior of straight, two-frame bridges with unrestrained and restrained in-span hinges. The non-linear parametric study produced a 3600 case database of the maximum relative hinge displacement and maximum relative abutment displacement responses. Results from this study were used to develop a new comprehensive restrainer design method. It was found that the maximum relative hinge displacement of a two-frame bridge depends primarily on the adjacent frame stiffness ratio and restrainer stiffness, while the maximum relative abutment displacement is governed by the sum of the stiffnesses of both frames. The wave passage effect results in small increases in the maximum relative hinge displacements and has little impact on the maximum relative abutment displacements. The AASHTO minimum seat width equation proved to be conservative. Similarly, it was shown that the CATRANS restrainer design method does not predict the maximum relative hinge displacements accurately. Note that neither design procedure accounts for spatial variability of the input ground motions. The restrainer design method proposed by the UW researchers was able to produce rational, consistent and safe predictions of the maximum relative hinge displacements and also account for varying ground motions.

1.3.10 UNR Design of Restrainers for Multi-Span Simply Supported Bridges (Randall et al., 1998)

The most recent study on the performance of seismic restrainers was conducted by researchers at the University of Nevada, Reno (UNR) in 1998. The objectives of this study were: (1) to review the performance of longitudinal cable restrainers on bridges with simply supported spans in past earthquakes, (2) to evaluate the adequacy of current restrainer design procedures, (3) to develop new restrainer design procedures that would prevent unseating, and, (4) to evaluate the adequacy of the new restrainer design procedures. Skew and non-skew, two- and five-span simply supported highway bridges with narrow and wide seats were modeled and studied. Ground motions were applied in the longitudinal direction for non-skew bridges and in both the longitudinal and transverse directions for skew bridges. Abutments, superstructure, columns, foundations, restrainers, bearings and expansion joints were all included in models. Element behavior was assumed to be non-linear with the exception of the superstructure that was treated as elastic. Cable restrainers connecting spans to their seat in the longitudinal direction were the only type of restrainers considered. Three new design procedures were developed: (1) an equivalent linear method, (2) the W/2 method, and, (3) the Modified CALTRANS method. The equivalent linear method is similar to the existing CALTRANS procedure in that it uses response spectra to determine the force a restrainer set must withstand. However, this method includes the effects of column, footing and bearing stiffness and strength, as well as abutment stiffness and strength in order to determine an equivalent vibration period that is combined with response spectra to determine restrainer forces. In the W/2 method, restrainers must withstand one-half of the weight of the span they are restraining. The Modified CALTRANS method combines a part of the equivalent linear method with the CALTRANS procedure. It was found that the Modified CALTRANS procedure is an effective method for designing restrainers to limit relative displacement at supports and prevent unseating and, therefore, is recommended for use in all cases. The equivalent linear method was also recommended for use in all cases except for skew bridges and structures with narrow seats when the substructure is very flexible. The CALTRANS method was found to be satisfactory but in skew cases the number of restrainers should be modified by the Skew Factor. The W/2 and AASHTO methods are also effective procedures for designing restrainers. However, their use should be limited to bridges that have wide seats and are not skewed. Another conclusion drawn was that the bearing strength has a great influence on the relative displacements at superstructure seats and should be considered in restrainer design. It was also shown that non-skew two- and five-span bridges do not need restrainers to prevent unseating if AASHTO seat width requirements are met. Finally, abutment restrainers were recommended unless wide abutment seats are provided.

1.4 Objectives and Scope

This experimental study focused on the dynamic performance of straight bridges with in-span hinges retrofitted with seismic restrainers and subjected to real time earthquake motion. Cable restrainers were the only type of restrainers that was considered.

The primary objectives of the research were:

- Investigate the pounding between adjacent spans at in-span hinges and the possible local damage and concrete spalling associated with the significant impact forces, which are developed during impact.
- Subject the specimen to a worst possible scenario ground motion and evaluate the performance and effectiveness of the hinge restrainers in inhibiting relative displacements across the hinges and preventing span unseating under simulated earthquakes with different intensities.
- Assess the effects of the restrainer gap, the number of restrainers, and, the peak ground acceleration on the response of the hinge.

In order to achieve the objectives, a specimen consisting of two large-scale concrete blocks representing the adjacent parts of a reference bridge at an in-span hinge was constructed and tested under incrementally increasing earthquake excitation. The blocks were placed on one of the two shake tables available in the Large Scale Structures Laboratory at the University of Nevada, Reno and were supported by elastomeric bearings simulating the stiffness of the substructure. The two blocks were tied with cable restrainers, the number and gap of which were varied during the experiments.

SECTION 2
TEST SPECIMEN

2.1 Introduction

The purpose of this chapter is to describe the test specimen that was used in the experimental study. A portion of a reinforced concrete box girder bridge, which includes the hinge, was constructed in order to test the impact of two adjacent bridge spans that are connected with longitudinal hinge restrainers. The development of the bridge model was based on data obtained from several representative bridges in California. The specimen was placed on one shake table and supported by bearings simulating the stiffness of the substructure. The bearings were designed such that their stiffness is equal to the scaled stiffness of the bent supporting the corresponding segment of the actual bridge. Cable restrainers were used to connect the two blocks representing the bridge segments. The restrainers were designed according to the current CALTRANS restrainer design procedure (CALTRANS, 1989).

2.2 Bridge Database

The bridge model was designed based on the average dimensions of the following six typical existing CALTRANS bridges with in-span hinges: (1) Fourth Street Viaduct, (2) Rudgear Road Undercrossing, (3) South Walnut Creek Overhead, (4) Laurel Drive Undercrossing, (5) Tompkins Hill Road Overhead, and, (6) Danville Overhead. The bridges included in the database were built in 1969, 1995, 1975, 1995, 1982, and 1975, respectively. All of them have been retrofitted to prevent unseating at the in-span hinges during major earthquakes because of the inadequacy of their seat widths. The majority of this retrofit work involves installation of high-strength steel cables anchored to the diaphragms or webs at hinges and joints. Type C-1 restrainers were used in most of the cases. The basic superstructure, spans, bents and hinge properties of these bridges were tabulated and statistical analysis of the data was carried out in order to obtain a reference representative bridge. The elevation of the bridge model is shown in figure 2-1.

2.2.1 Superstructure Properties

A summary of the superstructure properties of the six representative CALTRANS bridges is shown in table 2-1. It should be noted that reinforced concrete box girder was the only in-span hinge bridge type found in the CALTRANS database. In order to serve the rapidly increased traffic demands of California, four of the six bridges had been recently widened. Therefore, the section of the average bridge consisted of multispine boxes joined by link slabs located at both sides of the original structure. The average section width was approximately 36 m (118 ft), corresponding to eight lanes with two shoulders, while the average section depth was slightly greater than 1.6 m (5.3 ft). Furthermore, the average top slab, web, and bottom slab thickness were 18 cm (7 in), 24 cm (9.5 in) and 14.5 cm (5.7 in), respectively.

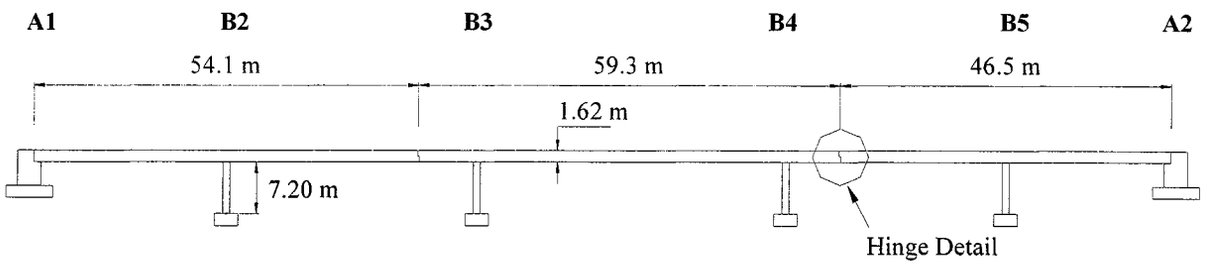

FIGURE 2-1 Average Bridge Elevation

2.2.2 Span Properties

Table 2-2 summarizes the main properties of the bridge spans. It should be noted that all the bridges had two in-span hinges. However, the number of spans in each bridge varied from four to eight. The two hinges divided the average bridge into three segments that were, respectively, 54 m (177 ft), 59 m (194 ft) and 47 m (154 ft) long. The segment between the two hinges was on average supported on two bents, while both end segments were supported on one bent only.

2.2.3 Substructure Properties

The bents of all the typical CALTRANS bridges considered in this study, except the Fourth Street Viaduct, consisted of more than one column. As it can be shown in table 2-3, the average number of columns at each bent was eight, while the average column height was approximately 7.2 m (23.6 ft). In three of the cases the columns had a rectangular cross section. For the two bridges in which the cross section was other than rectangular, an equivalent rectangular cross section was calculated based on equal areas. The column average dimensions were 254 cm (8.3 ft) by 98 cm (3.2 ft), while the pile-supported footing average dimensions were 434 cm (14.2 ft) by 331 cm (10.9 ft). The connection between the bridge sub- and superstructure was monolithic in all cases. The moment-resisting capacity of this type of connection created the potential for additional redundancy in the lateral force resisting path, particularly for longitudinal response.

2.2.4 Hinge Properties

The hinge properties of the six representative bridges are summarized in table 2-4. The average seat width was 264 mm (10.4 in). This relatively high value is not typical because it reflects the large seat widths of two of the bridges that were included in the database. Most of the bridges designed before 1971 had insufficient seat widths at hinge regions and this was one of the main reasons for span unseating and collapse during the 1971 San Fernando Earthquake. These

TABLE 2-1 Average Bridge Superstructure Properties

Superstructure	Fourth Street Viaduct	Rudgear Road Undercrossing	South Walnut Creek Overhead	Laurel Drive Undercrossing	Tompikns Hill Road Overhead	Danville Overhead	Average Properties
Year Constructed	1969	1995	1975	1995	1982	1975	-
interior web (cm)	20.32	25.40	20.32	30.48	22.86	20.32	23.28
no. of interior webs	4	19	14	20	8	15	13
exterior web (cm)	20.32	25.40	20.32	35.56	22.86	20.32	24.13
top width (m)	12.24	46.18	35.56	45.72	27.03	45.72	35.41
top slab thickness (cm)	15.87	17.15	18.10	16.19	21.59	17.78	17.78
bottom width (m)	11	38.05	30.04	-	21.08	30.16	26.07
bottom slab thickness (cm)	13.97	14.13	14.29	13.97	15.87	14.39	14.44
overhang thickness (cm)	17.78	-	17.78	-	15.24	17.78	17.15
overhang length (m)	0.62	-	1.21	-	0.91	0.94	0.92
total height (m)	1.37	1.83	1.83	1.47	1.83	1.41	1.62
net height (m)	1.07	1.52	1.51	1.17	1.45	1.08	1.30

TABLE 2-2 Average Bridge Span Properties

Spans	Fourth Street Viaduct	Rudgear Road Undercrossing	South Walnut Creek Overhead	Laurel Drive Undercrossing	Tompikns Hill Road Overhead	Danville Overhead	Average Properties
Year Constructed	1969	1995	1975	1995	1982	1975	-
no.	8	6	6	5	4	5	6
no. of hinges	2	2	2	2	2	2	2
abut. 1 - hinge 1 (m)	64.3	52.2	47.6	47.9	64.9	47.9	54.1
no. of bents	2	1	1	1	1	1	1
hinge 1 - hinge 2 (m)	100.1	80.5	82.9	29.0	34.3	29.0	59.3
no. of bents	3	3	3	2	1	2	2
hinge 2 - abut. 2 (m)	67.5	48.0	43.3	47.9	24.8	47.9	46.5
no. of bents	2	1	1	1	1	1	1

TABLE 2-3 Average Bridge Bent Properties

Bents	Fourth Street Viaduct	Rudgear Road Undercrossing	South Walnut Creek Overhead	Laurel Drive Undercrossing	Tompikns Hill Road Overhead	Danville Overhead	Average Properties
Year Constructed	1969	1995	1975	1995	1982	1975	-
type	tapered	elliptical	rectangular	-	rectangular	rectangular	-
no. of columns	1	5	3	15	6	13	8
column height (m)	4.7	8.9	8.2	7.8	6.3	7.4	7.2
column cross section (cm)	varies	411 x 135	366 x 76	-	122 x 107	119 x 76	254 x 98
footing cross section (cm)	503 x 503	-	594 x 274	-	366 x 274	274 x 274	434 x 331

TABLE 2-4 Average Bridge Hinge Properties

Hinge	Fourth Street Viaduct	Rudgear Road Undercrossing	South Walnut Creek Overhead	Laurel Drive Undercrossing	Tompikns Hill Road Overhead	Danville Overhead	Average Properties
Year Constructed	1969	1995	1975	1995	1982	1975	-
seat width (mm)	406	64	171	112	660	171	264
expansion joint gap (mm)	51	16	19	16	51	19	29
diaphragm thickness (mm)	914	1829	762	-	1676	762	1189

bridges had a hinge seat width of approximately 152 mm (6 in) that is significantly lower than the seat width considered in this study. Although current policy in California requires a seat width of 610 mm (24 in), the value of 264 mm is representative of most of the existing bridges with movement joints, and, thus, it was assumed to be appropriate for the purpose of this study. The average expansion joint gap and the diaphragm thickness were 29 mm (1.1 in) and 119 cm (3.9 ft), respectively. Although the diaphragm thickness seems to be large, it is not unrealistic since it includes the thickness of the bolsters. The bolsters were part of the retrofit work that had been carried out in bridges under consideration.

2.3 Specimen Design

In order to design the test specimen, the properties of the average bridge, including the superstructure mass and the substructure stiffness, had to be scaled down. Several researchers have pointed out that the dynamic response of structural systems can be simulated quite accurately only at reasonable model scales. It is well understood that confidence in the results of experimental model studies depends upon the selected scale factor. Small scale factors are unable to predict the behavior of full scale structures, especially when failure is initiated by localized phenomena, such as impact between adjacent spans or span unseating. Therefore, results from model tests with scale factor of 0.2 or smaller are usually viewed with a lot of skepticism. The primary selection of the scale factor in this study was to satisfy the pay load limitation of the shake table. Each of the University of Nevada, Reno shake tables has a pay load capacity of 445 KN (100 kips) for a table motion with a peak acceleration of 1 g. Thus, it was clearly anticipated that a scale factor greater than 1/3 could not be achieved.

2.3.1 Concrete Block Design

Based on the average properties presented in the preceding sections, the mass of the bridge cross section was estimated. Because of the symmetry about the longitudinal section centerline, only one half of the bridge was considered. All bridges were made of normal weight concrete, the unit weight of which was assumed to be 23.5 KN/m^3 (150 lb/ft^3). The distributed dead load along the bridge longitudinal axis was calculated to be approximately 344.7 KN/m (23.6 kips/ft). Since dynamic response in the longitudinal direction only would be considered and skewness effects would be neglected, it was decided that the estimation of the mass of the superstructure could be based on 1/8 of the superstructure. Since the actual average bridge consisted of eight lanes, 1/8 of the bridge corresponded to one lane of traffic flow. Further, in order to avoid in-phase motion and assure the impact of the two adjacent spans, only the heavier and the lighter of the bridge segments were considered. As a consequence, a scale factor of 1/4 was feasible, resulting in a total specimen weight of about 285 KN (64 kips). Therefore, the goal of not exceeding the shake table capacity but also designing a relatively large scale test was achieved.

Although the limitations imposed by the shake table dimensions and load carrying capacity prevented the selection of a scale factor greater than 1/4 for the modeling of the bridge mass and stiffness, it was decided that a full-scale structure in terms of dimensions would demonstrate the dynamic performance of the restrainers in a more explicit and convenient way. Thus, a realistic box girder bridge portion, with realistic hinge dimensions, was designed. The design was based on the average superstructure dimensions discussed in previous sections. A general layout of the

test specimen based on the average bridge properties is shown in figure 2-2. The specimen was 1.5 m (4.9 ft) high and 2 m (6.6 ft) wide. The combined length of the two concrete blocks representing the two adjacent bridge spans was 4.25 m (13.9 ft). The width and thickness of the specimen box girder elements are presented in table 2-5. It should be noted that during the actual retrofit work, which had been carried out in most of the bridges included in the database, a reinforced concrete bolster was cast against the existing hinge diaphragm. However, in order to simplify and expedite the construction process of the test specimen, this procedure was omitted and the bolster thickness was incorporated in the thickness of the diaphragm. The dimensions of the diaphragm were verified to be adequate through a punching shear model based on CALTRANS Seismic Design References (CALTRANS, 1994), based on forces of C-1 type restrainer.

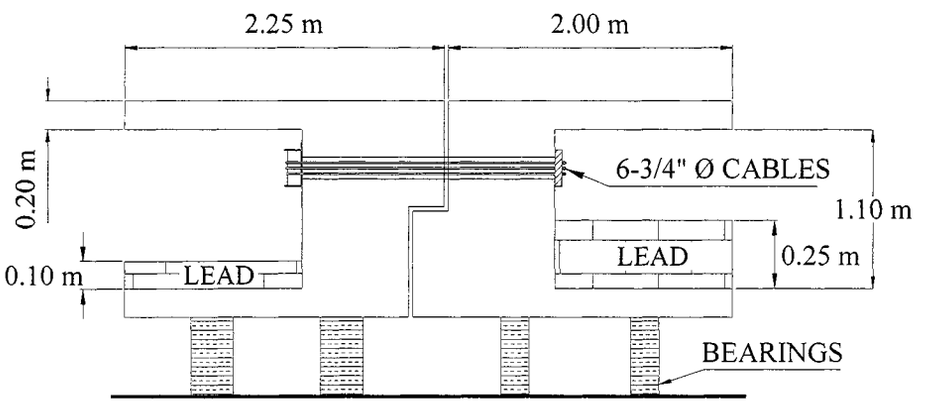

FIGURE 2-2 In-span Hinge Test Layout

The reinforcement used in the specimen is shown in figures 2-3 and 2-4. The bar sizes and locations were similar to those used in existing bridge hinges. The reinforcement used in top and bottom slabs, and web was designed according to the CALTRANS Seismic Design References (CALTRANS, 1993). For the design of the diaphragm, which was considered to be the critical region in terms of concrete strength, a strut-and-tie model was developed. The calculations for both the horizontal and the vertical reinforcement of the diaphragm were based on this model.

Based on this design, each concrete block weighs approximately 100 KN (22.5 kips). In order to obtain the scaled mass of the actual bridge model, supplemental weights had to be added to two concrete blocks. Lead bricks were used for this purpose.

2.3.2 Bearing Design

In order to design the bearings, the stiffness of the actual bridge substructure had to be calculated. A bridge column has a stiffness value between that of a cantilever column and a column fixed at both ends. To simplify the procedure of evaluating the bent stiffness, the average

TABLE 2-5 Dimensions of the Specimen and Type C-1 Cable Restrainer Hardware

Box Girder Element	Width of Thickness
top slab (cm)	20
bottom slab (cm)	20
diaphragm (cm)	75
web (cm)	20
seat (cm)	25
restrainer hardware	w x h x t *
Bearing plate (cm)	5 x 25 x 25
drum (cm)	11 x 41 x 25

* Width x Height x Thickness

of the two extremes was taken. Therefore, the elastic stiffness of each column was calculated using the following equations:

$$k = 7.5EI/h^3 + G\ A_s/h \tag{2-1}$$

where:
k = stiffness of one column
E = Young's modulus of concrete
I = cracked moment of inertia taken as one-half of gross moment of inertia
h = column height
G = shear modulus of concrete
A_s = shear area

All the columns within a bent were assumed to have the same stiffness. Thus, the total bent stiffness was calculated as follows:

$$K = nk \tag{2-2}$$

where:
K = total bent stiffness
n = number of columns in the bent

To form substructure stiffness, footing stiffness was also determined and combined with bent stiffness. Assuming that the springs simulating the columns and footing stiffnesses are connected in series, the total substructure stiffness was found from the following equation:

$$K_s = \frac{1}{1/K + 1/K_h + h^2/K_r} \tag{2-3}$$

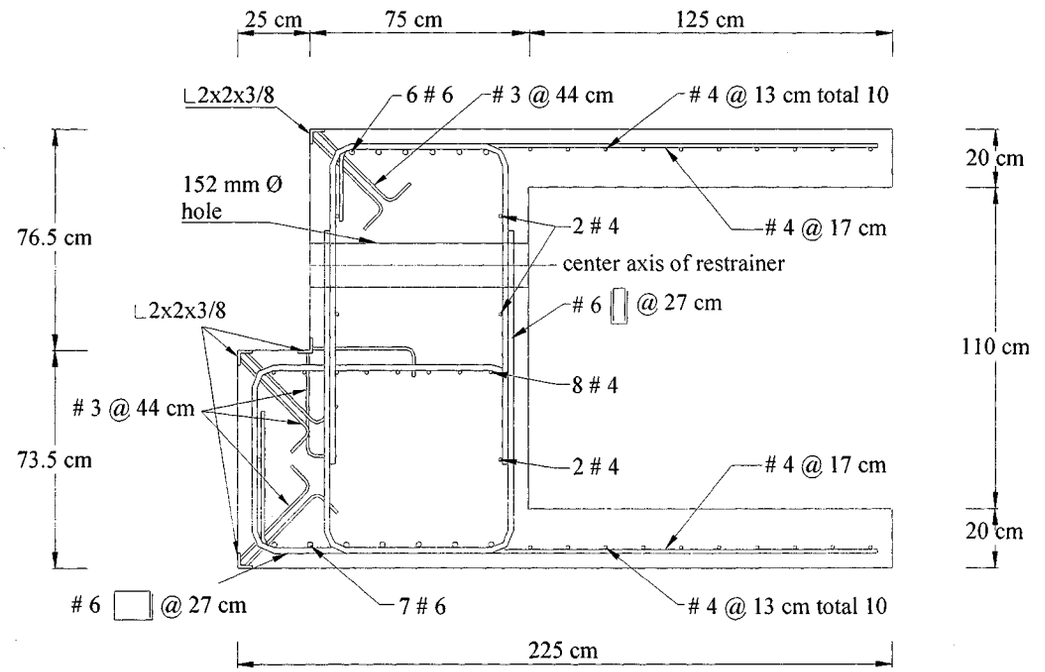

FIGURE 2-3 Reinforcement of East Block

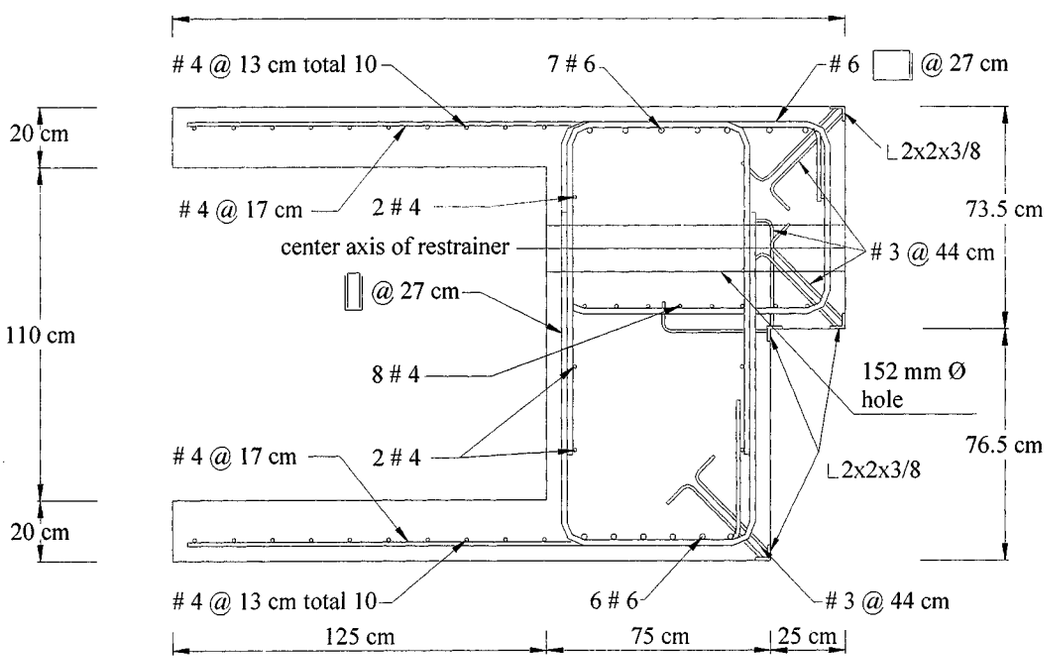

FIGURE 2-4 Reinforcement of West Block

where:
K_s = total substructure stiffness

Footing translational and rotational stiffnesses were calculated based on equations found in the Federal Highway Administration (FHWA) Seismic Design of Highway Bridge Foundations, Vol. II (FHWA, 1986). In order to simplify the calculations, the foundation was assumed to be surface. Thus, horizontal translational stiffness can be taken as:

$$K_h = 8 G_s \alpha / (2 - \nu) \tag{2-4}$$

where:
K_h = equivalent horizontal translational stiffness
G_s = shear modulus of soil
ν = Poisson's ratio of soil
α = equivalent radius

Similarly, rocking rotational stiffness is given by:

$$K_r = 8 G_s \alpha^3 / 3(1 - \nu) \tag{2-5}$$

where:
K_r = equivalent rocking rotational stiffness

The scaled substructure stiffness was obtained by multiplying K_s by the scale factor:

$$\tilde{K}_s = K_s l_r \tag{2-6}$$

where:
$\tilde{K}_s$ = scaled substructure stiffness
l_r = scale factor

The stiffness of the elastomeric bearing pads that were used to simulate the substructure stiffness was calculated as follows:

$$K_b = m G_b A_b / T_r \tag{2-7}$$

where:
G_b = shear modulus of rubber
A_b = bonded area of bearing pads
T_r = rubber thickness of bearing pads
m = number of bearing pads supporting each concrete block

Setting the stiffness of the bearing pads equal to the scaled substructure stiffness and performing simple algebraic calculations, the following equation was derived:

$$\frac{G_b A_b}{T_r} = \left(\frac{n}{m}\right)\left\{\frac{7.5EI/h^3 + G A_s/h}{1+\left(7.5EI/h^3 + G A_s/h\right)\left[(2-\nu)/8 G_s \alpha + 3h^2(1-\nu)/8 G_s \alpha^3\right]}\right\} l_r \qquad (2\text{-}8)$$

Equation (2-8) defines the stiffness of each bearing pad. In order to calculate this stiffness, several assumptions regarding material and soil properties were made. The modulus of elasticity and the shear modulus of concrete were assumed to be 27 GPa (3916 ksi) and 11 GPa (1595 ksi), respectively. The cracked moment of inertia was taken equal to 50 percent of the gross section moment of inertia. Since most of the columns of the six typical bridges in CALTRANS database had rectangular cross section, a shear area reduction factor of 5/6 was used in the calculations. The rubber used for the bearing pads was assumed to have a shear modulus of 1.2 MPa (174 psi). Furthermore, the Poisson's ratio of soil was taken equal to 0.33. The shear modulus of soil depends on the local soil conditions and the shear strain level developed due to earthquake excitation. For the purpose of this study, the shear modulus was assumed to be 19.2 MPa (2785 psi). This value corresponds to soft clays with a shear strength of 19.2 KPa (2.8 psi) and shear strain level equal to 10^{-2} (Carter and Bentley, 1991). Although each bent of the average bridge consisted of eight columns, n was taken equal to one because only 1/8 of the bridge was considered. Based on stability considerations, it was decided that each concrete block should be supported on four bearing pads. Based on these assumptions and the dimensions of the average bridge model, the stiffness of each of the bearings supporting each concrete block was calculated. For the block corresponding to the heavier bridge segment, the resulting value was multiplied by two because this segment was supported on two bents. Table 2-6 summarizes the basic properties of the two types of bearing pads that were used in this research study. As it can be seen in this table, type A pads had an effective horizontal stiffness of 161 KN/m (0.92 kips/in), while type B pads had an effective horizontal stiffness of 74 KN/m (0.42 kips/in). The reinforcing shims were made of steel. The contribution of the rotational flexibility of the bearing pads to lateral flexibility was neglected.

TABLE 2-6 Elastomeric Bearing Pads Properties

Bearing Pads	Type A	Type B
effective stiffness (KN/m)	161	74
overall height (cm)	15.6	19.2
diameter (cm)	17.8	17.8
rubber layer thickness (mm)	6.0	6.0
no. of rubber layers	12	16
shim thickness (mm)	3.2	3.2
no of shims	11	15
isolator hardware	w x h x t *	w x h x t *
bottom mounting plate (cm)	20.3 x 20.3 x 1.3	20.3 x 20.3 x 1.3
top mounting plate (cm)	35.6 x 35.6 x 1.3	35.6 x 35.6 x 1.3

* Width x Height x Thickness

2.3.3 Restrainer Design

The CALTRANS method, which was used for the restrainer design, requires an equivalent static analysis of the restrainers. It should be noted that the method was applied to the two segments of the actual bridge and the calculated number of restrainers was scaled down in order to obtain a scaled restrainer stiffness, based on the previously selected scale factor of 1/4.

According to the CALTRANS restrainer design procedure (CALTRANS, 1989), the following steps were followed:

1. The maximum permissible restrainer deformation was computed and limited to the available seat width. The maximum permissible restrainer deformation is given by:

$$D_r = D_y + D_g \tag{2-9}$$

where:
D_r = maximum permissible restrainer deformation
D_y = restrainer deformation at yield
D_g = slack in the restrainer gap

For the purpose of this study, the restrainer gap was assumed to be 25.4 mm (1 in). Furthermore, the yield deformation was obtained from the following equation:

$$D_y = F_y L / E_r \tag{2-10}$$

where:
F_y = yield stress in restrainer
L = restrainer length
E_r = initial modulus of elasticity of restrainer (before stretching)

Since type C-1 restrainers had been used in most of the typical box girder CALTRANS bridges that had been retrofitted, this type of restrainers was considered in this study. Type C-1 restrainers consist of 19-mm (3/4 in) diameter galvanized cables, bearing plates, drum and bolster. CALTRANS has used 19-mm (3/4 in) diameter cable in guard rails for more than two decades. The application of cables for restrainers was derived from their use in guard rails. The yield stress for these cables is 1.214 GPa (176.1 ksi), while their modulus of elasticity is approximately 69 GPa (10000 ksi). The restrainer length was assumed to be 2.0 m (6.6 ft). Thus, the calculated value of the maximum permissible restrainer deformation was 60 mm (2.4 in).

According to the CALTRANS Seismic Design References (CALTRANS, 1989), the available seat width can be calculated as follows:

$$\text{Available Seat Width} = \text{Seat Width} - \text{Expansion Joint Gap} - 102\ \text{mm} \tag{2-11}$$

All the preceding dimensions are shown in figure 2-5. The seat width and the expansion joint gap were directly taken from the average bridge hinge properties. The 102 mm (4 in) dimension is presumed to provide for a minimum 'reasonable' allowable seat width, below which the concrete cover in both segments would spall. By substituting the corresponding values into equation (2-11), the available seat width was found to be approximately 133 mm (5.2 in). Since this value was greater than the maximum permissible restrainer deflection, the restrainer design was considered to be acceptable.

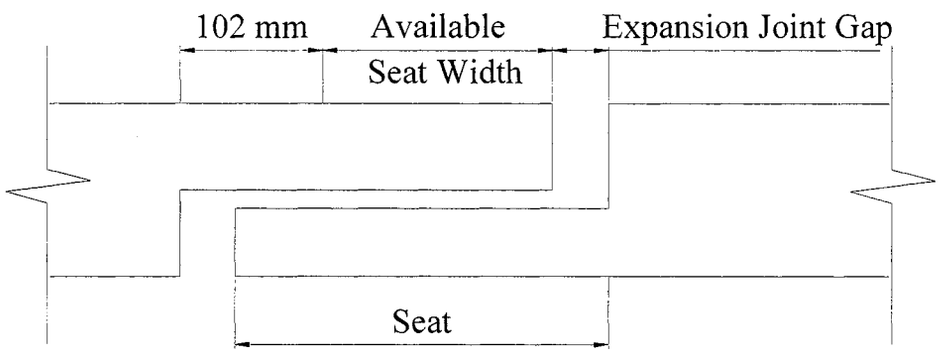

FIGURE 2-5 In-span Hinge Seat Width Detail

2. The maximum longitudinal earthquake deformations on both adjacent bridge spans under consideration were calculated. Restrainers were not included in this calculation. In order to calculate the unrestrained system stiffness, four cases were considered: (1) the left segment moving away from the hinge, (2) the right segment moving away from the hinge, (3) the left segment moving towards the right segment, and, (4) the right segment moving towards the left segment . In the last two cases both segments were mobilized. Having calculated the unrestrained system stiffness, the longitudinal displacement, corresponding to each one of the four cases, was derived from the following equation:

$$D_{eq} = ARS(W)/K_u \qquad (2\text{-}12)$$

where:

D_{eq} = longitudinal earthquake deformation of the unrestrained system

ARS = the acceleration in g for a given period of vibration, T. The period is given by: $T = 2\pi\sqrt{W/K_u g}$

W = weight of the segment under consideration

K_u = unrestrained system stiffness

In order to design the restrainers, the assumed ground acceleration was 0.4 g, while the subsoil was considered to be 3.1 m (10 ft) - 24.4 m (80 ft) alluvium, based on the relevant

CALTRANS example regarding hinge retrofit. Having the seismic data, CALTRANS smooth elastic response spectra (CALTRANS, 1993) were used to obtain ARS. The calculated earthquake deformations, corresponding to each one of the four cases that had been considered, were 530 mm (20.9 in), 713 mm (28.1 in), 505 mm (19.9 in) and 502 mm (19.8 in), respectively.

3. The maximum permissible restrainer deformation from step 1 and the smallest of the earthquake deformations from step 2 were compared and the course of action was determined. Because D_{eq} was greater than D_r by a significant amount, analysis indicated that a large number of restrainers was required.
4. The number of restrainers required was determined as follows:

$$N_r = K_u(D_{eq} - D_r)/(F_y A_r) \tag{2-13}$$

where:
N_r = number of restrainers required
A_r = area of one restrainer

For C-1 type cables, A_r is equal to 1.43 cm^2 (0.222 in^2). By substituting into equation (2-13), the required number of restrainers was calculated to be six.

5. The deformation of the restrained system was determined from the following equation:

$$D_t = ARS(W)/K_t \tag{2-14}$$

where:
D_t = deformation of the restrained system
K_t = total restrained system stiffness = K_u+K_{RS}
K_{RS}= 'equivalent' restrainer stiffness = $F_y(N_r)A_r/D_r$

Because the deformation of the restrained system was greater than the maximum permissible restrainer deformation, the adjustment procedure had to be used. This adjustment was accomplished by increasing the number of restrainers. Since all the initial assumptions were still valid, only step 5 had to be repeated in order to assure that D_r was not less than D_t with the new restrainer configuration. After several iterations it was found that 20 2.0-m long cables (2 units of 10 cables each) were required for the two segments of the actual bridge. This number was multiplied by the scale factor of 1/4 to obtain the number of restrainers that had to be used in the test specimen, because it was the restrainer stiffness that was being scaled.

2.4 Material Properties

The specified and measured properties of concrete and steel are described in the following sections. Since specified and measured material properties do not usually coincide, the evaluation of the differences can facilitate a better understanding of the specimen behavior.
The concrete for the two concrete blocks was specified to have a compressive strength of 5000 psi (34.5 MPa), with a maximum aggregate size of 3/8 in (9.5 mm). In order to facilitate the necessary formwork, the construction joint was decided to be between the bottom slab and the

diaphragm. Therefore, the specimen construction process was completed in two phases. Nine 152 mm x 304 mm (6 in x 12 in) cylinders were taken during the first phase, while six more were taken while pouring the diaphragm and the top slabs. The specimens were capped with sulfur in accordance with American Society for Testing and Materials (ASTM) C617-87 (ASTM, 1987). The tests were performed at the University of Nevada, Reno using a Riley screw type testing machine in accordance with ASTM C39-86 (ASTM, 1986). All 15 cores failed in an explosive manner with a conical failure surface. Tables 2-7 and 2-8 summarize the test results.

TABLE 2-7 Measured Concrete Compressive Strength-Bottom Slabs

(a) 7 Days (08/20/1999)

Sample No.	f'_c (MPa)
1	26.42
2	30.04
3	27.16
Average	27.87

(b) 14 Days (08/27/1999)

Sample No.	f'_c (MPa)
1	27.59
2	26.60
3	29.12
Average	27.77

(c) 28 Days (09/10/1999)

Sample No.	f'_c (MPa)
1	27.28
2	30.47
3	29.12
Average	28.96

TABLE 2-8 Measured Concrete Compressive Strength-Diaphragm & Top Slabs

(a) 7 Days (09/07/1999)

Sample No.	f'_c (MPa)
1	29.61
2	29.37
3	28.08
Average	29.02

(b) 28 Days (09/27/1999)

Sample No.	f'_c (MPa)
1	31.95
2	31.76
3	30.66
Average	31.46

Grade 60 reinforcement was specified to be used in the specimen. The material properties of the steel were in compliance with CALTRANS specifications (CALTRANS, 1993). Since the reinforcement was not expected to yield during the test, verification of the specified steel properties was not considered to be necessary.

2.5 Computer Software

In order to predict the dynamic behavior of the test specimen on the shake table, an analytical finite element model was formulated and analyzed using the personal computer software DRAIN 3DX (Prakash et al., 1993). DRAIN is a non-linear finite element structural analysis program. It features elements such as an inelastic truss element, an elastic beam column element, two different fiber beam column elements, inelastic connections, a friction bearing element and an inelastic compression/tension link element.

DRAIN can be used to perform many types of analyses with many different types of loading. The program is able to calculate mode shapes and perform both spectral and response history analysis. Furthermore, loads can be specified in several different manners. For instance, dynamic loads can be ground acceleration or displacement records, nodal force records, nodal initial velocity patterns or response spectra. For the purpose of this study, ground acceleration records were used for loading of the model and response history analysis was performed. In order to obtain solutions for consecutive time steps that converged, the selected time step was 0.0005 sec.

DRAIN uses Rayleigh damping method to formulate the damping matrix (Clough and Penzien, 1993). According to this method, damping is proportional to a combination of the mass and the stiffness matrices:

$$\mathbf{c} = \alpha_o \mathbf{m} + \alpha_1 \mathbf{k} \tag{2-15}$$

where:
$\mathbf{c}$ = damping matrix
$\mathbf{m}$ = mass matrix
$\mathbf{k}$ = stiffness matrix
α_o = mass proportional damping factor
α_1 = stiffness proportional damping factor

Assuming a constant damping ratio, the proportionality factors are given by the following equation:

$$\begin{Bmatrix} \alpha_o \\ \alpha_1 \end{Bmatrix} = \frac{2\zeta}{\omega_1 + \omega_2} \begin{Bmatrix} \omega_1 \omega_2 \\ 1 \end{Bmatrix} \tag{2-16}$$

where:
ω_1 = fundamental circular frequency of the structure
ω_2 = circular frequency of the structure with the second greatest contribution to the dynamic response
ζ = damping ratio

Since damping is based on initial stiffness, the application of constant stiffness proportional damping factors implies that very stiff elements will have very high viscous damping forces even after yielding. In bearing elements, high damping forces could have a great impact on the model response and may not represent real behavior. However, constant stiffness proportional damping was used in this study for bearing elements too because they are supposed to simulate the actual bridge piers and not real bearing pads.

2.6 Analytical Model

The analytical model that was formulated in this study is shown in figure 2-6. Three element types were used. The first was the compression/tension link element. This element is an inelastic bar element that resists axial force only. The main advantage of this element is that it can be specified to act either in tension only or in compression only. As a tension element, it has finite stiffness in tension and becomes slack in compression, while as a compression element, it has finite stiffness in compression and gap opens in tension. Thus, it enables researchers to model bridge elements that act either in tension or in compression exclusively, such as cable restrainers and expansion joints. Furthermore, it can be prestrained to a specific negative deformation giving the analyst the opportunity to account for the initial restrainer slack or expansion joint gap. The force deformation behavior of the element is depicted in figure 2-7. It should be noted that, if stiffness proportional damping is specified, a linear viscous damping element is added in parallel

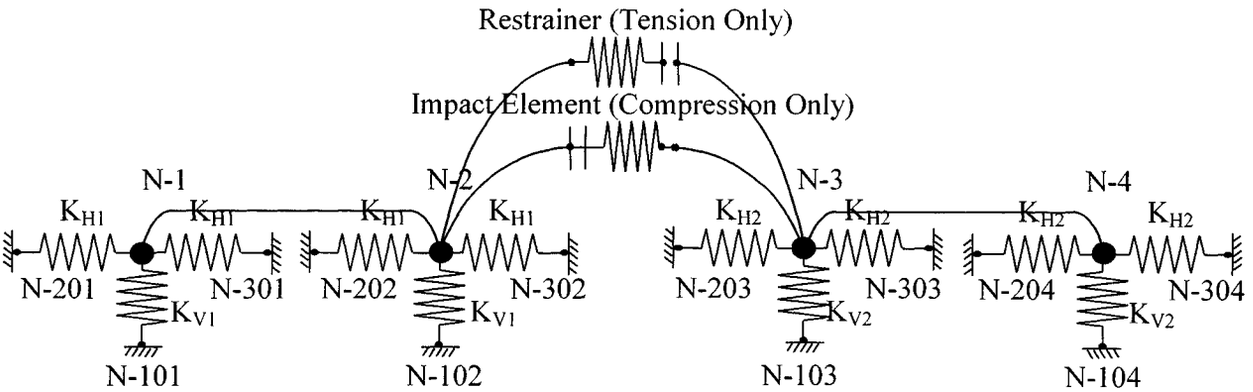

FIGURE 2-6 Analytical Model

with the basic element. However, if the element acts in tension and has initial slack or acts in compression and has an initial gap, the initial stiffness is zero and, hence, the viscous damping force is zero.

The second element used was the elastic beam-column element. It is a simple linear beam-column element. The required input data for this element includes material and cross sectional properties, stiffness factor sets to account for non-prismatic elements and rigid end zone types. The element was used to connect the two lumped masses simulating the total mass of each concrete block. In order to account for the large rigidity of the block, an unrealistically high modulus of elasticity was input.

The last element that was used in this study was the friction bearing element. This is a simple inelastic element for modeling supports that resist normal force in bearing and lateral force through friction. The element connects two coincident nodes. It consists of a bearing (normal) component and a friction (lateral) component. The force deformation behavior of the two components is shown in figures 2-8 and 2-9, respectively. The stiffnesses of the bearing component can be different in tension and compression. Although the stiffness in tension can be very small, it is not allowed to be exactly zero. Furthermore, when the resultant friction force exceeds the bearing force multiplied by a specified friction coefficient, friction slip occurs. Since it is unlikely that the friction force will be exactly equal to the nominal slip force, a tolerance is introduced mainly for computational purposes in order to avoid unnecessary stiffness change events.

2.7 Preanalysis Results

In order to analyze the analytical model described above, several earthquakes and earthquake records were considered as input. Six records were finally selected:

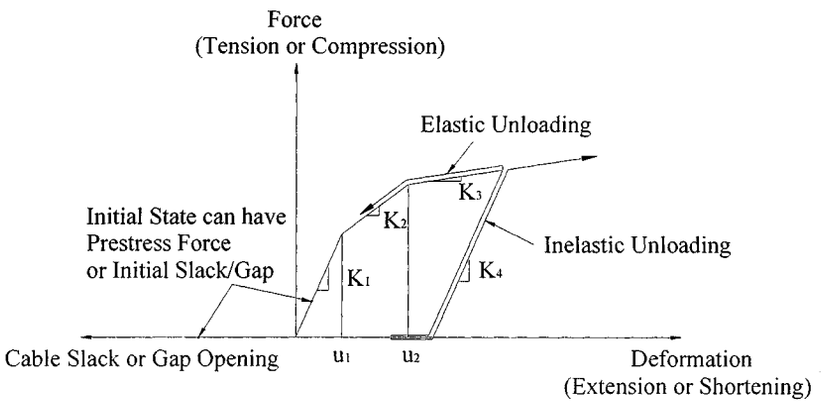

FIGURE 2-7 Compression/Tension Link Element Behavior

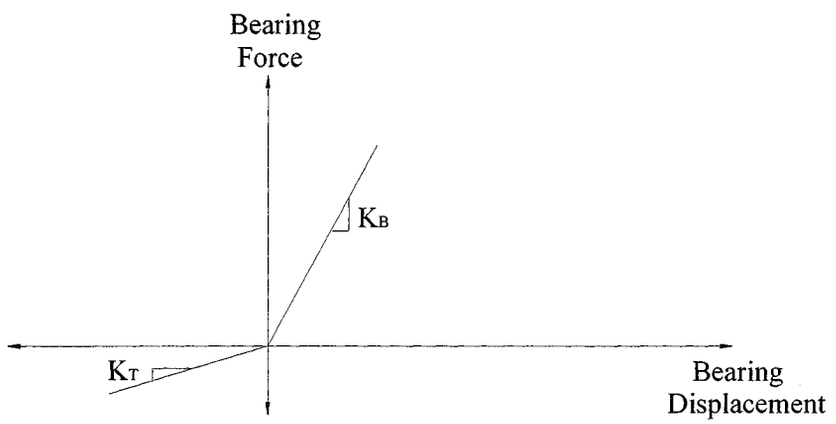

FIGURE 2-8 Friction Bearing Element Behavior (a) Bearing Component

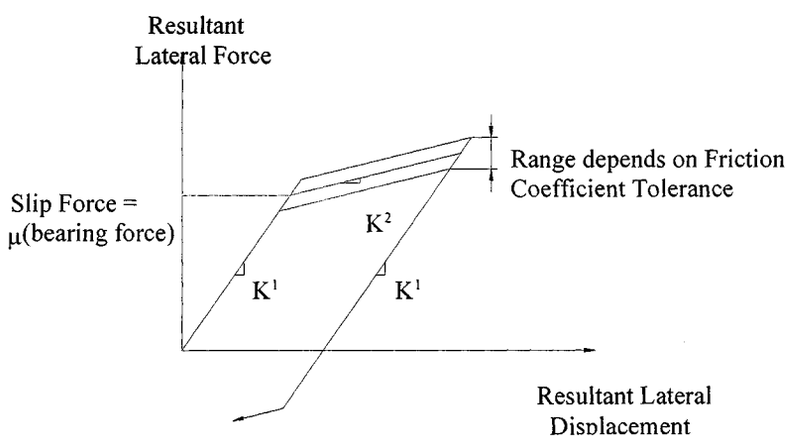

FIGURE 2-9 Friction Bearing Element Behavior (b) Friction Component

1. Imperial Valley Earthquake, El Centro Record, 1940
2. San Fernando Earthquake, Pacoima Dam Record, 1971
3. San Fernando Earthquake, 8244 Orion Blvd Record, 1971
4. Loma Prieta Earthquake, Oakland Outer Harbor Record, 1989
5. Northridge Earthquake, Sylmar County Hospital Parking Lot Record, 1994
6. Northridge Earthquake, Santa Monica City Hall Record, 1994

Earthquakes were chosen based on their amplitude, frequency content and duration characteristics. The peak ground accelerations of these records were 0.348 g, 1.07 g, 0.178 g, 0.27 g, 0.60g and 0.75 g, respectively. The peak ground accelerations were scaled to a wide range between 0.4 g and 0.9 g. Based on review of the acceleration response spectra for these earthquakes, the time axes were not scaled from the accelerograms in order to ensure the out-of-phase motion of the two blocks and, therefore, obtain higher restrainer forces.

Preanalysis results indicated that the 'weak link' in the specimen design was the bearing pads. According to the bearings manufacturers, the maximum displacement on the pads should not exceed 3 in. This limitation was mainly attributed to the special design characteristics of the bearings, including their unusually low stiffness and large height compared to common pads. As a consequence, time history analysis had to be adjusted to this restriction. However, because of the high safety factor applied to the bearings design, it was decided that, if only few cycles of loading resulted in displacement greater than 3 in for the bearings, exceeding this limit would not affect the specimen stability. In this case, the pads would experience some small amount of stiffness degradation without any severe impact on their overall behavior.

Preanalysis also showed that, unlike the actual bridge condition, the resulting restrainer forces were much closer to the yielding force when the lighter concrete block was supported on the stiffer bearings. This was primarily due to the much higher period ratio of the two blocks that caused significant out-of-phase motion and, thus, larger forces in the bridge model elements. Since there are several existing CALTRANS bridges, such as the South Connector of the Interstate 5/State Route 14 Interchange, in which the heavier spans are supported on the more flexible bents, it was decided to switch the masses in the current setup, in order to have a chance of failing the restrainer cables.

It should be mentioned that the purpose of the preliminary analytical model was to provide an initial input about the response of the specimen and facilitate the selection of a worst-case excitation scenario. A detailed comparison between analytical and experimental results was not performed as part of this study and, therefore, no more detail analytical models were developed

SECTION 3
EXPERIMENTAL SETUP AND TEST PROCESS

3.1 Introduction

This section describes the procedure of setting up the test specimen on the shake table, illustrates the instrumentation of the specimen and presents the test series performed in order to evaluate the seismic behavior of the hinge restrainers. As several previous analytical studies have indicated, the most important parameters in bridge restrainer design for seismic retrofit are the restrainer cross sectional area and the initial restrainer slack (Saiidi et al., 1992, Saiidi et al., 1993, Trochalakis et al., 1995). The objective of this study was to investigate experimentally the effects of these parameters on the dynamic response of the hinge-restrainer system. Therefore, different number of restrainer cables and gap lengths were attempted and a series of tests were conducted under incrementally increasing earthquake motion.

3.2 Experimental Setup

A system of steel plates and threaded rods were utilized to tie down the elastomeric bearing pads to the shake table deck. The dimensions and the hole pattern of the plates were based on the existing pattern on the shake table surface and the number of tie downs needed to prevent plate uplift during the test. The top plates, which were bolted to the top mounting plates of the bearing pads, were then bonded to the bottom concrete surface of the two box girder segments using a multi-purpose construction epoxy. Furthermore, dowels were bolted to the top mounting plate of each of the bearing pads and, subsequently, passing through the top steel plates, anchored to the specimen. The dowels were mainly utilized to increase the bonding capacity of the connection and prevent the possible slippage due to shear failure of the epoxy at the interface between concrete and steel during the shake table test. Complete details on the dimensions of the steel plates used to connect the bearing pads to the shake table and the concrete blocks are given in Appendix A.

After the two concrete blocks representing the adjacent bridge spans had been tied down to the shake table deck, the restrainer unit installation procedure commenced (Appendix A). As noted before, the scaled number of restrainers required based on the scale factor of 1/4 was five. In C-1 type restrainers, cables connecting the two bridge segments under consideration are fixed at the bearing plate mounted on one side of the diaphragm, are looped around two 90° bends on the drum attached to the other edge of the hinge, and are anchored to the second bearing plate of the original side (figure 3-1). Therefore, even if design requires an odd number of cables, an even number of cables is used in the field. Hence, although the CALTRANS restrainer design method resulted in five cables for the scaled bridge model, six cables were used in this study.

The final step in setting up the test was the placement of the lead bricks providing the supplementary mass. Two alternatives were considered for the placement of the weights: the first was to set them in weight baskets on the top of the blocks, and the second was to place the lead inside the box girder. Based on stability considerations it was decided to use the second alternative. The types and number of the lead bricks used in this study are thoroughly discussed in Appendix A.

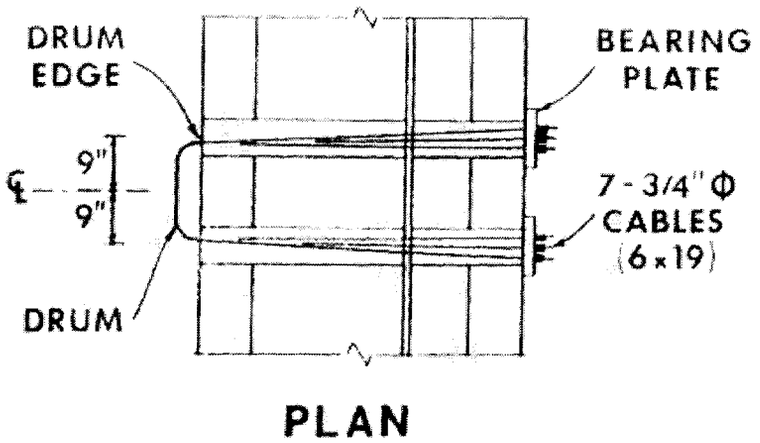

FIGURE 3-1 C-1 Type Cable Restrainer (CALTRANS, 1989)

3.3 Data Acquisition Equipment

A Megadac 3415 DC control unit (OPTIM Corporation, 1993) was used to collect the experimental data. This system has a variety of features for accurately capturing dynamic analog and digital data from a wide range of active and passive sensors. The system has a capacity of up to 512 channels of input and a maximum sampling rate of 25,000 samples per second. Analog output was available for on-line control of any selected input parameter. The instruments used to monitor the behavior of the specimen during the test were connected to screw terminal blocks, which consisted of an AD 885D analog input module. The AD 885D module was used to set addressing, resolution and range of the connected instrumentation by setting the hardware jumpers. The currently used module configuration had the capacity of supporting 15 constant voltage instruments, such as displacement transducers and accelerometers. All the collected data were temporarily stored in a mass storage device and then passed to a host computer.

3.4 Instrumentation

The relative displacements at the joint between the two segments of the specimen were measured by three direct current displacement transducers (DCDTs). The analytical model predicted that the maximum relative hinge displacement of the unrestrained system was not to exceed 15 cm (5.9 in), while this displacement was further decreased to 3 cm (1.2 in) for the restrained system case. The transducers used were Novotechniks LWG-225 with a stroke of ± 22.5 cm (8.9 in). The Novotechniks were placed one on each side and one on the top of the hinge region of the specimen spanning the expansion joint gap between the two blocks (figure 3-2). They were mounted on 5-mm-diameter threaded rods cast integrally to the specimen.

Four Temposonic LA-Series 36-in (91.4 cm) stroke DCDTs were used to measure the absolute displacements of the two concrete blocks. These transducers were attached off the shake table, three on plywood boards and one on a vertical I-shape steel column attached to the lab wall. Previous tests have concluded that the wall vibration during shake table operation is insignificant and, therefore, the wall can be considered as a fixed reference. Each Temposonic was connected to the specimen through wire, which was looped around a pulley and attached to a small

aluminum bracket anchored to the corresponding web of the box girder segment (figure 3-2). To obtain each block displacement relative to the shake table, the shake table displacement, given by an internal shake table displacement transducer, must be subtracted from the block absolute displacement, measured by the Temposonics. Furthermore, by using the Temposonics measurements the relative hinge displacement can be calculated, which allows to verify the readings of the Novotechniks.

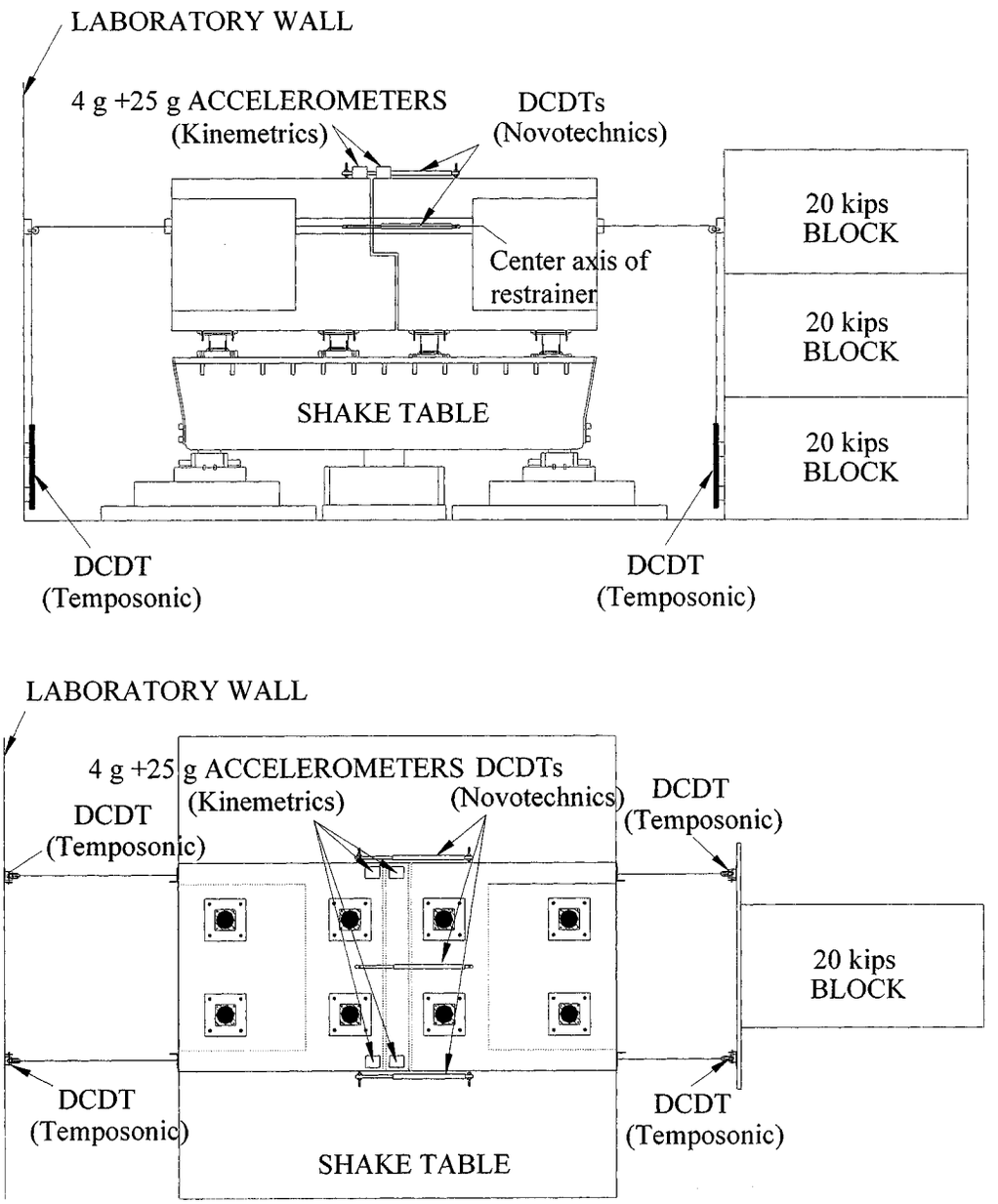

FIGURE 3-2 Instrumentation (a) Elevation, (b) Plan

The acceleration levels at the top of the blocks were measured by eight accelerometers. Four of them were Kinemetrics FBA-11 with a measurement range of ± 4 g, while the other four could sense up to ± 25 g and they were used to capture the high instantaneous acceleration levels occurring during the impact between the two blocks. The accelerometers were placed on the upper surface of the two concrete segments. They were located on the corners of the edges close to the expansion joint gap between the two blocks as shown in figure 3-2. These instruments pass through a Kinemetrics Signal Conditioning Strongmotion Accelerograph Model SMA-3 conditioner.

All incoming signals were processed by the Pacific Instruments 5530 signal conditioning cards. All channels were sampled at 250 Hz. The Pacific Instruments data acquisition software digitally high pass filtered the data at a 20 Hz corner.

3.5 Selection of Earthquake Records

Several earthquake motions were considered as possible input records for preanalysis purposes. These included the 1940 Imperial Valley Earthquake (El Centro), the 1971 San Fernando Earthquake (Pacoima Dam and 8244 Orion Blvd.), the 1989 Loma Prieta Earthquake (Oakland Outer Harbor), and the 1994 Northridge Earthquake (Sylmar County Hospital Parking Lot and Santa Monica City Hall). Based on the results of the initial analysis, it was decided that the Loma Prieta Earthquake Record was the most appropriate for this experimental study. Since this study is a nondestructive test, the excitation selection was mainly based on frequency content rather than acceleration amplitude criteria. As shown in figure 3-3, the Oakland Outer Harbor Record is characterized by a wide frequency content with two distinctive predominant periods. Thus, it was considered capable of generating out-of-phase motion of the two concrete blocks and, therefore, producing higher impact and restrainer forces. The peak ground acceleration (PGA) of the record is 0.27 g (104.3 in/s^2), which corresponds to a moderate earthquake. Preanalysis performed using DRAIN 3DX indicated that the selected motion could be amplified by 1.5 without exceeding significantly the displacement capacity of the bearing pads. The duration of the original ground motion is 40 s. As dictated by modeling rules, this length should be scaled by $\sqrt{l_r}$. The scale factor of 1/4 resulted in a time scaling of 0.50. However, in order to avoid compression of the frequency content, which would significantly reduce the intensity of the impact between the two segments as well as the chances of failing the restrainer cables, it was decided to use the original earthquake motion instead of compressing the time axis by 0.50. From this point of view, the used earthquake subject the specimen to a worst-case scenario, but does not produce the response of the hinge under a realistic historical earthquake motion.

3.6 Test Process
3.6.1 General

The tests presented in this study were conducted at the Large Scale Structures Laboratory at the University of Nevada, Reno (UNR). The tests were completed in three days. Several different configurations of the restrained system were tested on each day by varying the number of restrainer cables and the initial restrainer gap. The values for the restrainer gap, which were used in this study, are representative of restrainer gap values used in the illustrative examples of the CALTRANS design manual (CALTRANS, 1989).

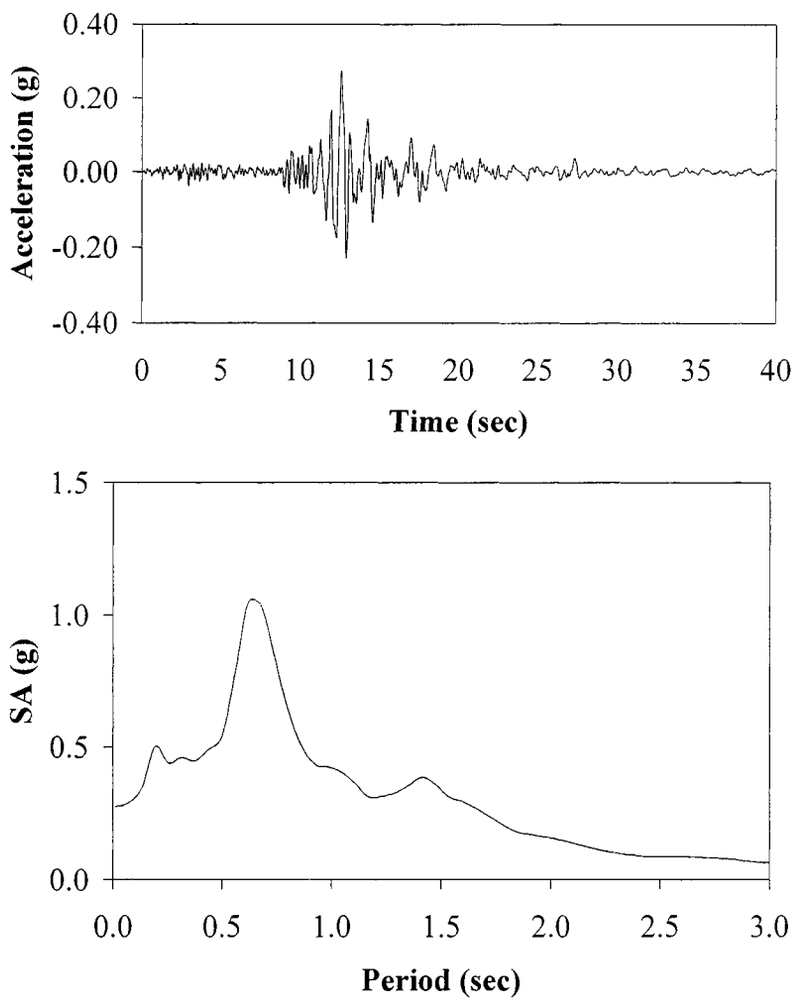

FIGURE 3-3 Loma Prieta Earthquake – Oakland Outer Harbor Record (PGA = 0.27 g) and Acceleration Response Spectrum

Since the primary objective of this experimental study was to examine the impact between adjacent bridge spans at in-span hinges and evaluate the performance of the seismic restrainers under normal operating and failure conditions, several levels of excitation were used. The test specimen was subjected to gradually increasing shake table acceleration, corresponding to different fractions of the chosen Loma Prieta Earthquake Record (table 3-1). It should be noted that only the acceleration amplitudes were changed for the input motions by multiplying the acceleration values by a corresponding scalar, while the record duration was kept at 40 s.

3.6.2 Preliminary Test

Initial shake table tuning was done at very low levels of random motion in order to allow the 469D shake table software to counterbalance the mass of the specimen and the shake table own response. This process lasted approximately 30 min. The acceleration levels generated by the shake table during tuning corresponded to 30 percent of 0.1 g Root Mean Square (RMS) random acceleration from 1 Hz to 30 Hz.

Based on the free vibration response of the specimen, damping values were estimated. The estimated damping did not exceed 3% of critical. This low value is due to the fact that the actual boundary conditions, which include the effects of the response of the rest of the structure at the ends of the tested configuration, were not included. The two blocks were free to vibrate at their ends and were just supported on elastomeric bearings pads, simulating the equivalent elastic stiffness of the substructure. Therefore, the test specimen cannot capture the actual structural damping of the whole bridge, which could result in a much higher damping value.

TABLE 3-1 Test Schedule

Test Day 1 (Preliminary Test)

Series I	No. of Cables	Restrainer Gap	Earthquake Record
I1	6	25 mm (~1 in)	0.15*Loma Prieta (PGA=0.04g)
I2	6	25 mm (~1 in)	0.19*Loma Prieta (PGA=0.05g)
I3	6	25 mm (~1 in)	0.25*Loma Prieta (PGA=0.07g)
I4	6	25 mm (~1 in)	0.37*Loma Prieta (PGA=0.10g)

Test Day 2

Series II	No. of Cables	Restrainer Gap	Earthquake Record
II1	6	25 mm (~1 in)	0.50*Loma Prieta (PGA=0.14g)
II2	6	25 mm (~1 in)	0.75*Loma Prieta (PGA=0.20g)
II3	6	25 mm (~1 in)	1.00*Loma Prieta (PGA=0.27g)
II4	6	25 mm (~1 in)	1.25*Loma Prieta (PGA=0.34g)
II5	6	25 mm (~1 in)	1.50*Loma Prieta (PGA=0.41g)

Series III	No. of Cables	Restrainer Gap	Earthquake Record
III1	6	13 mm (~0.5 in)	0.50*Loma Prieta (PGA=0.14g)
III2	6	13 mm (~0.5 in)	0.75*Loma Prieta (PGA=0.20g)
III3	6	13 mm (~0.5 in)	1.00*Loma Prieta (PGA=0.27g)
III4	6	13 mm (~0.5 in)	1.25*Loma Prieta (PGA=0.34g)
III5	6	13 mm (~0.5 in)	1.50*Loma Prieta (PGA=0.41g)

Test Day 3

Series IV	No. of Cables	Restrainer Gap	Earthquake Record
IV1	6	0 mm (0 in)	0.50*Loma Prieta (PGA=0.14g)
IV2	6	0 mm (0 in)	0.75*Loma Prieta (PGA=0.20g)
IV3	6	0 mm (0 in)	1.00*Loma Prieta (PGA=0.27g)
IV4	6	0 mm (0 in)	1.25*Loma Prieta (PGA=0.34g)
IV5	6	0 mm (0 in)	1.50*Loma Prieta (PGA=0.41g)

TABLE 3-1 Test Schedule (cont'd)

Series V	No. of Cables	Restrainer Gap	Earthquake Record
V1	2	0 mm (0 in)	0.50*Loma Prieta (PGA=0.14g)
V2	2	0 mm (0 in)	0.75*Loma Prieta (PGA=0.20g)
V3	2	0 mm (0 in)	1.00*Loma Prieta (PGA=0.27g)
V4	2	0 mm (0 in)	1.25*Loma Prieta (PGA=0.34g)
V5	2	0 mm (0 in)	1.50*Loma Prieta (PGA=0.41g)

Series VI	No. of Cables	Restrainer Gap	Earthquake Record
VI1	0	-	0.50*Loma Prieta (PGA=0.14g)
VI2	0	-	0.75*Loma Prieta (PGA=0.20g)

After the completion of the initial shake table tuning, the restrainer slack was adjusted to 1 in (25.4 mm) and the specimen was subjected to a low amplitude motion of 0.15×Loma Prieta (0.04 g). This initial motion was mainly used to evaluate the overall specimen behavior under dynamic loads and address necessary modifications. Furthermore, instrumentation and shake table control operation were checked. Preanalysis had determined that a peak ground acceleration of approximately 0.08 g was the threshold beyond which impact between the two blocks would occur. Two motions with peak accelerations of 0.05 g and 0.07 g, corresponding to 0.19×Loma Prieta and 0.25×Loma Prieta, respectively, were used to confirm this prediction.

Indeed, although the relative hinge displacement was visibly higher with increasing input motion, the measurements of both displacement transducers and accelerometers showed that no impact had occurred. As shown in table 3-1, the next motion chosen was 0.37×Loma Prieta (0.10 g), which was the last record used in the preliminary test. Two or three minor impacts were observed during the test. The instruments verified this observation, showing closure of the expansion joint gap between the two blocks and instantaneous increase of the acceleration levels at the time when impact occurred. The measured data will be discussed in the next section.

One of the conclusions drawn based on the preliminary test series was that there was a quite significant difference between the target peak earthquake accelerations and the achieved values. The error, varying from 15 percent to 20 percent for the four selected input motions of Test Series I, was mainly attributed to the influence of the test specimen, including the high structural mass and the flexibility of the bearing pads. Thus, although the UNR shake table has the capability to generate very accurate ground motions relative to the target motion through software incorporated in the system, the achieved signals did not coincide with the target motions. In order to obtain a better correlation between the achieved and target records, it was decided to amplify the target input earthquake motion by a scale factor equal to 1.20 before running each test of the following test series. This will be further discussed in Section 4.

3.6.3 Test Series II and III

Test series II and III were completed in one day. A summary of these tests is presented in table 3-1, which includes the number of restrainer cables used, the restrainer gap and the input earthquake motion.

Test series II was a continuation of the preliminary test described in the preceding section. Five earthquake runs were simulated, varying from 0.50×Loma Prieta to 1.50×Loma Prieta. The acceleration amplitude was increased in the steps shown in table 3-1. It should be noted that there was no apparent damage of the specimen during the first two motions except for minor cracking in the vicinity of the expansion joint gap, although several major collisions between the two blocks occurred. Under the 1.00×Loma Prieta motion, concrete spalling occurred at the bottom of the ledge diaphragm on the north side. The 1.25×Loma Prieta motion produced some additional spalling due to the increased intensity of the impact. Furthermore, more cracks were visible on both sides of the hinge, indicating vertical bending of the diaphragm between the top and bottom slabs. Although the spalled region increased after the 1.50×Loma Prieta motion, the damage was limited to the concrete cover and no reinforcement bars were exposed (figure 3-4).

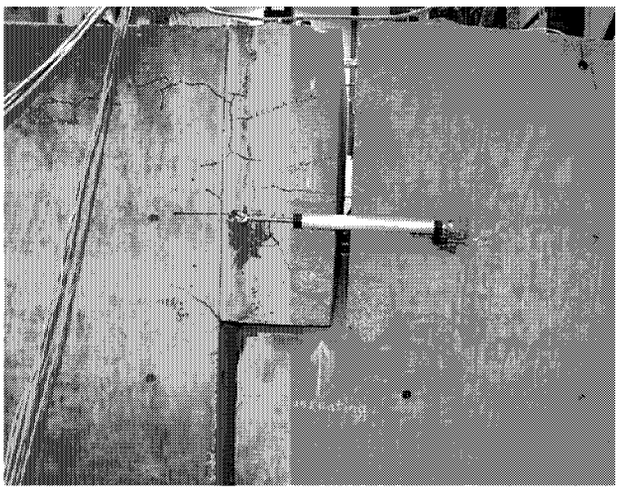

FIGURE 3-4 Damage under run II5 (see table 3-1)

After test series II was completed, the restrainer gap was reduced to 0.5 in (12.7 mm) by tightening the cables from the adjustment end simultaneously a distance equal to 0.5 in (12.7 mm). Similarly to the previous series, the specimen was subjected to five motions with the acceleration amplitude increasing from 0.14 g (0.50×Loma Prieta) to 0.41 g (1.50×Loma Prieta). The reduction of the restrainer slack did not have any apparent effect on the overall specimen behavior. However, due to the smaller gap, the restrainers were engaged sooner and, therefore, the intensity of the impact between the two blocks was slightly reduced. In addition, even though the width of the existing cracks was increased and new cracks were formed, no other significant damage occurred.

3.6.4 Test Series IV, V and VI

In the last three test series the variable was the number of restrainer cables. Restrainers were gradually reduced from six to zero, corresponding to an unrestrained system case. As shown in table 3-1, the same loading pattern that had been used for the previous two series, was also adopted for series IV and V. When no restrainers were utilized, it was anticipated that the collision between the two concrete blocks could cause the bearing pads to undergo excessive displacements, which could result in significant damage of the specimen. Hence, it was decided that the applied acceleration amplitude should not exceed 0.20 g, and, therefore, the specimen was loaded with only two motions, corresponding to 0.50×Loma Prieta and 0.75xLoma Prieta, respectively.

Before starting test series IV, the restrainer gap was further reduced to 0 in (0 mm). This case, which in practice represents condition under very low ambient temperature, was shown to be the most critical in assessing restrainer stresses by most of the previous analytical studies investigating the seismic performance of bridge restrainers (Saiidi et al., 1992, Saiidi et al., 1993). The restrainer gap reduction was accomplished by tightening the cables an additional 0.5 in (12.7 mm). The lack of any restrainer slack was also indicated by the corresponding closure of

the gap between the disc springs installed on the adjustment end of the cables. Since the restrainer gap was set to zero, the immediate engagement of the restrainers reduced even further the intensity of the impacts. No additional major damage was observed.

As soon as test series IV was completed, four of the restrainer cables were removed, thus reducing the number of cables to zero, and the whole series was repeated. The same general trends described in the previous tests were noticed. It should be mentioned at this point, that in all the tests in-plane rotations of the blocks were recorded. In practice, these rotations occur primarily in the case of skew bridges (Bjornsson et al., 1997). However, due to construction imperfections, in-plane rotations occurred in this test, although there was no skewness. The main difference between test series IV and V was that the in-plane rotations of the two blocks were more prominent during test series V, especially under high amplitude motions. This was mainly attributed to the fact that the reduction of restrainers had 'weakened' the longitudinal linkage between the two blocks and, therefore, the contribution of the torsional mode to the dominant translational mode was now greater.

The last two tests, which were performed without restrainers, demonstrated clearly the effectiveness of seismic restrainers in reducing the relative longitudinal displacements across in-span hinges and preventing span unseating. As anticipated, even though the specimen was subjected to relatively low amplitude motions, the elastomeric bearings experienced significant displacements. Furthermore, the impact between the two blocks was noticeably more intense, resulting in large hinge displacements. It should be noted that, as it will be further discussed in the next section, in both cases the hinge relative displacements exceeded the scaled seat width value of 65 mm (2.6 in). This indicates that in a real bridge span unseating would have occurred.

SECTION 4
EXPERIMENTAL RESULTS

4.1 Introduction

The following sections present the results of the experimental testing and the related analysis of the hinge-restrainer system. The comparison of the achieved and target signals is also thoroughly discussed. The results are mainly categorized based on the parameters that were varied, including the number of cables and the restrainer gap. The acceleration of the two blocks is plotted for all motions and the impacts between the two blocks are shown. Using displacement data, the hinge relative displacement as well as the relative displacement of the two blocks with respect to the shake table are calculated and plotted. The measured peak hinge relative displacement for different motions is compared to the scaled seat width and the possible span unseating is identified. The restrainer forces are computed based on the measured restrainer displacements and the specified cable properties. Finally, several comparative plots are presented in order to evaluate the effects of the parameters on the overall hinge-restrainer system.

4.2 Comparison of the Achieved and Target Signals

As noted in the preceding section, five main test series were performed. In all but the last test series, five earthquake records were used, corresponding to different fractions of the Loma Prieta motion peak ground acceleration (table 3-1).

A satisfactory correlation between the achieved table acceleration histories and the target earthquake motions was accomplished by amplifying each shake table driven file by 1.20. A comparison of the achieved and target signals was made through elastic response spectra (figures 4-1 to 4-6). The spectral acceleration was plotted for a period range of zero to three seconds and a damping ratio of 5 percent, which was considered to be representative of the actual damping levels developed during the tests. All the response spectra had similar shape with two characteristic peaks at 0.9 s and 1.5 s. These two periods are close to the fundamental period of the west and the east block, respectively. This fact confirms that the selected earthquake motion was a good choice for producing strong excitation of the test specimen. Figures 4-1 to 4-3 show the acceleration response spectra for the achieved and target signals of three of the motions used in Test Series II, the 0.50×Loma Prieta, the 1.00×Loma Prieta, and the 1.50×Loma Prieta, respectively. It can be seen that the generated peak table acceleration (PTA) values match perfectly the peak ground acceleration values of the target earthquake motions. Furthermore, the maximum spectral accelerations coincide. Another observation, which can be made based on figures 4-1 to 4-3, is that the correlation between target and achieved signals diverges slightly as the amplitude of the earthquake motion increases. This observation is more apparent for the period range between one and two seconds. However, the achieved signal generally overestimates the target motion by a small percent. The same trends can be also shown in figures 4-4 to 4-6, which depict the acceleration spectra for the three corresponding motions of Test Series IV. It is worth noting that the reliability of the shake table system can be verified by the resemblance of the achieved signals for the two test series.

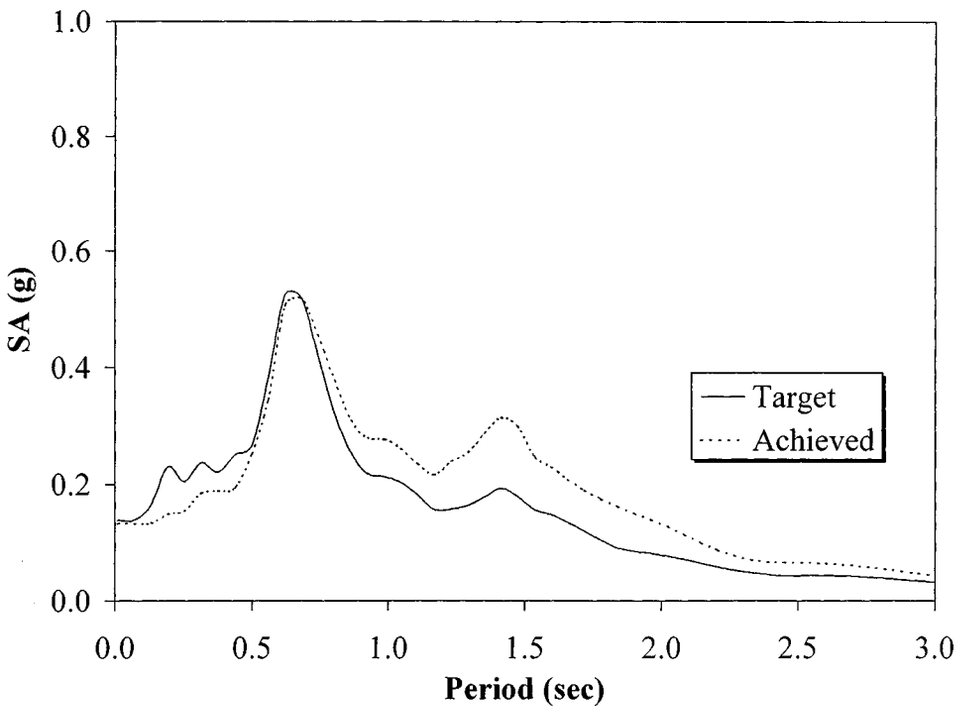

FIGURE 4-1 Target vs. Achieved Table Acceleration Spectrum (6 Restrainer Cables, 25.4 mm Restrainer Gap, 0.50×Loma Prieta, PTA = 0.13 g)

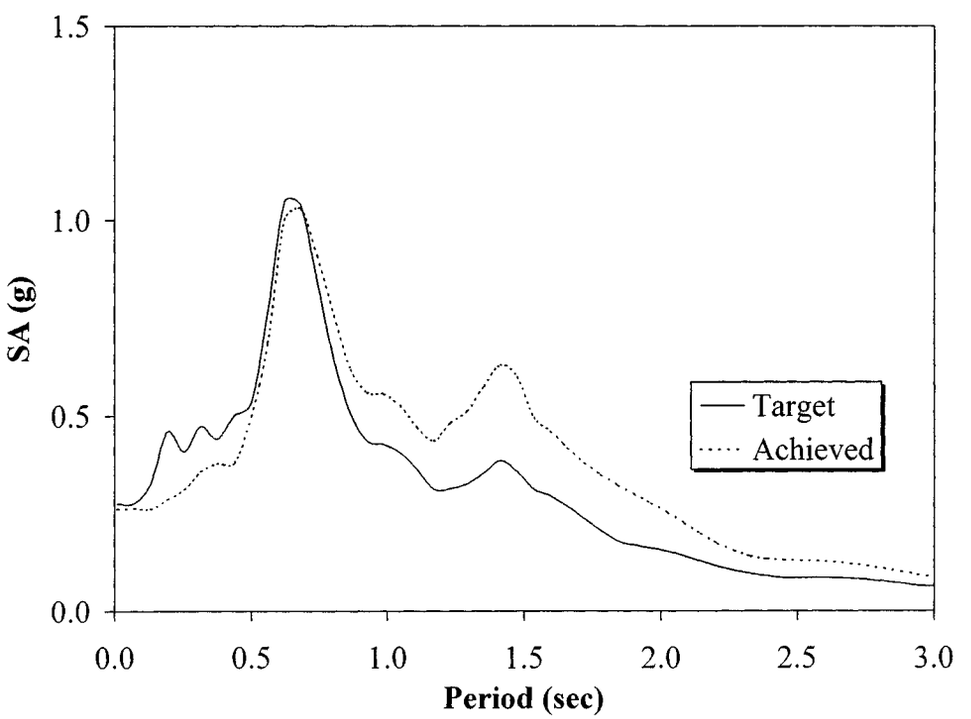

FIGURE 4-2 Target vs. Achieved Table Acceleration Spectrum (6 Restrainer Cables, 25.4 mm Restrainer Gap, 1.00×Loma Prieta, PTA = 0.26 g)

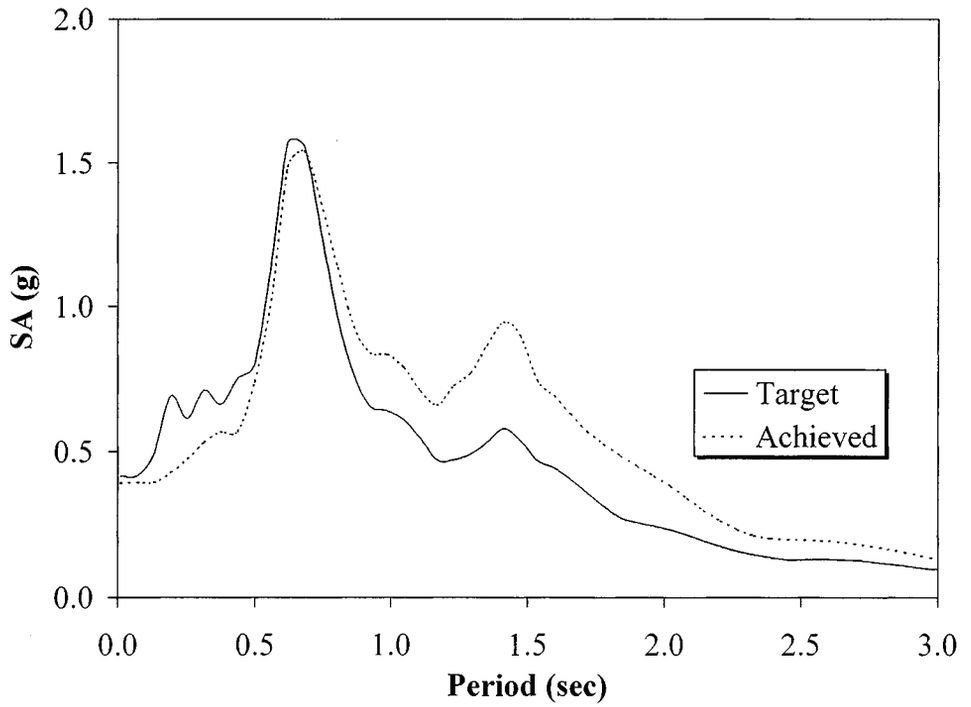

FIGURE 4-3 Target vs. Achieved Table Acceleration Spectrum (6 Restrainer Cables, 25.4 mm Restrainer Gap, 1.50×Loma Prieta, PTA = 0.39 g)

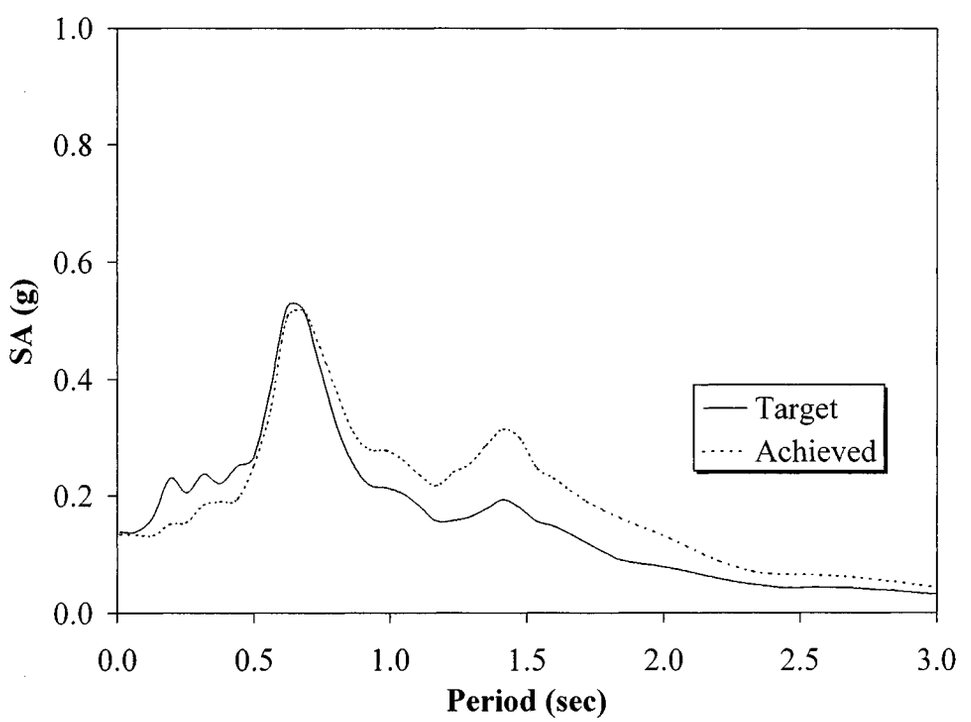

FIGURE 4-4 Target vs. Achieved Table Acceleration Spectrum (6 Restrainer Cables, 0 mm Restrainer Gap, 0.50×Loma Prieta, PTA = 0.13 g)

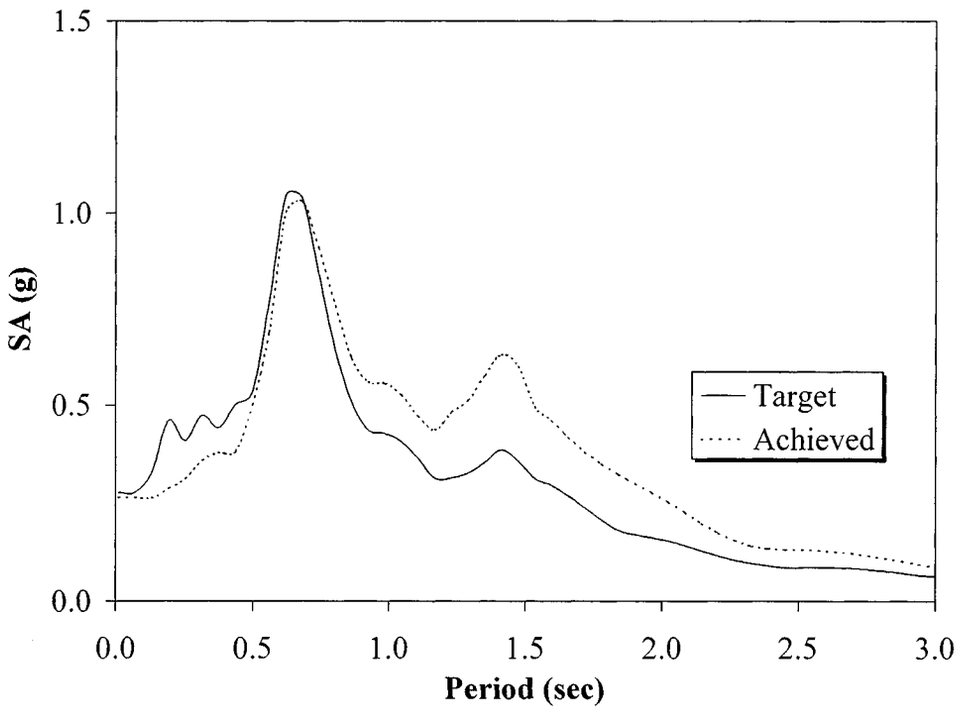

FIGURE 4-5 Target vs. Achieved Table Acceleration Spectrum (6 Restrainer Cables, 0 mm Restrainer Gap, 1.00×Loma Prieta, PTA = 0.26 g)

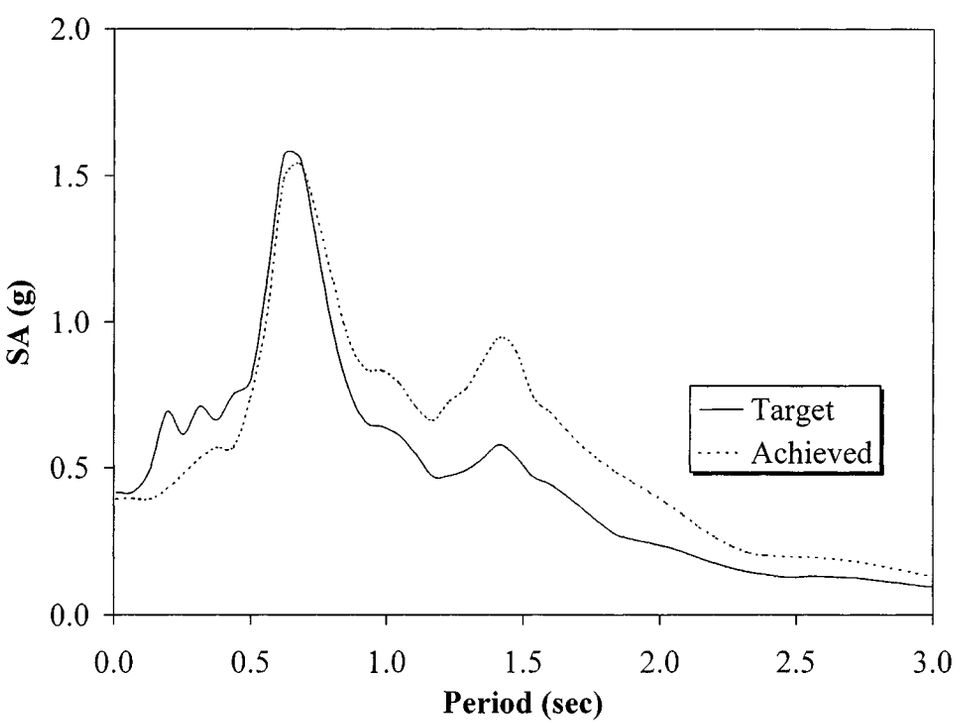

FIGURE 4-6 Target vs. Achieved Table Acceleration Spectrum (6 Restrainer Cables, 0 mm Restrainer Gap, 1.50×Loma Prieta, PTA = 0.39 g)

4.3 Test Series II, III and IV

The number of restrainers in all these series was six. The variable among series II to IV was the restrainer gap.

4.3.1 Absolute Accelerations

Figures 4-7 to 4-24 show the measured absolute acceleration response of the two blocks. For each earthquake motion, two figures are plotted. The first figure shows the acceleration response of the blocks during the 40 s of the excitation, while the second figure depicts the same response during the specified range of interest, when most of the impacts occurred. Acceleration data for each block was measured by eight accelerometers attached to the four corners of the deck slabs adjacent to the expansion joint gap (figure 3-2). Due to in-plane rotations, which occurred after the first impact between the blocks during all the conducted tests, the readings of the two accelerometers on each corner were not identical to the readings of the two antisymmetric accelerometers on the opposite corner of each box girder segment. However, the differences in the measurements were not considered to be significant and, therefore, the average acceleration was calculated and plotted for each block. It should be noted that for the lower acceleration levels the measurements of the accelerometers with ± 4 g measurement range were used to calculate the average acceleration, since they were considered to be more sensitive than the accelerometers that could measure up to ± 25 g. The readings of the accelerometers with the ± 25 g measurement range were mainly used to compute the high accelerations experienced by the two blocks during the impacts.

In all the measured acceleration histories, the occurrence of impact was indicated by an abrupt increase of the acceleration value. In all cases, the majority of impacts occurred within the range 11 s to 17 s. The major impacts had peak accelerations that varied between 0.70 g and 3.50 g. The intensity and the number of collisions increased with increasing earthquake motion. Based on figures 4-7 to 4-24, it can be also deduced that the accelerations experienced by the east block during impact were generally higher than the corresponding accelerations of the west block.

The maximum recorded accelerations for each block are given in table 4-1. It can be concluded that the cases with higher restrainer slack produced slightly higher impact accelerations. As shown in table 4-1, the maximum accelerations ranged from 1.10 g to 3.01 g and from 1.51 g to 3.77 g, for the west and the east block, respectively.

4.3.2 Relative Displacements

The hinge relative displacement response is given in figures 4-25 to 4-33. The maximum recorded hinge displacements are also shown in table 4-2. The hinge relative displacement at each time was calculated as the average of the measurements of the three Novotechnik displacement transducers, which were located one on each side and one on the top of the test specimen spanning the expansion joint gap. The readings of the two side Novotechniks were also confirmed using the data recorded by the four Temposonics measuring the absolute displacements of the two blocks. If $\Delta_{i,1}$ and $\Delta_{i,2}$ are the recorded absolute displacements of the

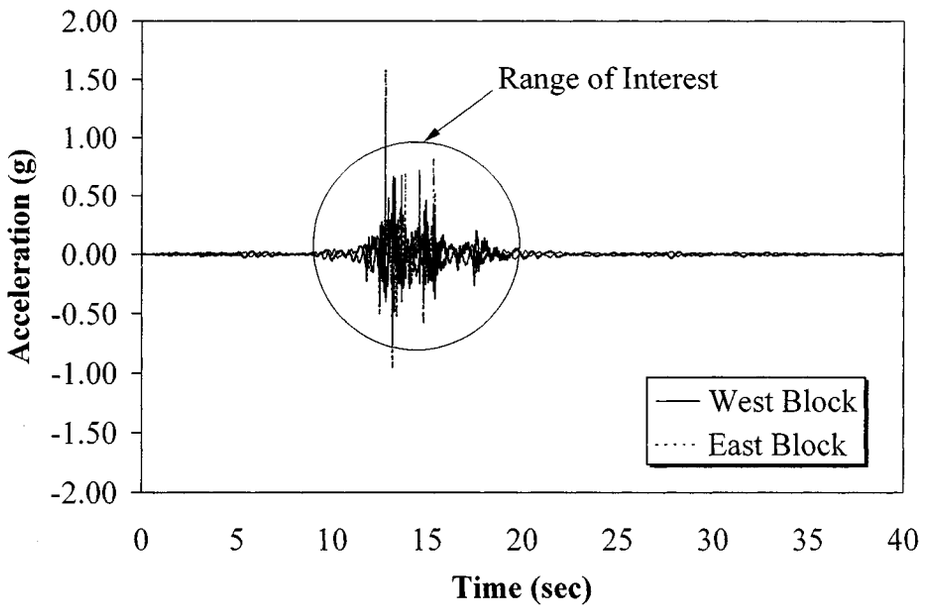

FIGURE 4-7 Block Accelerations History for Run IV1

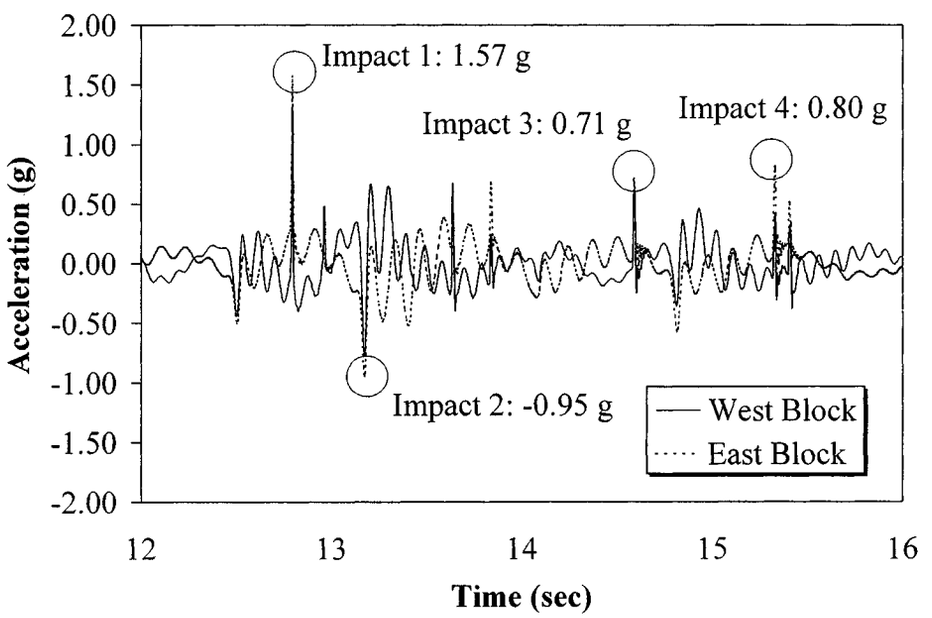

FIGURE 4-8 Block Accelerations History for Run IV1

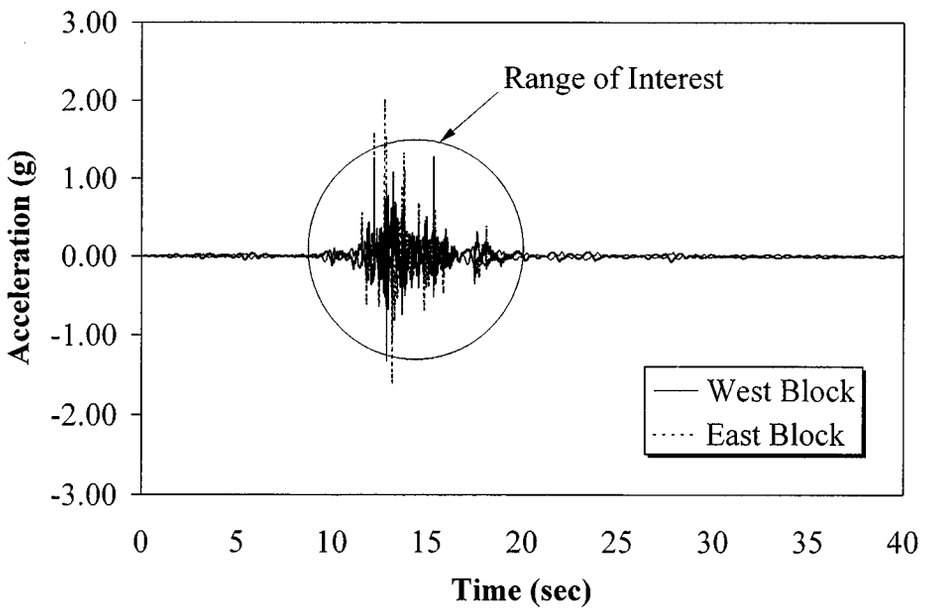

FIGURE 4-9 Block Accelerations History for Run IV3

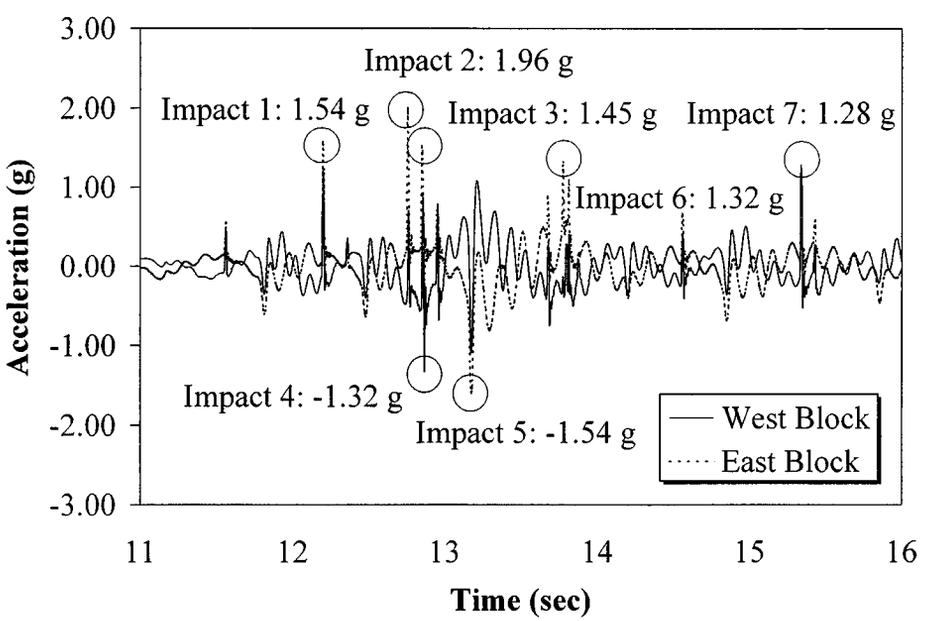

FIGURE 4-10 Block Accelerations History for Run IV3

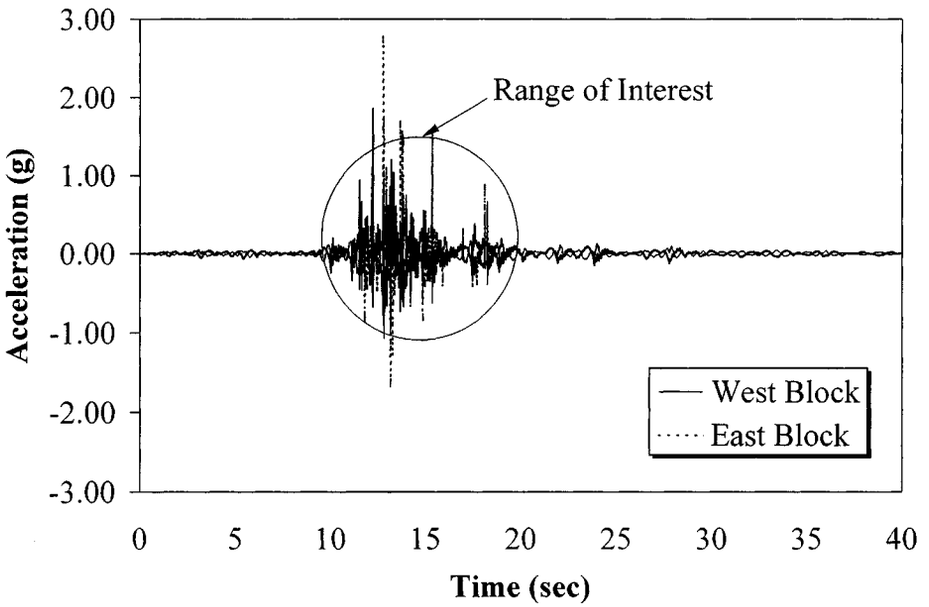

FIGURE 4-11 Block Accelerations History for Run IV5

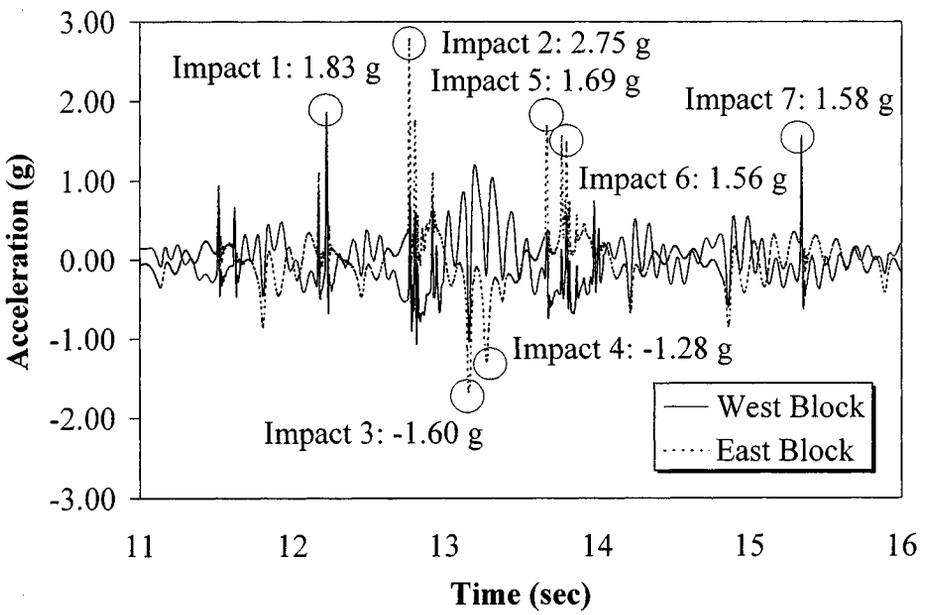

FIGURE 4-12 Block Accelerations History for Run IV5

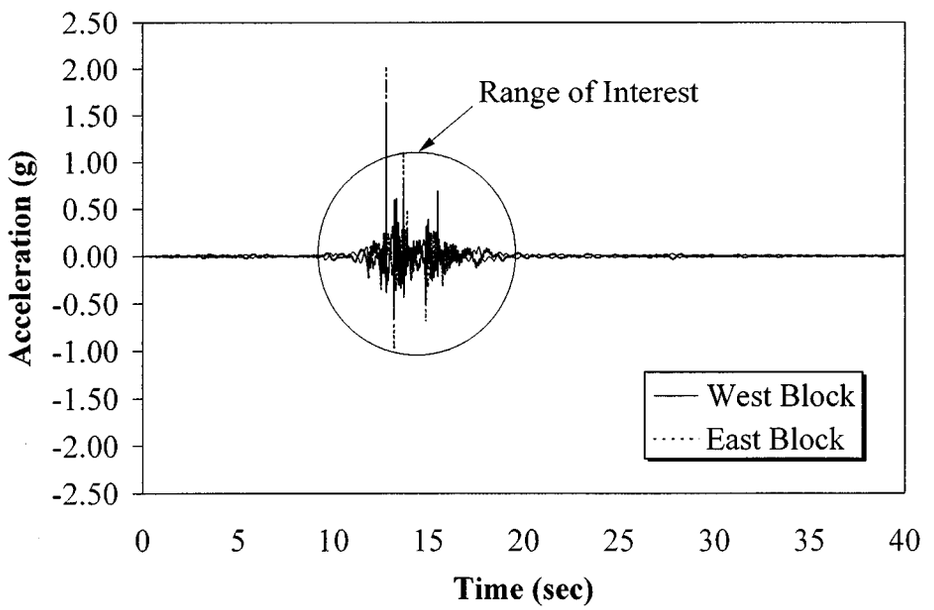

FIGURE 4-13 Block Accelerations History for Run III1

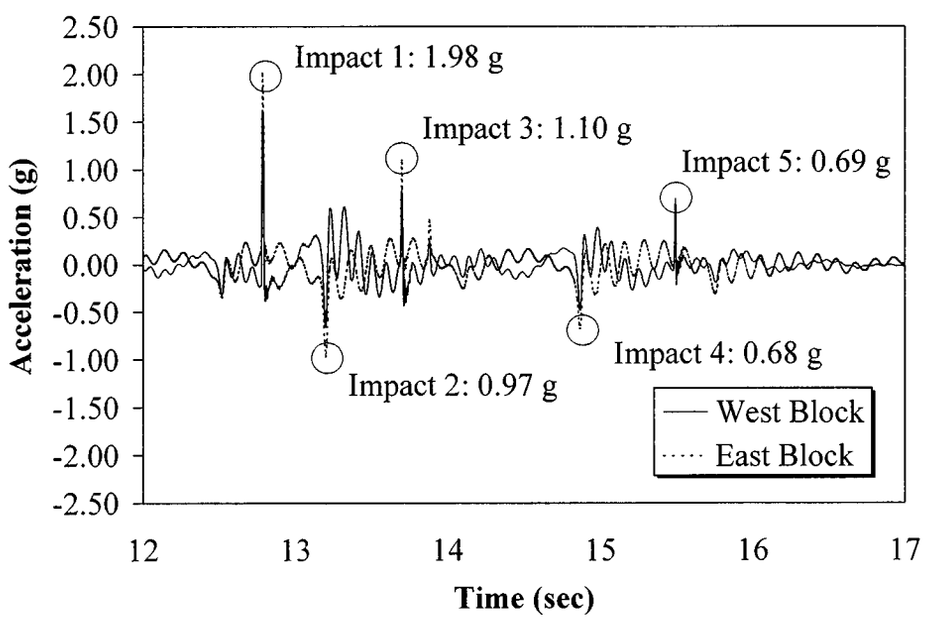

FIGURE 4-14 Block Accelerations History for Run III1

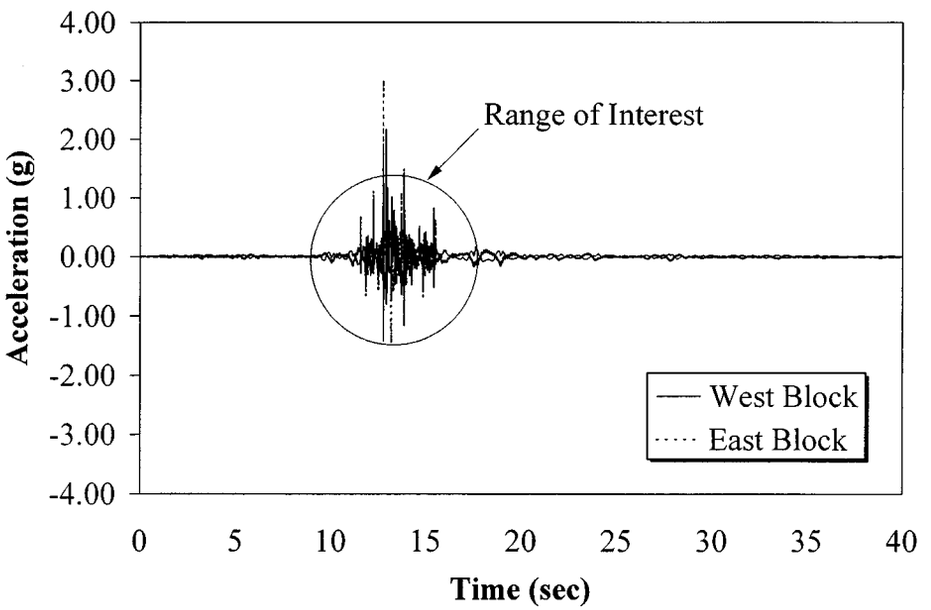

FIGURE 4-15 Block Accelerations History for Run III3

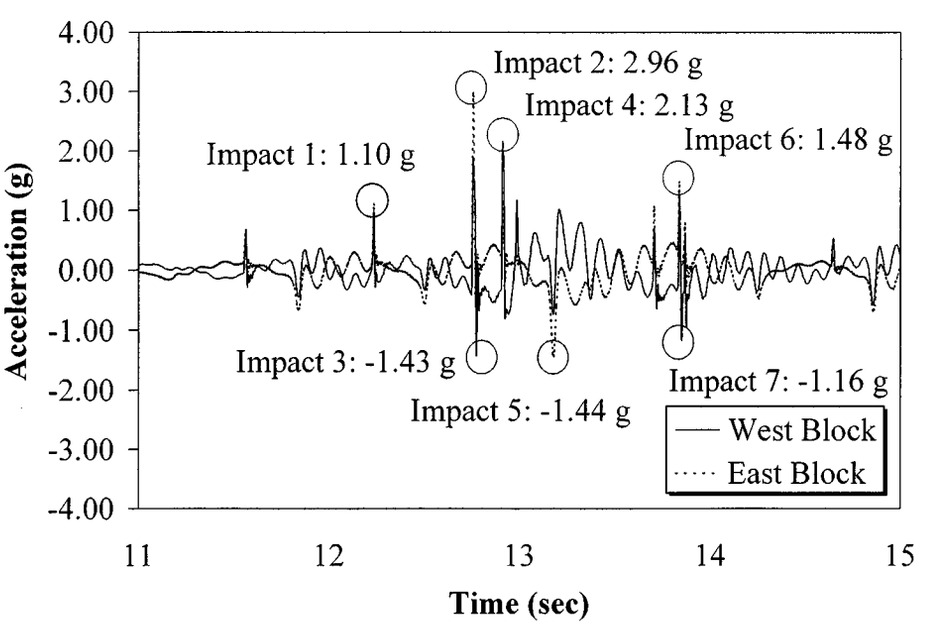

FIGURE 4-16 Block Accelerations History for Run III3

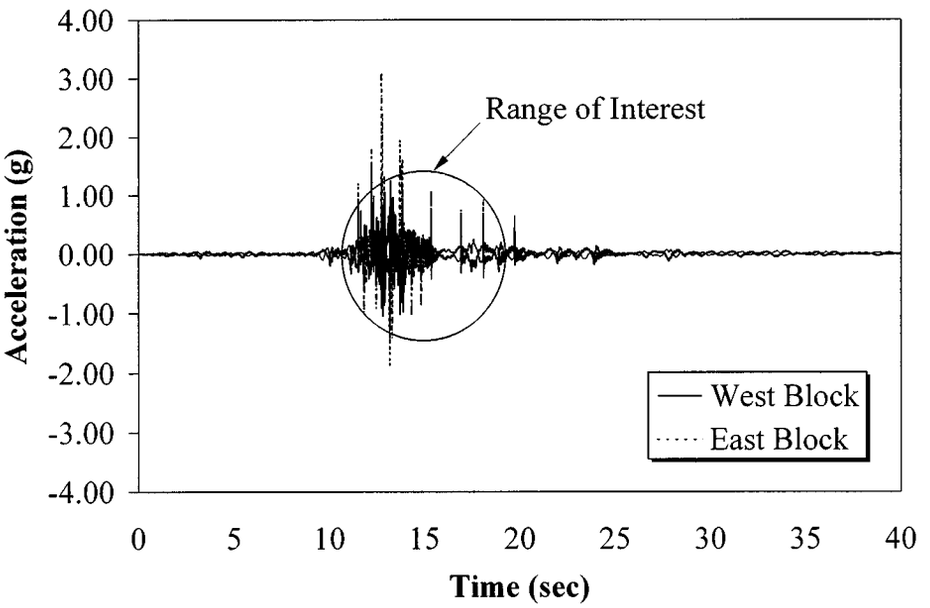

FIGURE 4-17 Block Accelerations History for Run III5

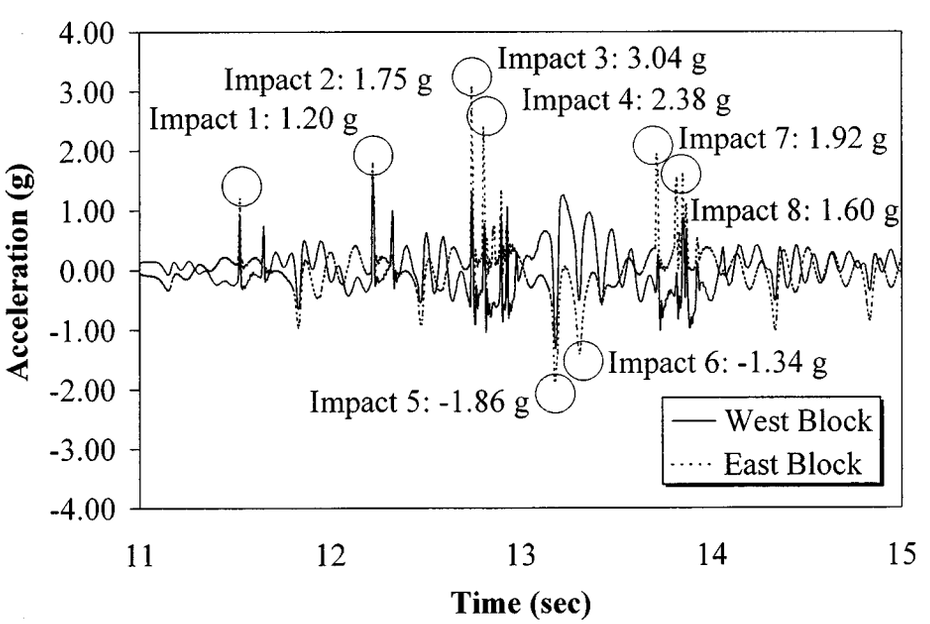

FIGURE 4-18 Block Accelerations History for Run III5

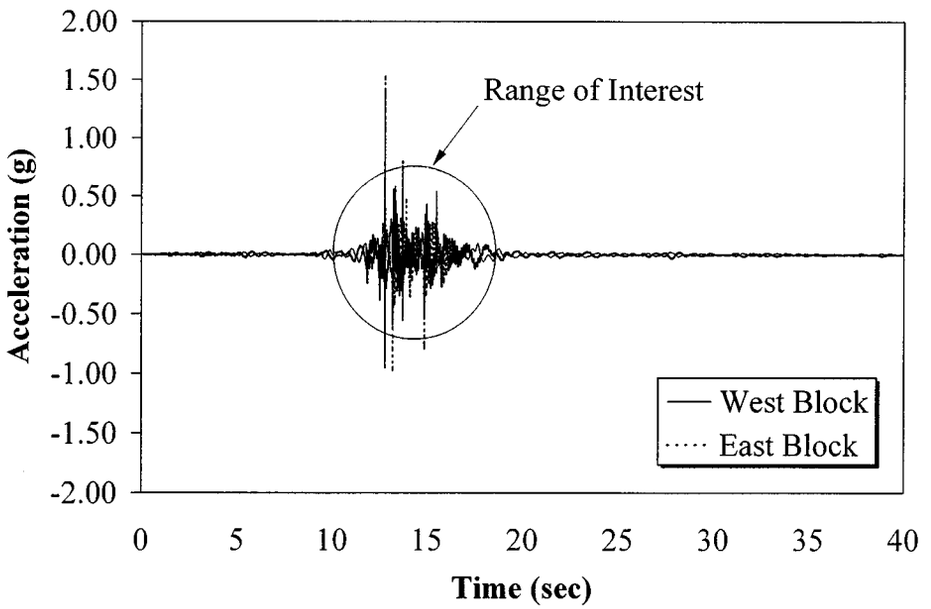

FIGURE 4-19 Block Accelerations History for Run II1

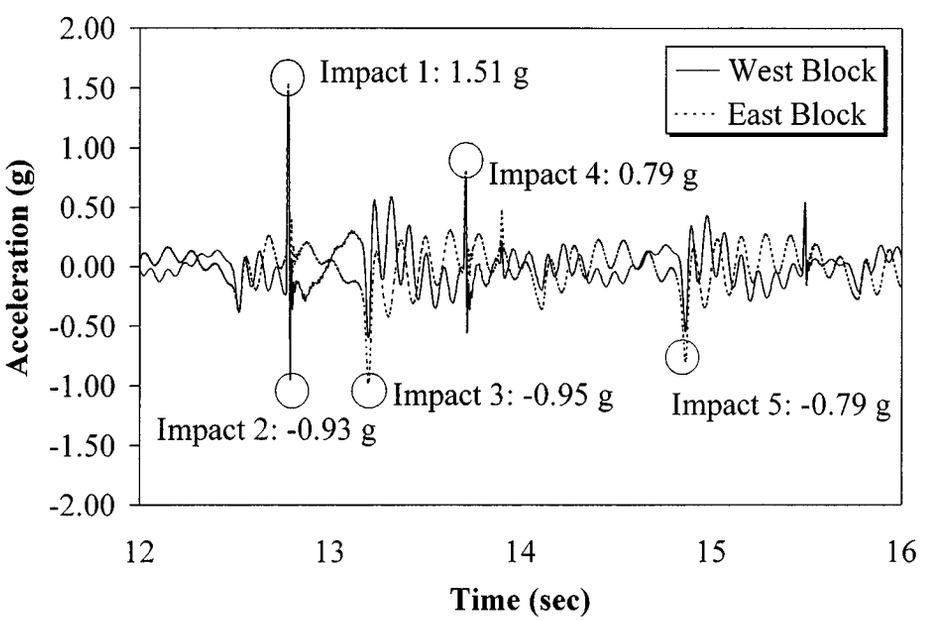

FIGURE 4-20 Block Accelerations History for Run II1

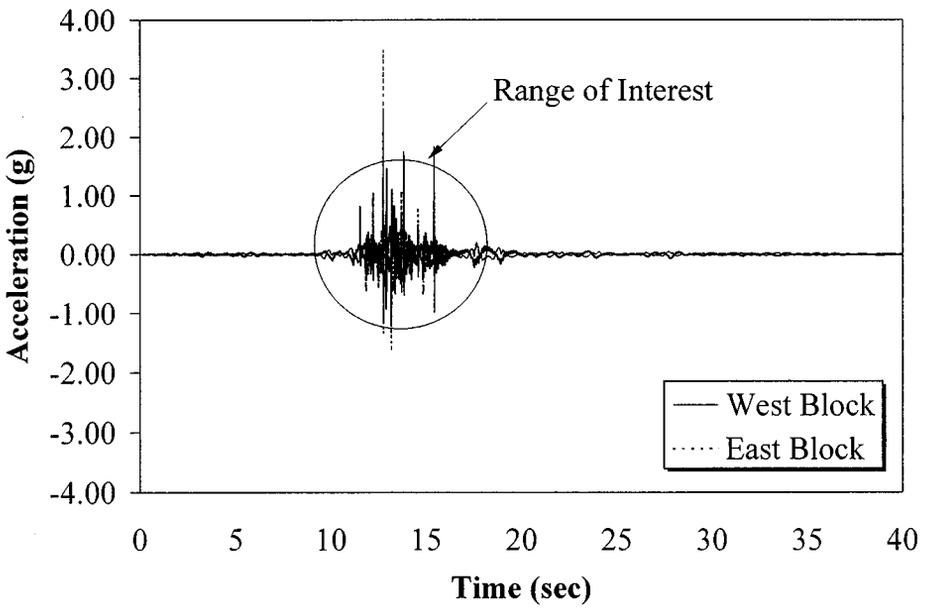

FIGURE 4-21 Block Accelerations History for Run II3

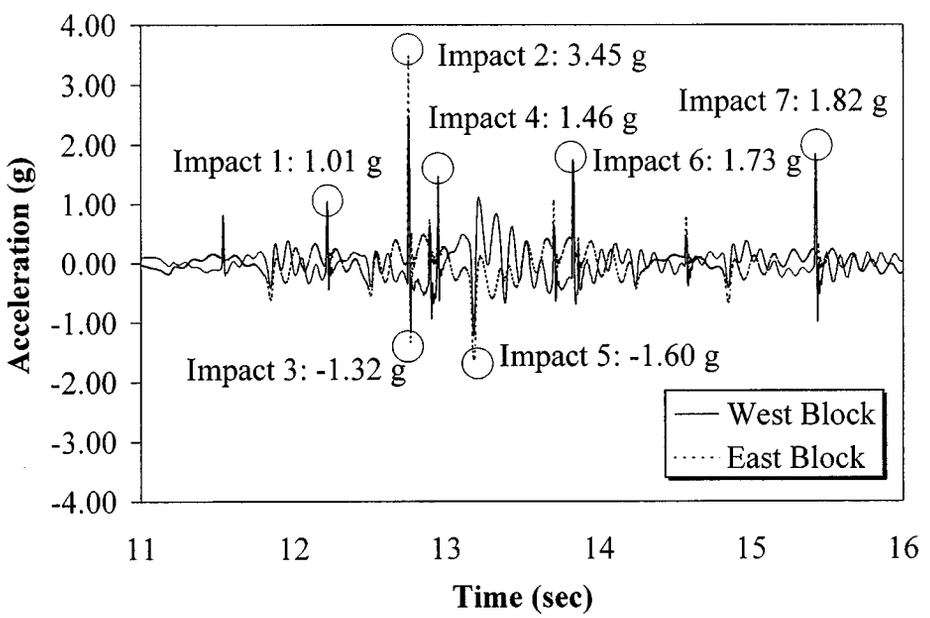

FIGURE 4-22 Block Accelerations History for Run II3

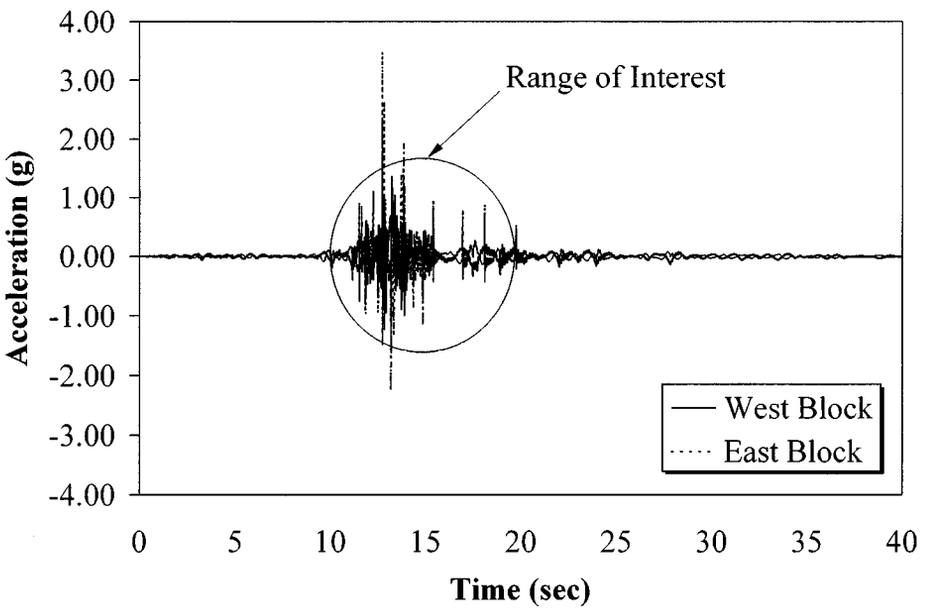

FIGURE 4-23 Block Accelerations History for Run II5

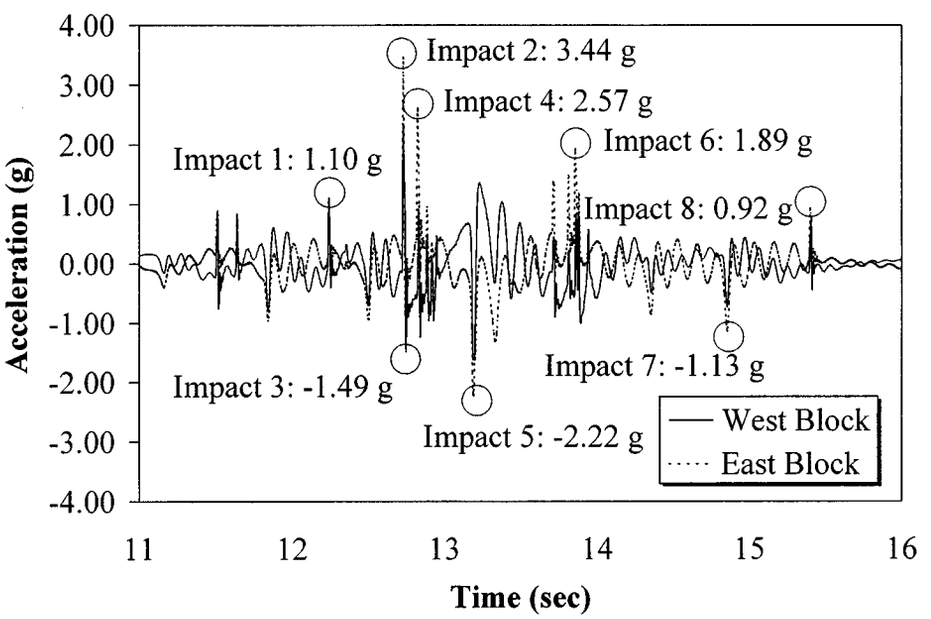

FIGURE 4-24 Block Accelerations History for Run II5

west and the east block, respectively, at any time step i, the hinge relative displacement, $\Delta_{i,12}$ can be calculated as follows:

$$\Delta_{i,12} = -(\Delta_{i,1} + \Delta_{i,2}) \tag{4-1}$$

TABLE 4-1 Maximum Recorded Accelerations for the Cases with Six Restrainers

Restrainer Gap (mm)	Earthquake Motion	Maximum Acceleration (g)	
		West Block	East Block
0.0	0.50×Loma Prieta	1.32	1.57
0.0	0.75×Loma Prieta	1.10	1.69
0.0	1.00×Loma Prieta	1.32	1.96
0.0	1.25×Loma Prieta	1.61	2.69
0.0	1.50×Loma Prieta	1.79	2.75
12.7	0.50×Loma Prieta	1.60	1.98
12.7	0.75×Loma Prieta	1.41	2.03
12.7	1.00×Loma Prieta	2.13	2.96
12.7	1.25×Loma Prieta	2.44	3.32
12.7	1.50×Loma Prieta	1.52	3.04
25.4	0.50×Loma Prieta	1.42	1.51
25.4	0.75×Loma Prieta	1.93	1.80
25.4	1.00×Loma Prieta	2.45	3.45
25.4	1.25×Loma Prieta	3.01	3.77
25.4	1.50×Loma Prieta	2.28	3.44

The negative sign is included because, based on the adopted sign convention, the extension of the expansion joint gap was considered as positive relative displacement, while the closure of the gap was considered to be negative relative displacement. However, due to the sign convention of the Temposonics, the extension of the gap was measured as negative displacement and, therefore, the negative of the summation of the two readings had to be taken. It was found that the Temposonics readings produced good overlay with the hinge displacements recorded by the Novotechniks. Some minor discrepancies were noted but were mainly attributed to the different sensitivity of the two types of transducers.

Figures 4-25 to 4-33 and table 4-2 indicate that, in general, for a certain restrainer gap, the hinge relative displacement increases slightly with the level of the input acceleration. It can be also seen that the level of the hinge relative displacement increases as the restrainer gap increases from 0 mm (0 in) to 25.4 mm (1 in) by 40 to 50 percent. The maximum displacement at the hinge occurred during the 1.50×Loma Prieta motion with 1 in (25.4 mm) restrainer gap and was approximately 15.7 mm (0.62 in). Since the scaled available seat width was 65 mm (2.6 in), it can be concluded that, even in the most critical case of hinge relative displacement, the span did not become unseated.

Ideally, the minimum hinge displacements should always be equal to 25.4 mm (1 in), which is the size of the expansion joint gap. However, due to construction imperfections, the gap between the two blocks was not constant but varied from 25.4 mm (1 in) to 50.8 mm (2 in) in both transverse and vertical directions. As a consequence of the variations in the expansion joint gap and the in-plane rotations associated with them, the recorded values illustrated fluctuations in the minimum hinge displacement. It should be also noted that the expansion joint gap was measured after the completion of each run and no residual displacements were observed, indicating elastic behavior of the elastomeric pads that simulated the column stiffness.

TABLE 4-2 Maximum Recorded Hinge Displacements for the Cases with Six Restrainers

Restrainer Gap (mm)	Earthquake Motion	Maximum Hinge Displacement (mm)
0.0	0.50×Loma Prieta	8.8
0.0	0.75×Loma Prieta	9.4
0.0	1.00×Loma Prieta	10.0
0.0	1.25×Loma Prieta	10.2
0.0	1.50×Loma Prieta	10.2
12.7	0.50×Loma Prieta	11.0
12.7	0.75×Loma Prieta	11.8
12.7	1.00×Loma Prieta	12.0
12.7	1.25×Loma Prieta	13.0
12.7	1.50×Loma Prieta	13.1
25.4	0.50×Loma Prieta	12.9
25.4	0.75×Loma Prieta	13.7
25.4	1.00×Loma Prieta	14.3
25.4	1.25×Loma Prieta	15.0
25.4	1.50×Loma Prieta	15.7

Figures 4-34 to 4-42 show the block displacement histories relative to the shake table. Shake table displacement was measured by an internal transducer in the shake table. The relative displacement was calculated by subtracting shake table displacement from the absolute displacement measured by the Temposonics transducers. The average of the two relative displacement values, corresponding to the two webs of each block, was then computed to obtain the relative displacement of the block. Based on figures 4-34 to 4-42, it is evident that the two box girder segments did not experience significant out-of-phase motion, even though their fundamental periods were considerably different. This is mainly attributed to the presence of restrainers that provided a relatively stiff linkage between the two blocks. Out-of-phase motion of the two blocks was actually initiated only after the first collision occurred, lasted for the entire impact duration and gradually decayed. It can be also concluded that the east block, which was supported on the more flexible bearings, generally underwent higher displacements compared to the west block. The displacements for both blocks increased with increasing earthquake excitation and varied from approximately 50 mm (2.0 in) to 150 mm (5.9 in).

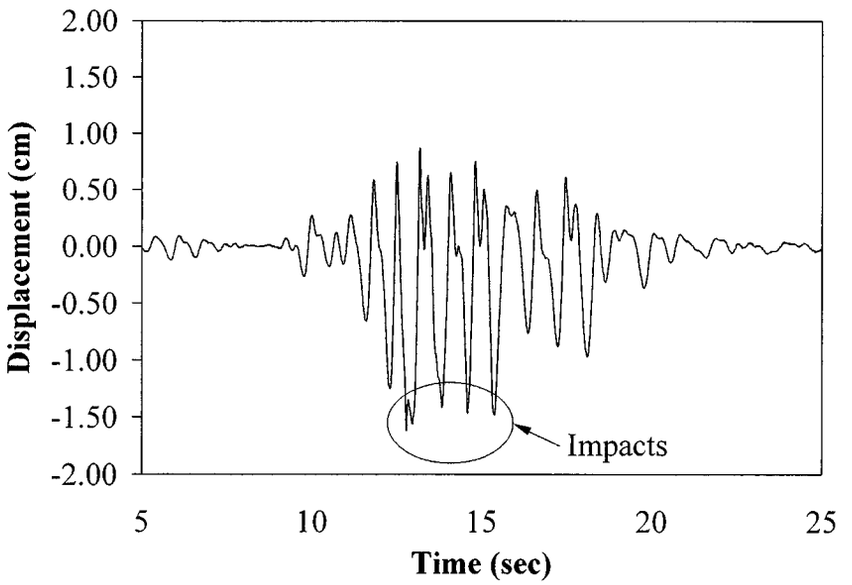

FIGURE 4-25 Hinge Relative Displacement History for Run IV1

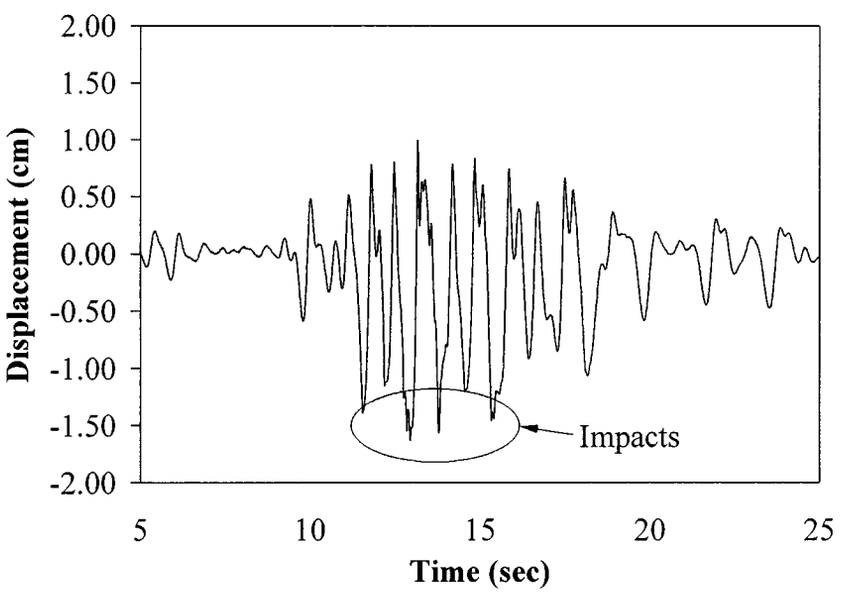

FIGURE 4-26 Hinge Relative Displacement History for Run IV3

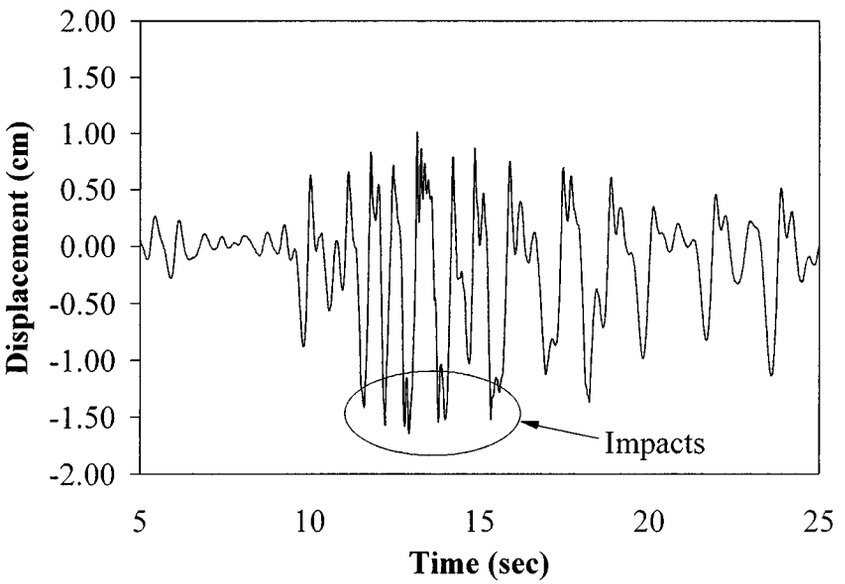

FIGURE 4-27 Hinge Relative Displacement History for Run IV5

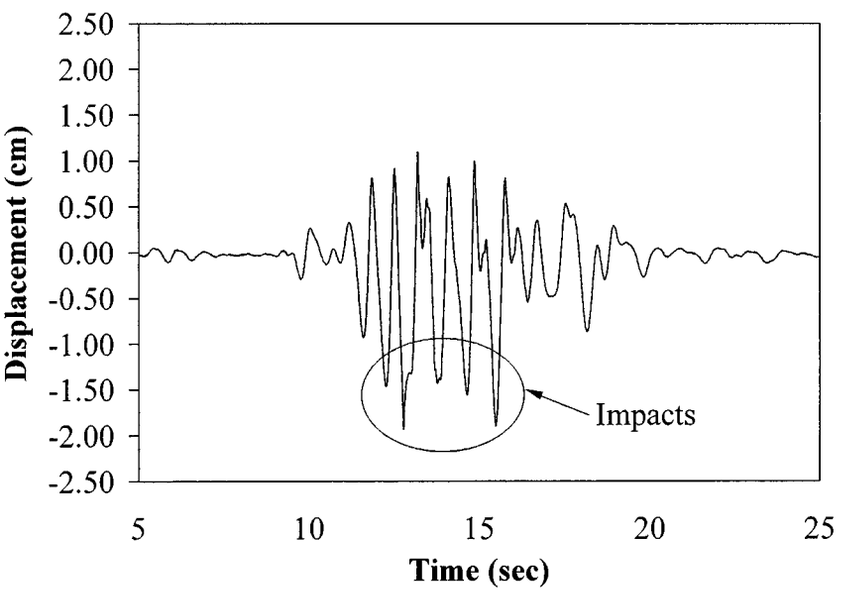

FIGURE 4-28 Hinge Relative Displacement History for Run III1

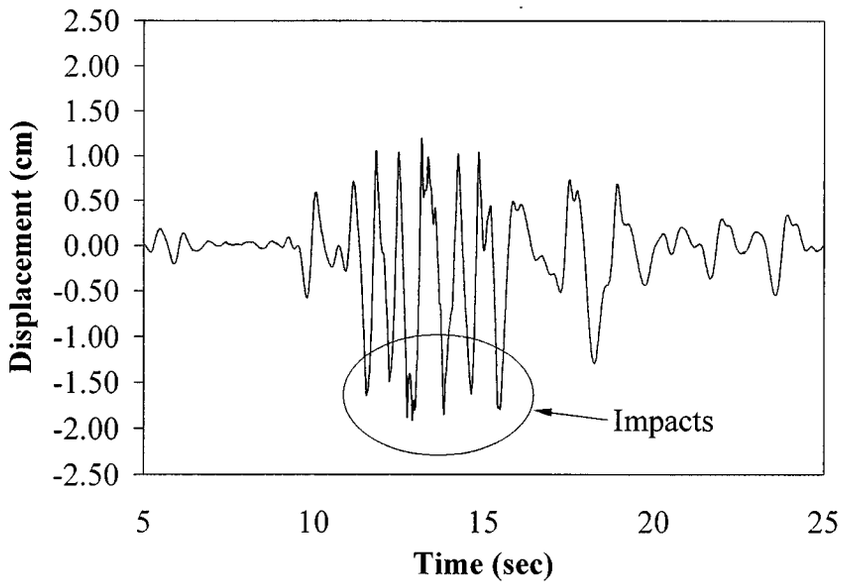

FIGURE 4-29 Hinge Relative Displacement History for Run III3

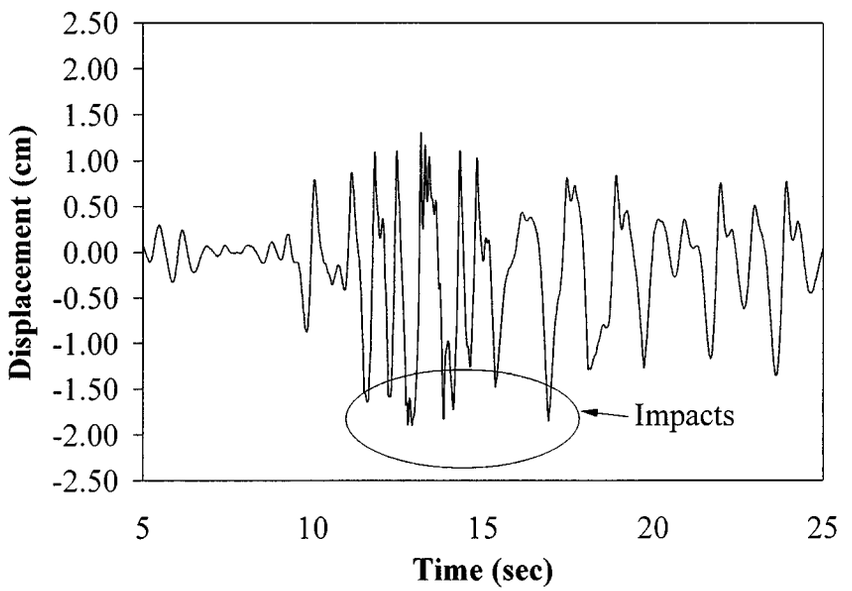

FIGURE 4-30 Hinge Relative Displacement History for Run III5

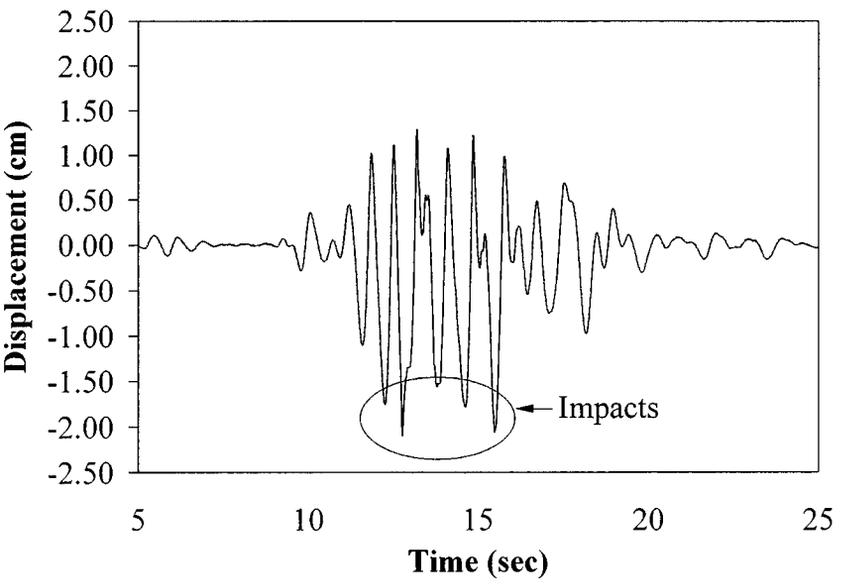

FIGURE 4-31 Hinge Relative Displacement History for Run II1

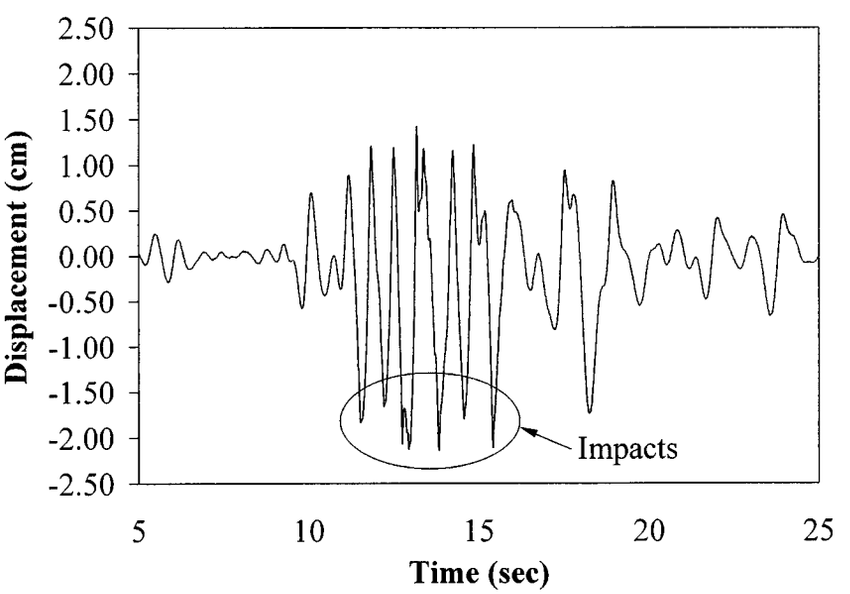

FIGURE 4-32 Hinge Relative Displacement History for Run II3

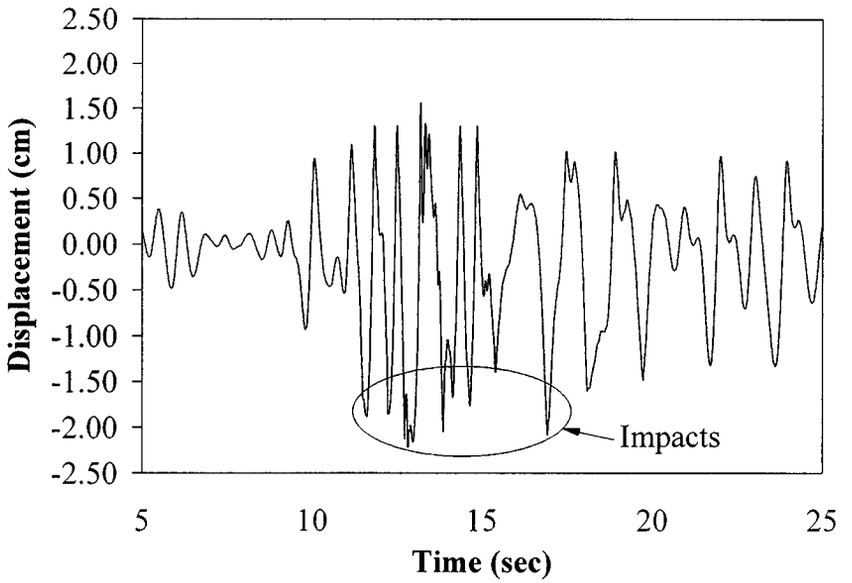

FIGURE 4-33 Hinge Relative Displacement History for Run II5

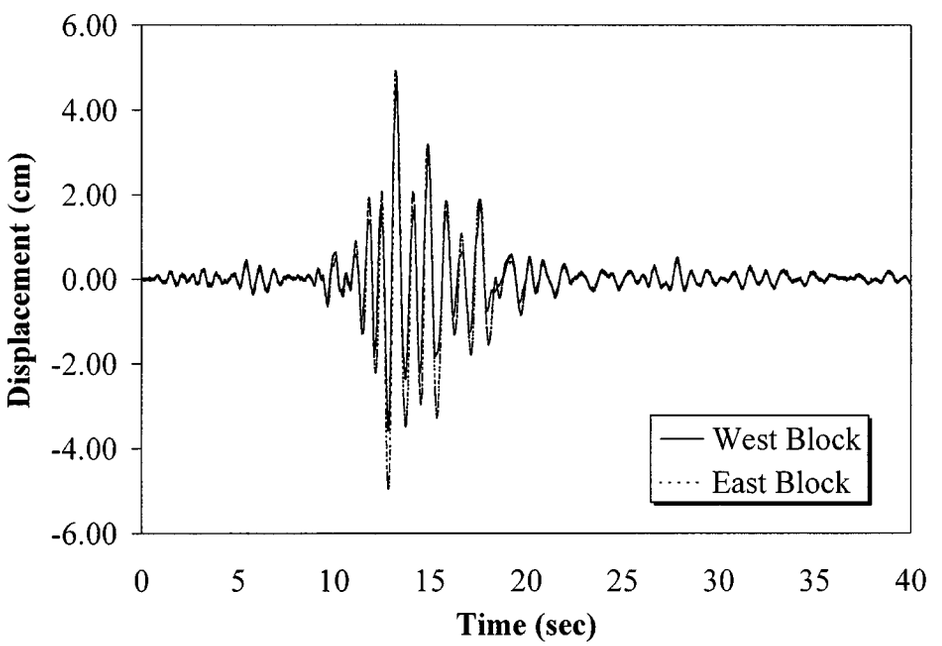

FIGURE 4-34 Block Displacements Relative to the Shake Table History for Run IV1

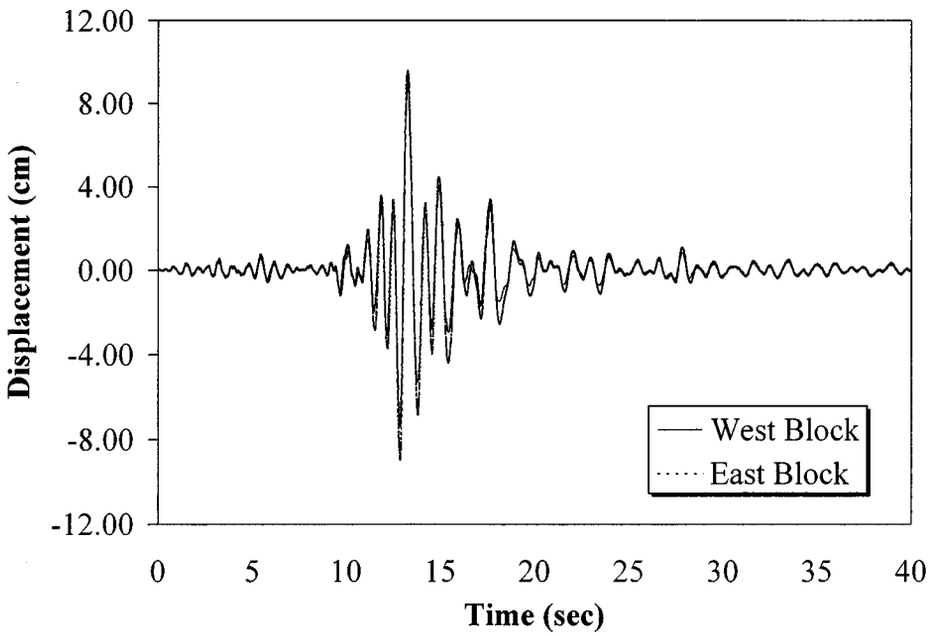

FIGURE 4-35 Block Displacements Relative to the Shake Table History for Run IV3

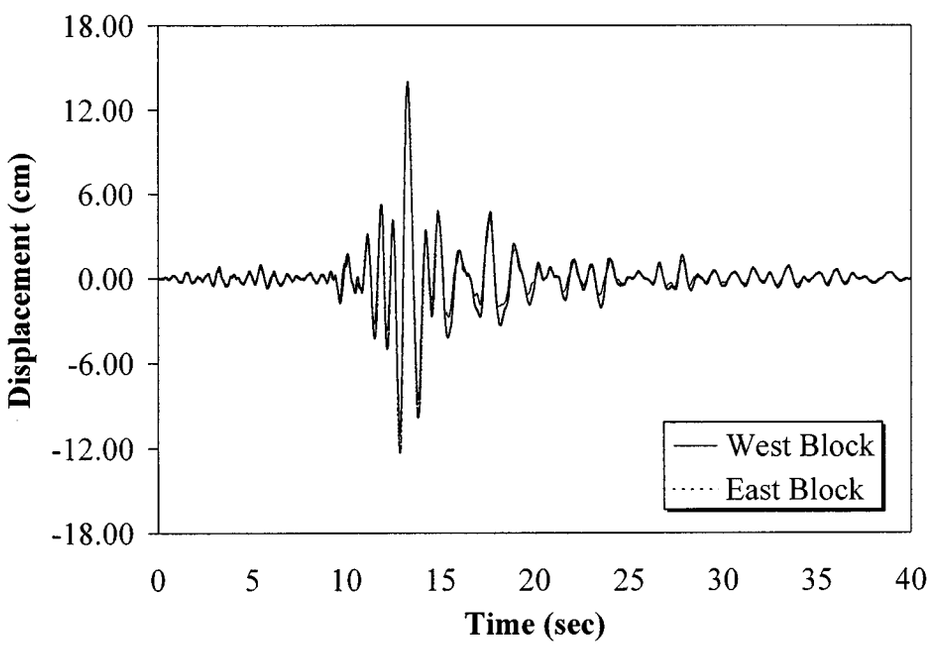

FIGURE 4-36 Block Displacements Relative to the Shake Table History for Run IV5

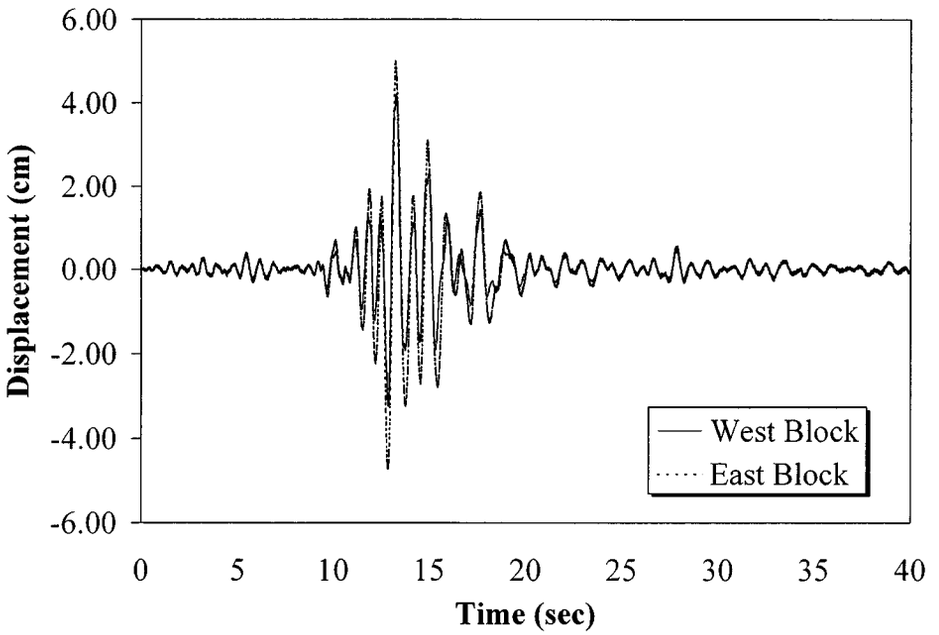

FIGURE 4-37 Block Displacements Relative to the Shake Table History for Run III1

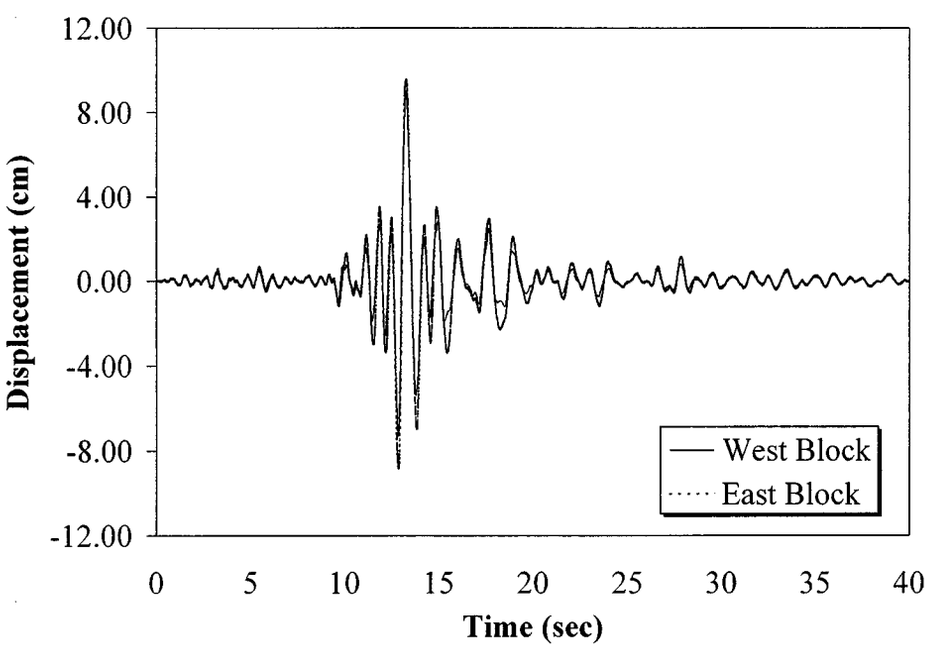

FIGURE 4-38 Block Displacements Relative to the Shake Table History for Run III3

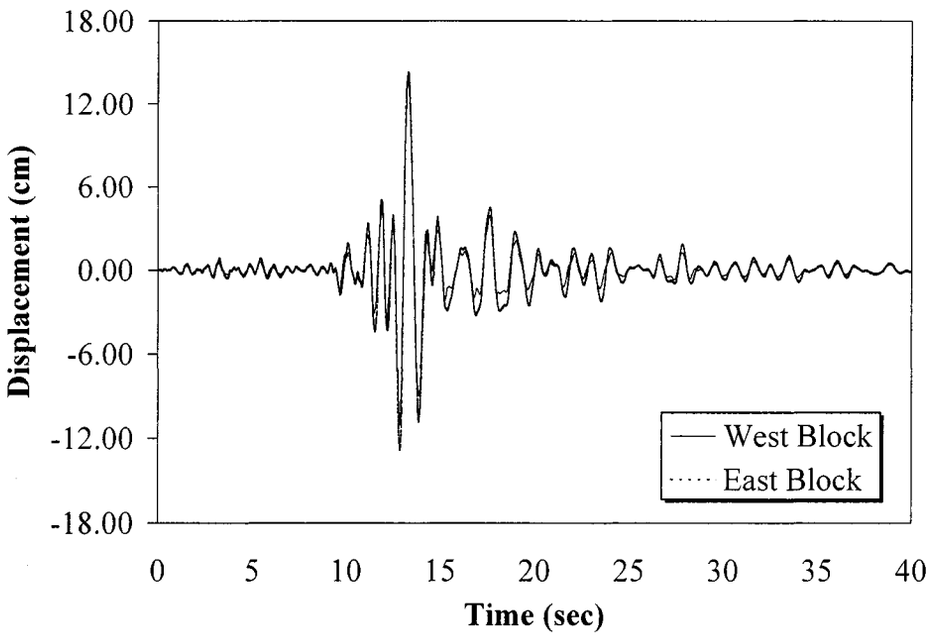

FIGURE 4-39 Block Displacements Relative to the Shake Table History for Run III5

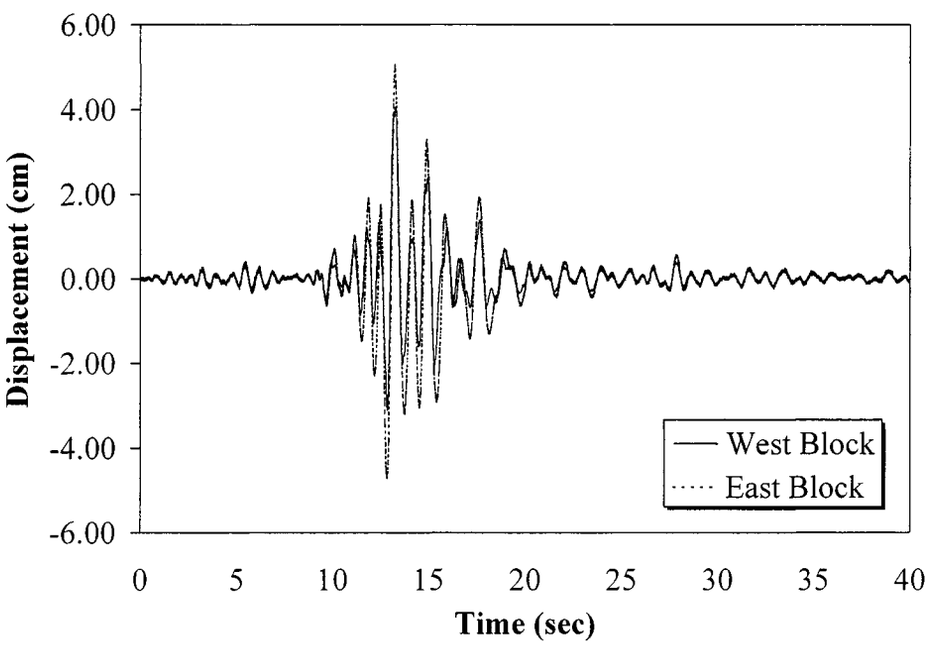

FIGURE 4-40 Block Displacements Relative to the Shake Table History for Run II1

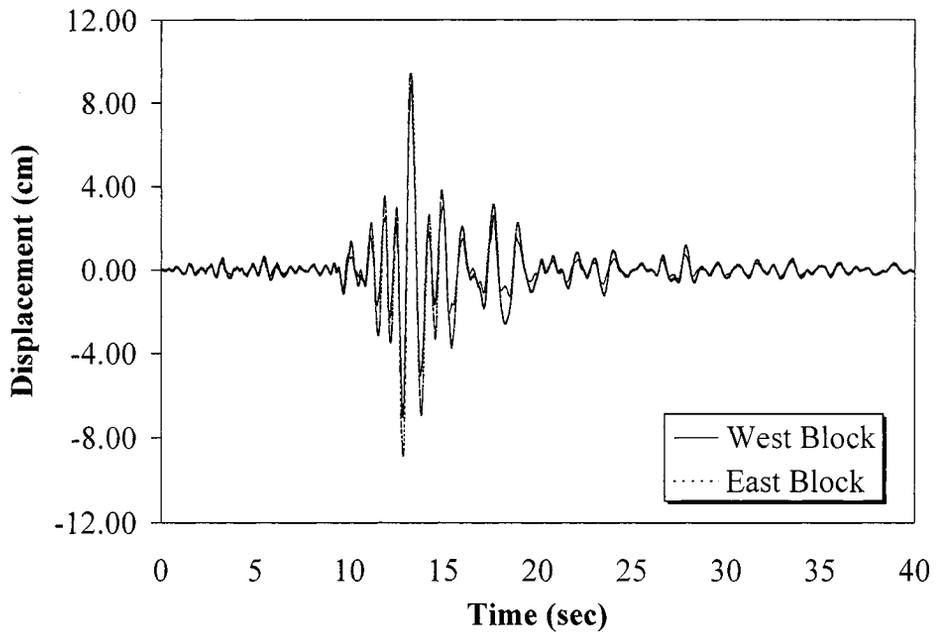

FIGURE 4-41 Block Displacements Relative to the Shake Table History for Run II3

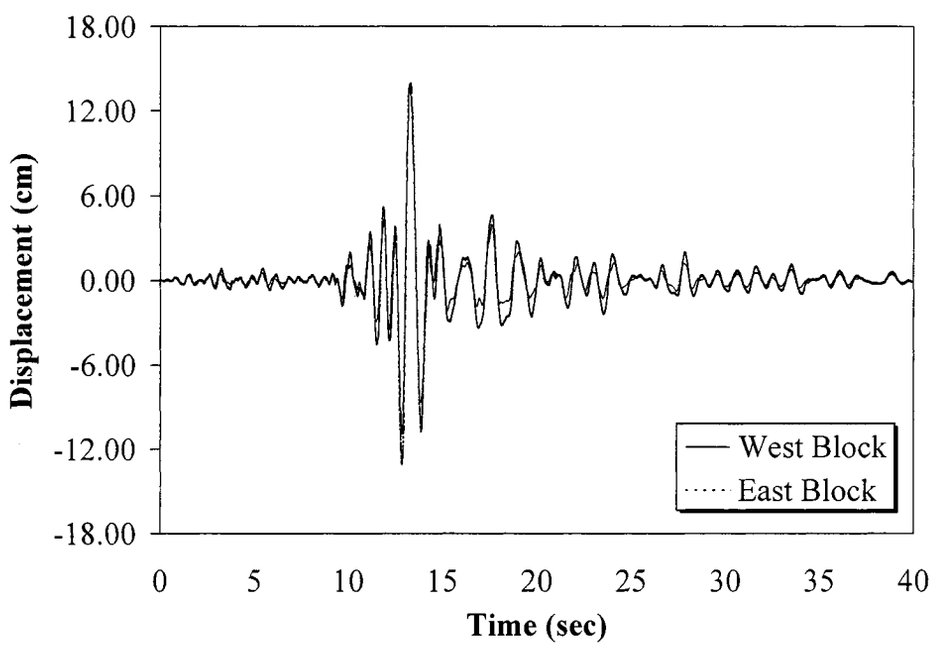

FIGURE 4-42 Block Displacements Relative to the Shake Table History for Run II5

4.3.3 Restrainer Elongation and Forces

The restrainer elongation histories are plotted in figures 4-44 to 4-52. Since the restrainers can take only tension, they are activated after the relative displacement at the hinge exceeds the initial restrainer slack. Therefore, the actual elongation of the cables, when the two cables move apart, is equal to the difference between the relative movement of the blocks and the initial restrainer slack. When there is no restrainer slack, the restrainers are activated immediately after the two blocks start moving apart. When the two bridge segments move towards each other, the cables become loose. Restrainer yielding was assumed to occur when the restrainer displacement reached the scaled restrainer yield deformation (figure 4-43), even though the actual restrainers, which had not been scaled, did not yield. For the 2.0 m (6.6 ft) long cables, which were utilized in this study, with a specified yield stress of 1.214 GPa (176.1 ksi) and a modulus of elasticity of approximately 69 GPa (10000 ksi), the unscaled yield deformation was calculated to be 35.3 mm (1.39 in). This displacement was then multiplied by the scale factor of 1/4 to give a scaled value of 8.8 mm (0.35 in).

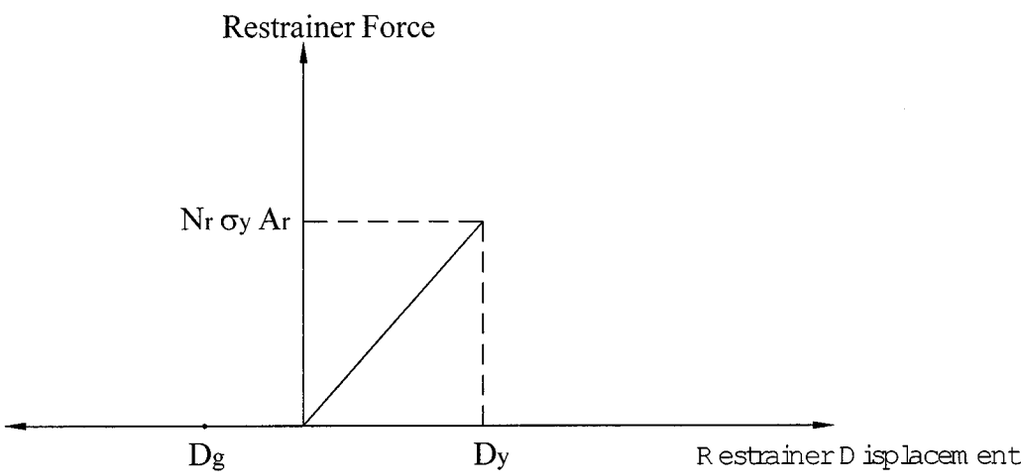

FIGURE 4-43 Restrainer Behavior

As shown in Figures 4-44 to 4-46, corresponding to 0 in (0 mm) restrainer gap, the restrainers nearly yielded during the 0.50×Loma Prieta excitation, while they experienced significant yielding during both the 1.00×Loma Prieta and the 1.50×Loma Prieta motions. In the 0.5 in (12.7 mm) slack case, yield deformation was barely exceeded when the specimen was loaded with the 1.00×Loma Prieta motion but notable yielding occurred during the 1.50×Loma Prieta run. Finally, when the restrainer gap was set to 1 in (25.4 mm), the restrainers yielded only during the 1.50×Loma Prieta excitation. The results clearly demonstrate that the force demand on the restrainer is critical when the slack is zero (during the cold season) and are in agreement with the conclusions of the study by Saiidi et al. (Saiidi et al., 1992).

The restrainer forces are given in Figures 4-53 to 4-61. Restrainer force was calculated as the product of the restrainer stiffness and displacement as follows:

$$F_r = (N_r \sigma_y A_r / D_y)(D - D_g) \qquad (4\text{-}2)$$

where:

F_r = restrainer force

N_r = number of restrainers used

σ_y = yield stress in restrainer

A_r = area of one restrainer

D_y = unscaled restrainer deformation at yield

D = measured restrainer displacement

D_g = scaled restrainer gap

The unscaled yield deformation is used in equation (4-2) to calculate the restrainer stiffness because stiffness has been already scaled down by multiplying the number of restrainers required by the scale factor of 1/4. The scaled restrainer yield force, F_y, can be determined by substituting D_r for D into equation (4-2). In this case, D_r is the scaled maximum permissible restrainer deformation given by equation (2-9). For six restrainer cables, F_y was calculated to be 260.9 KN (58.6 kips).

As expected the trend in restrainer forces is similar to that in displacements. Extent of yielding increases with increasing peak earthquake acceleration but decreases with increasing restrainer gap. As shown in table 4-3, the maximum calculated restrainer force was equal to 301.1 KN (67.7 kips) and corresponded to the 1.50×Loma Prieta excitation with 0 in (0 mm) restrainer gap.

TABLE 4-3 Maximum Restrainer Forces for the Cases with Six Restrainers

Restrainer Gap (mm)	Earthquake Motion	Maximum Restrainer Force (KN)
0.0	0.50×Loma Prieta	259.4
0.0	0.75×Loma Prieta	278.7
0.0	1.00×Loma Prieta	296.3
0.0	1.25×Loma Prieta	301.0
0.0	1.50×Loma Prieta	301.1
12.7	0.50×Loma Prieta	231.6
12.7	0.75×Loma Prieta	256.7
12.7	1.00×Loma Prieta	261.6
12.7	1.25×Loma Prieta	290.5
12.7	1.50×Loma Prieta	293.1
25.4	0.50×Loma Prieta	195.1
25.4	0.75×Loma Prieta	217.7
25.4	1.00×Loma Prieta	234.7
25.4	1.25×Loma Prieta	256.8
25.4	1.50×Loma Prieta	275.7

It should be noted that, in a field case, the system behavior could be substantially different after the restrainers yield, especially if the ultimate restrainer displacement was also reached. Cable failure would convert the restrained system to unrestrained and span unseating would probably occur. Also, in a field case, after yielding occurs, the forces given by the formula 4-2 will not be accurately since only initial stiffness is considered. It should be emphasized that neither restrainer yielding nor span unseating were visually seen during the tests, since the actual unscaled restrainer properties, seat width and hinge gap were used in this experimental study. Yielding and unseating were calculated by comparing the test results to the scaled values of restrainer yield deformation and seat width.

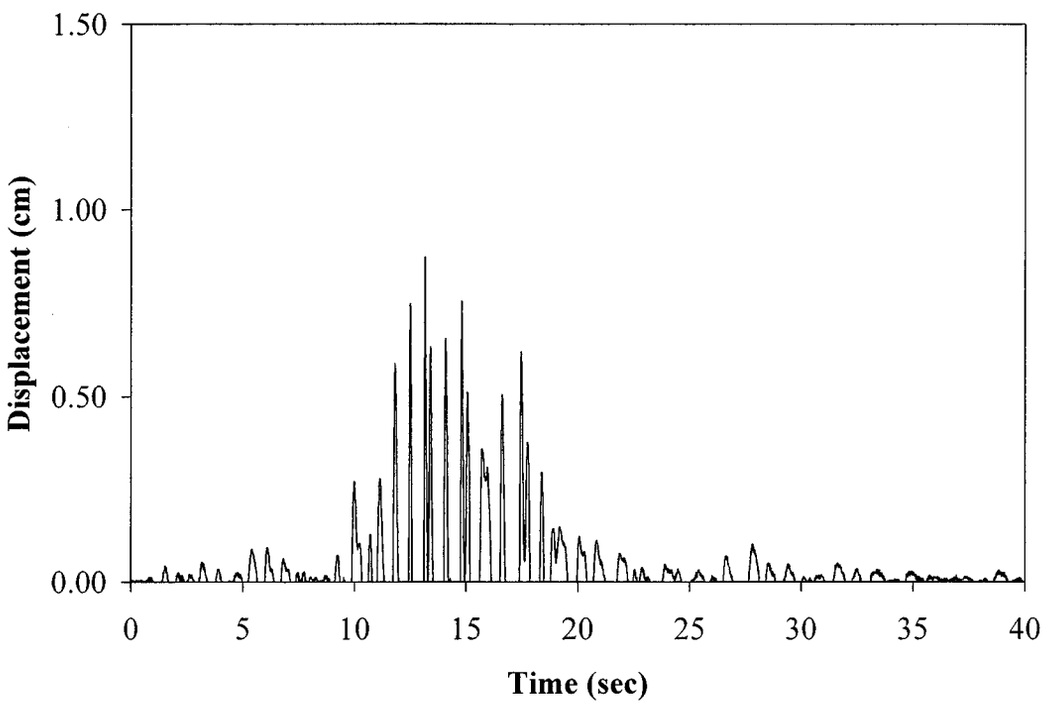

FIGURE 4-44 Restrainer Cable Elongation History for Run IV1

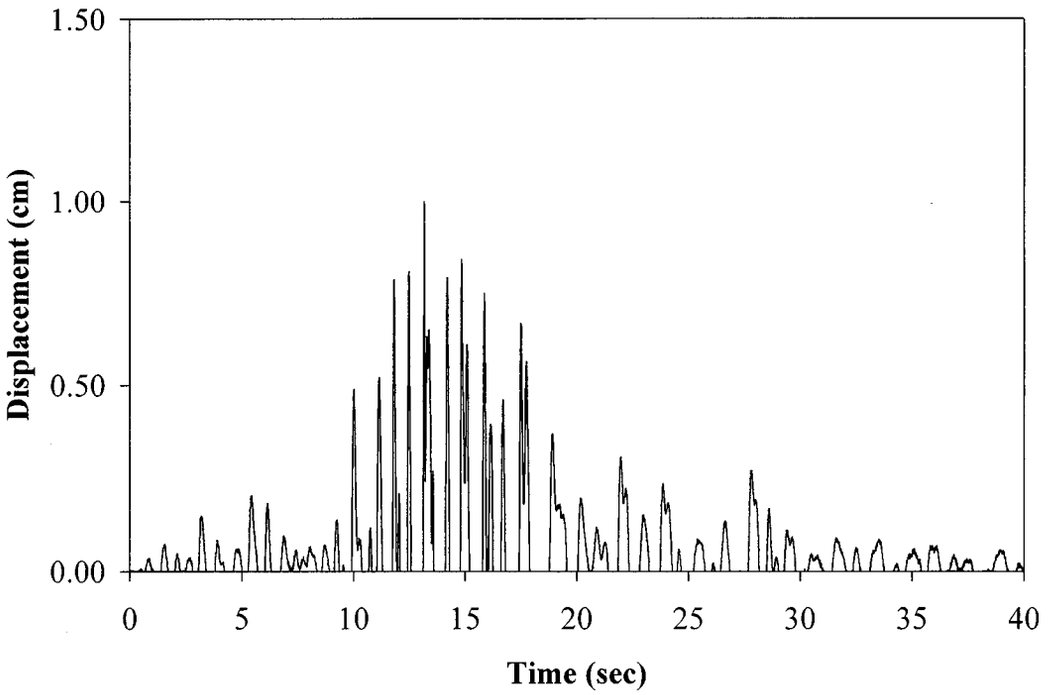

FIGURE 4-45 Restrainer Cable Elongation History for Run IV3

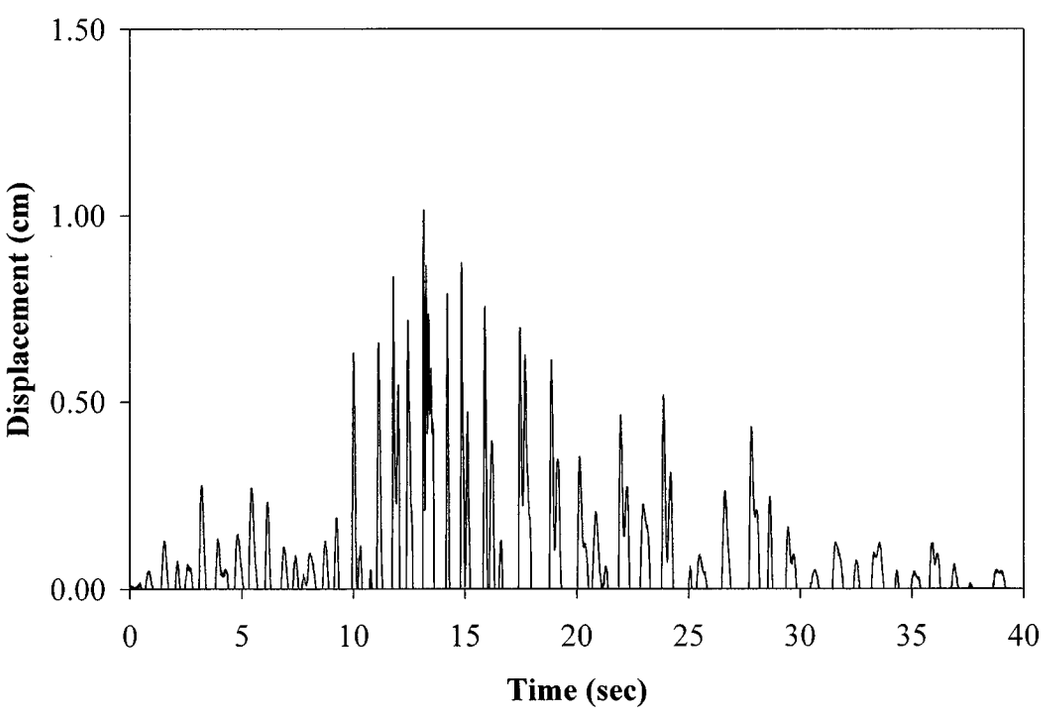

FIGURE 4-46 Restrainer Cable Elongation History for Run IV5

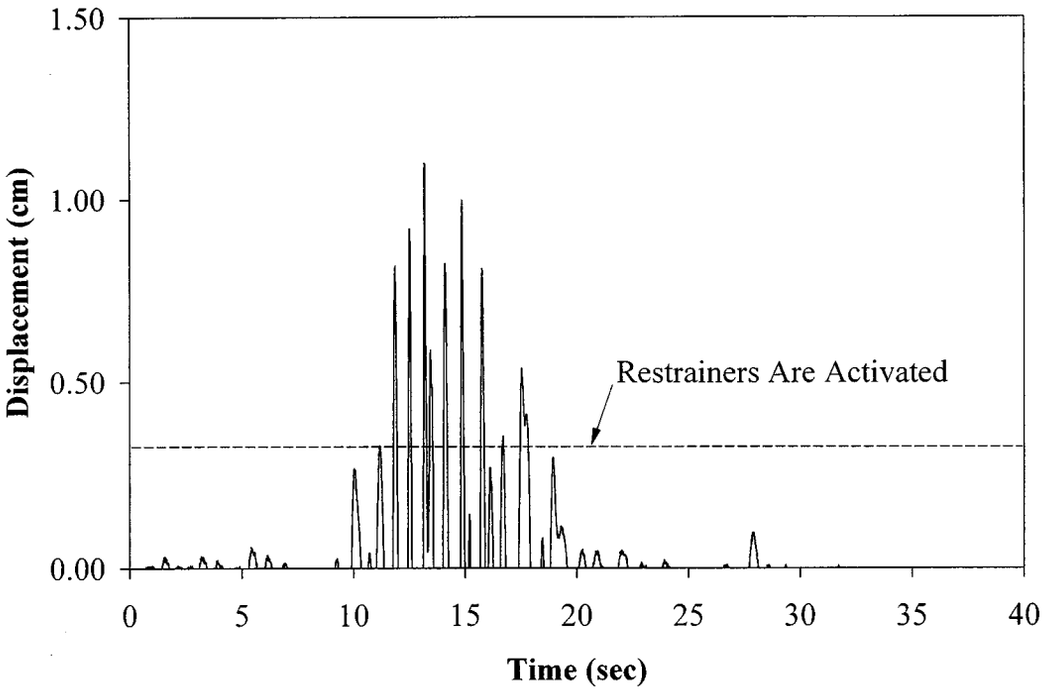

FIGURE 4-47 Restrainer Cable Elongation History for Run III1

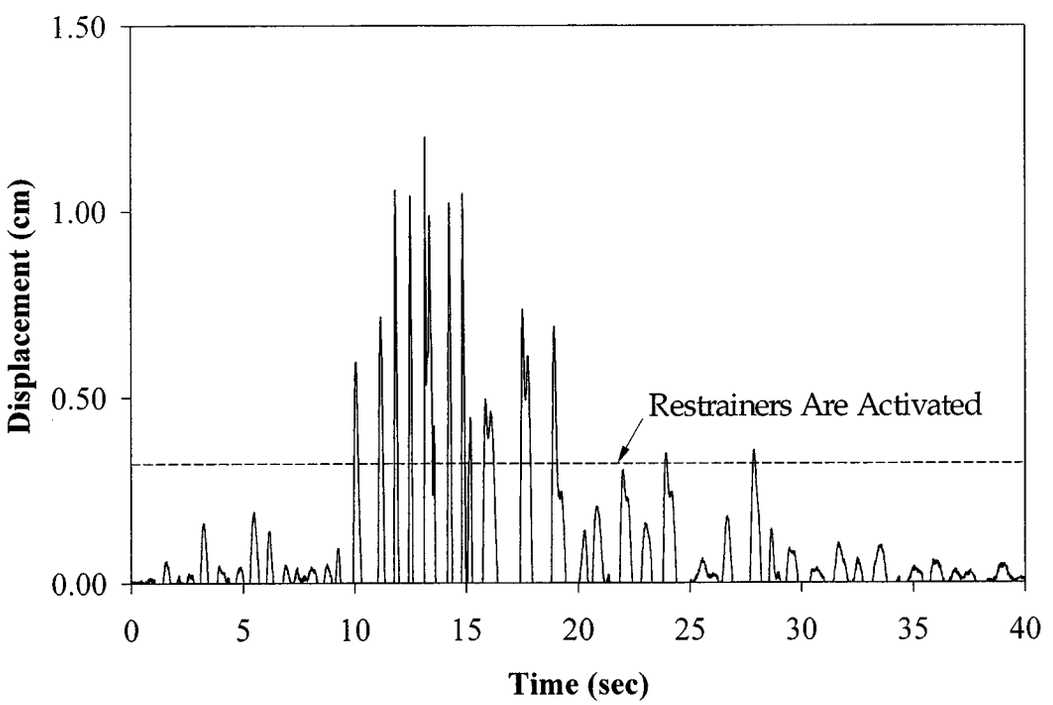

FIGURE 4-48 Restrainer Cable Elongation History for Run III3

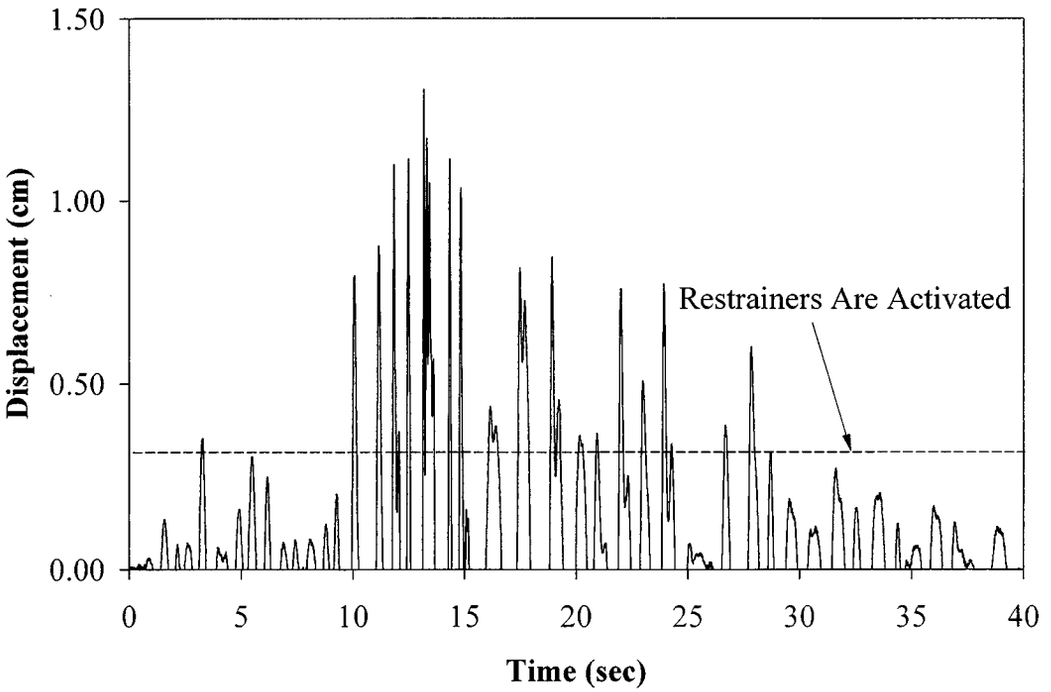

FIGURE 4-49 Restrainer Cable Elongation History for Run III5

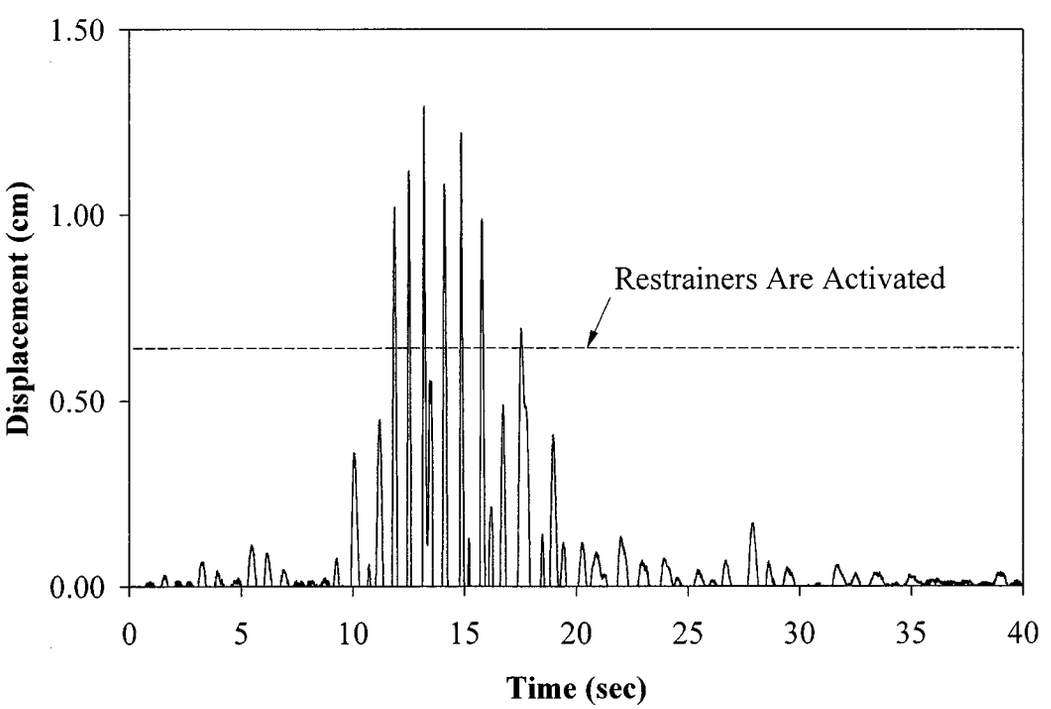

FIGURE 4-50 Restrainer Cable Elongation History for Run II1

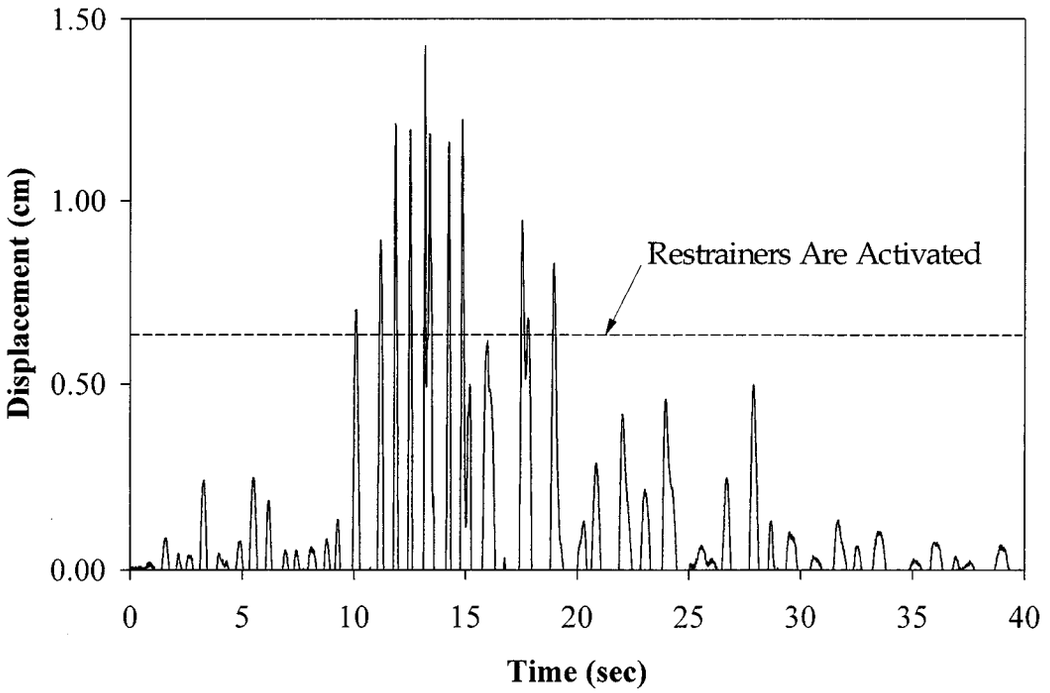

FIGURE 4-51 Restrainer Cable Elongation History for Run II3

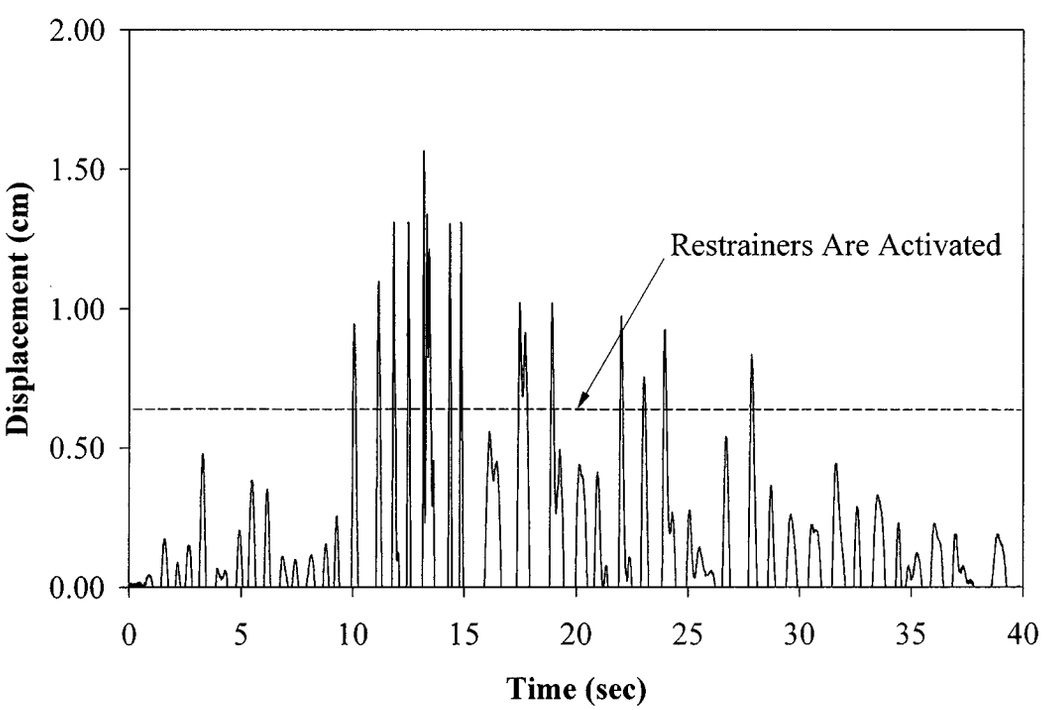

FIGURE 4-52 Restrainer Cable Elongation History for Run II5

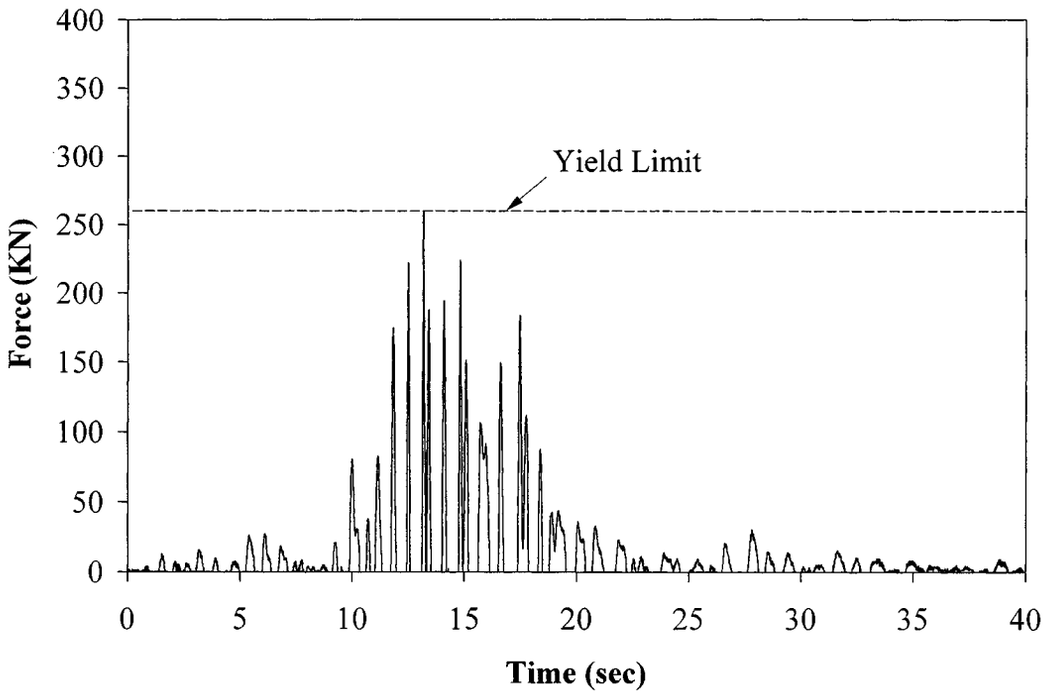

FIGURE 4-53 Restrainer Cable Force History for Run IV1

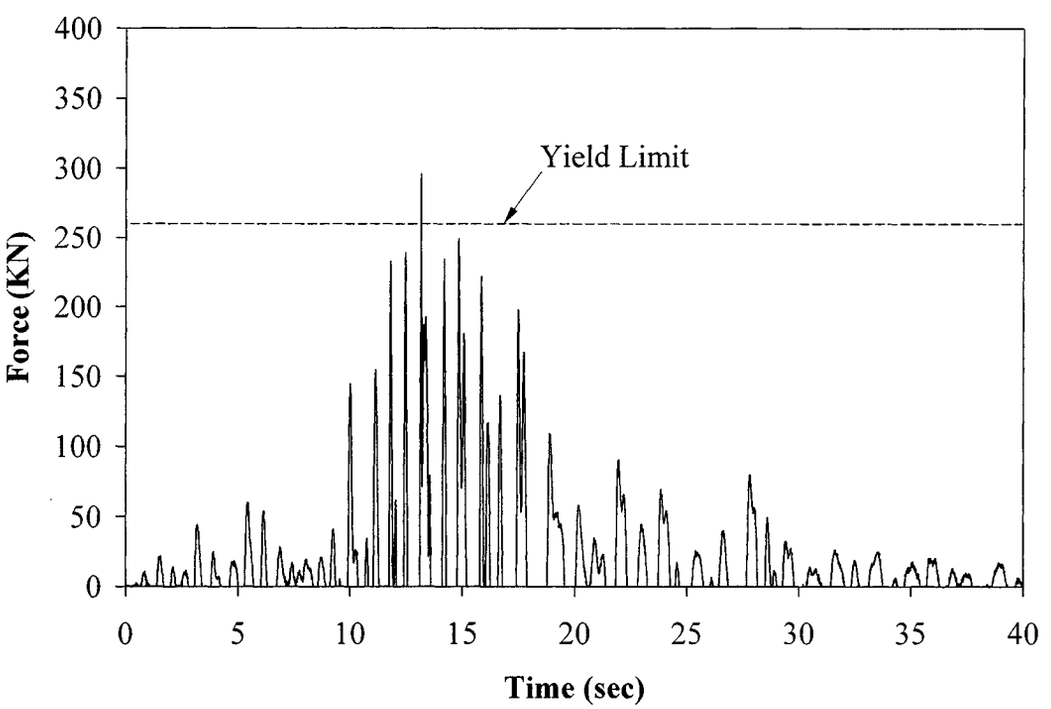

FIGURE 4-54 Restrainer Cable Force History for Run IV3

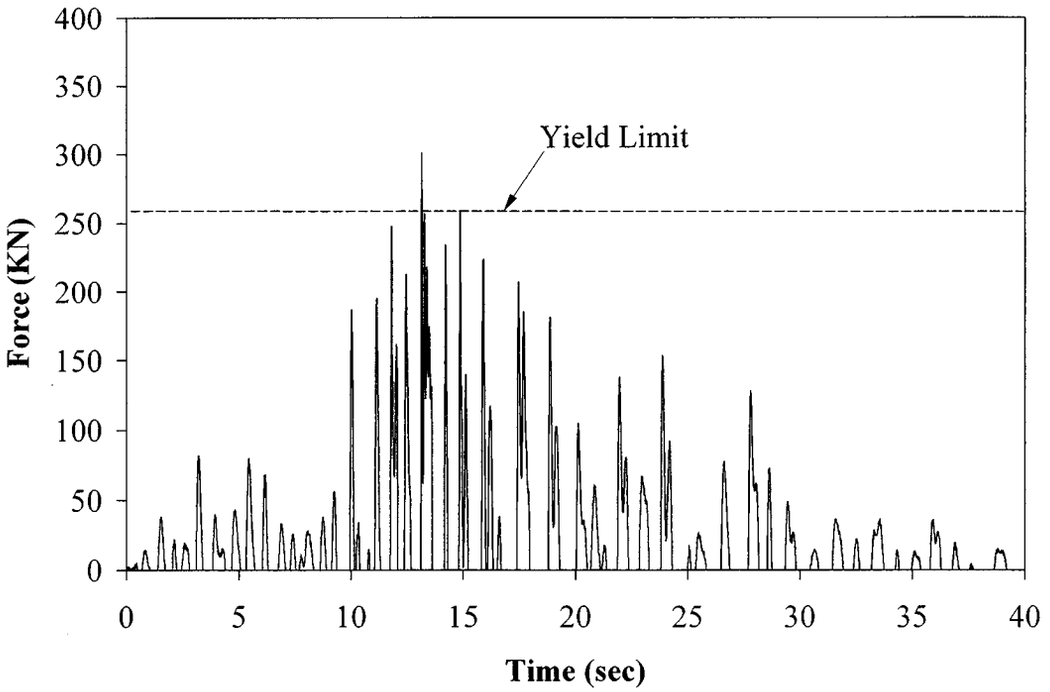

FIGURE 4-55 Restrainer Cable Force History for Run IV5

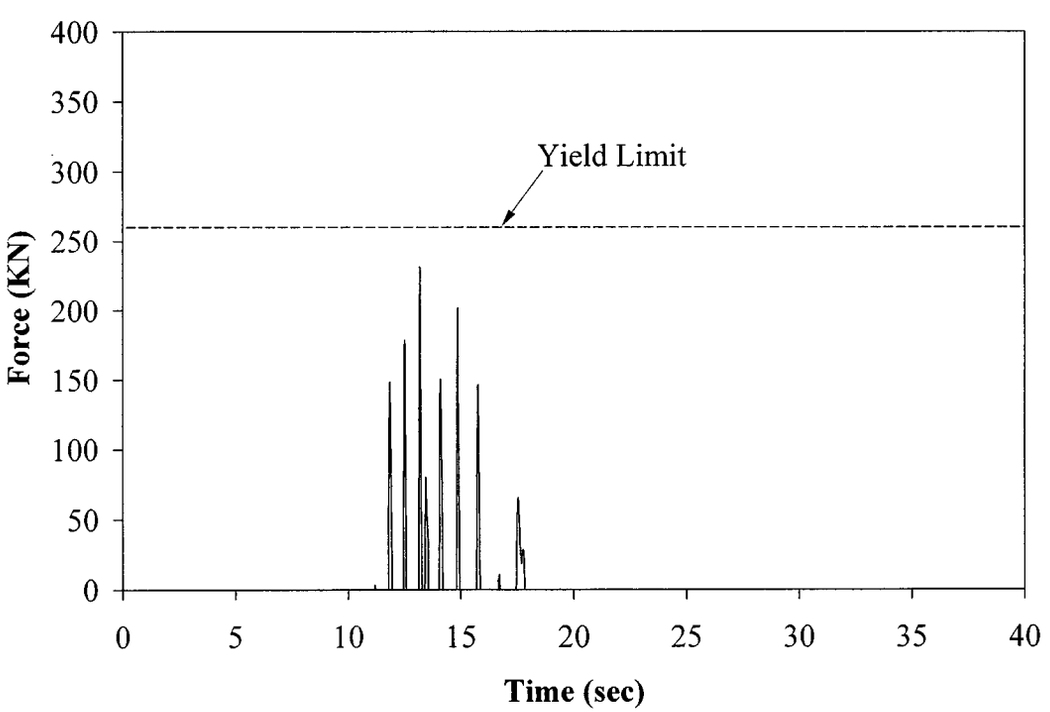

FIGURE 4-56 Restrainer Cable Force History for Run III1

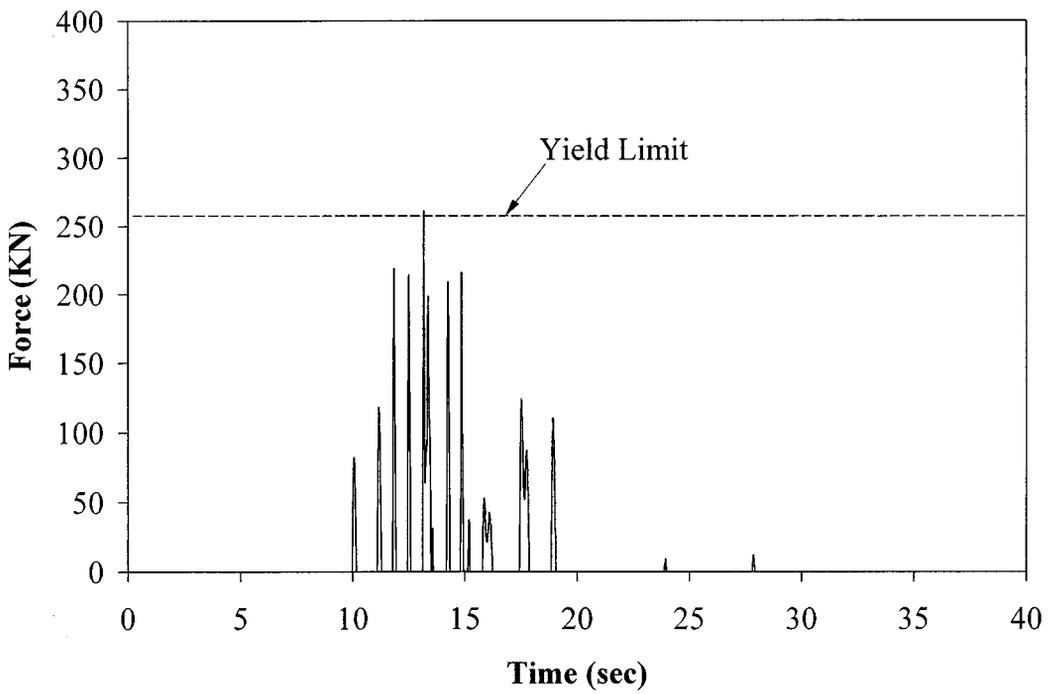

FIGURE 4-57 Restrainer Cable Force History for Run III3

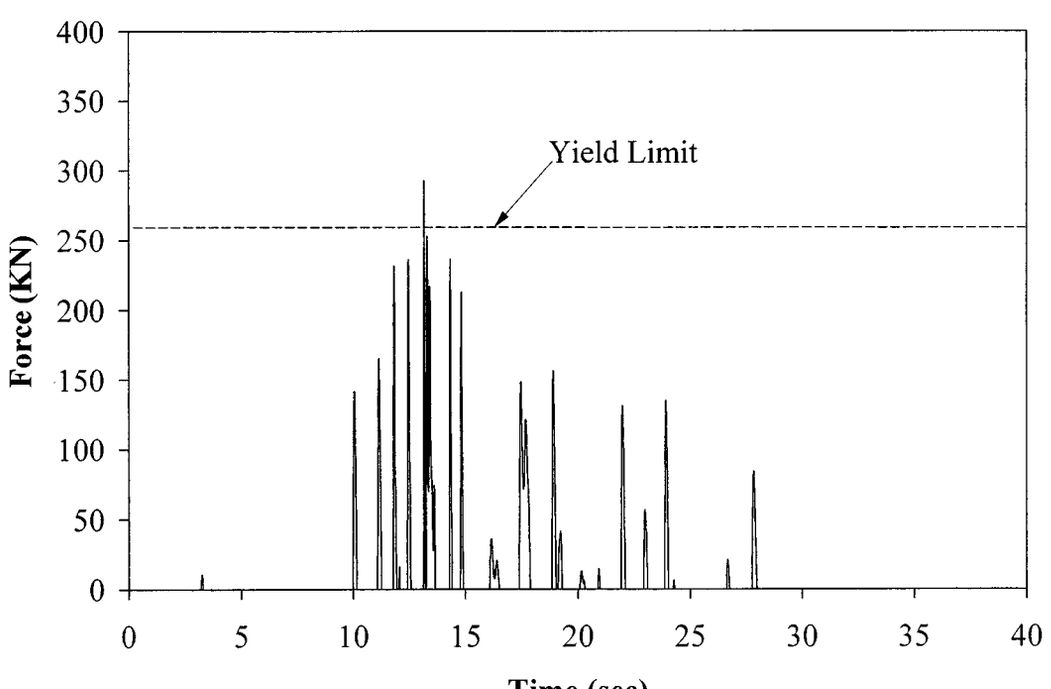

FIGURE 4-58 Restrainer Cable Force History for Run III5

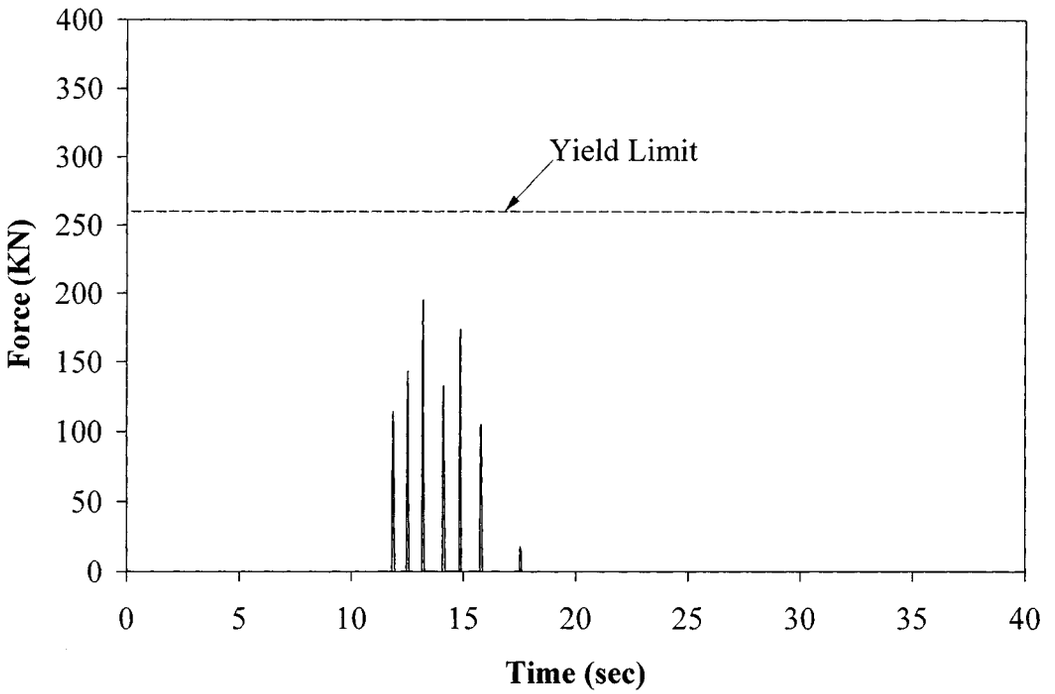

FIGURE 4-59 Restrainer Cable Force History for Run II1

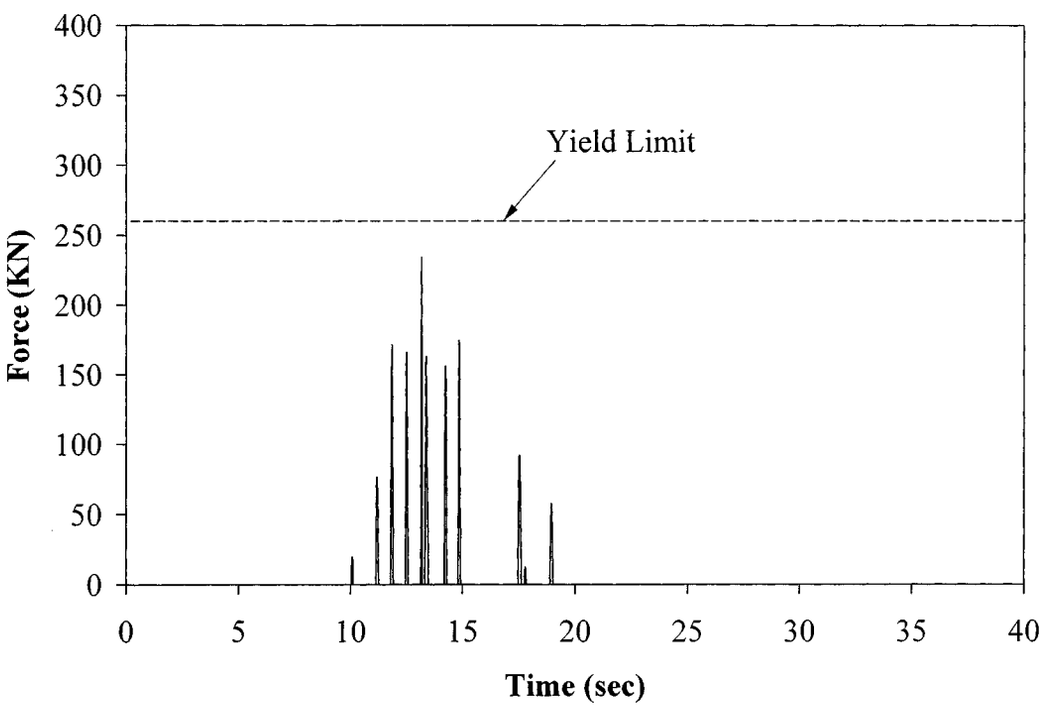

FIGURE 4-60 Restrainer Cable Force History for Run II3

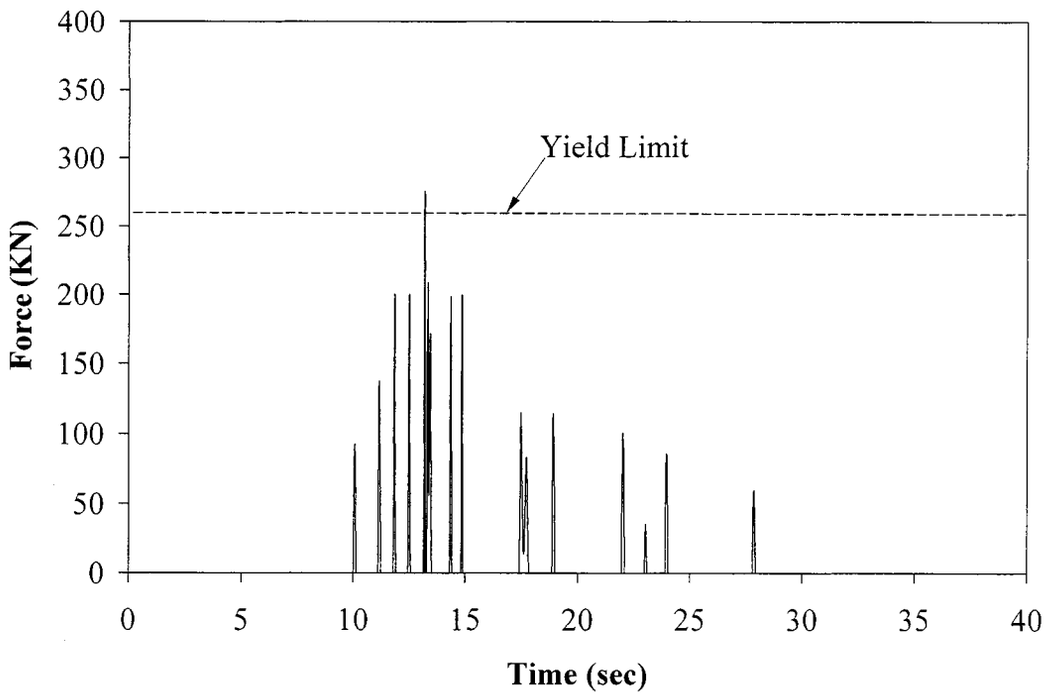

FIGURE 4-61 Restrainer Cable Force History for Run II5

4.4 Test Series V

The number of restrainers in these series was equal to two, while the restrainer gap was equal to zero.

4.4.1 Absolute Accelerations

Figures 4-62 to 4-67 show the absolute acceleration histories of the two blocks. In-plane rotations were more pronounced when only two restrainer cables were used. However, the average of the readings of the two antisymmetric Kinemetric accelerometers was considered to calculate the acceleration levels of each block, since the impacts between the two blocks and not the in-plane rotations were mainly examined in this experimental study. Similarly to the six restrainer cables case, the number and intensity of the impacts between the two box girder segments increased with increasing input motion. The peak accelerations, which were recorded, varied within the range 1.06 g to 1.75 g and 1.26 g to 3.11 g, for the west and the east block, respectively. These values are slightly lower than the maximum recorded accelerations, corresponding to six restrainer cables and zero restrainer gap.

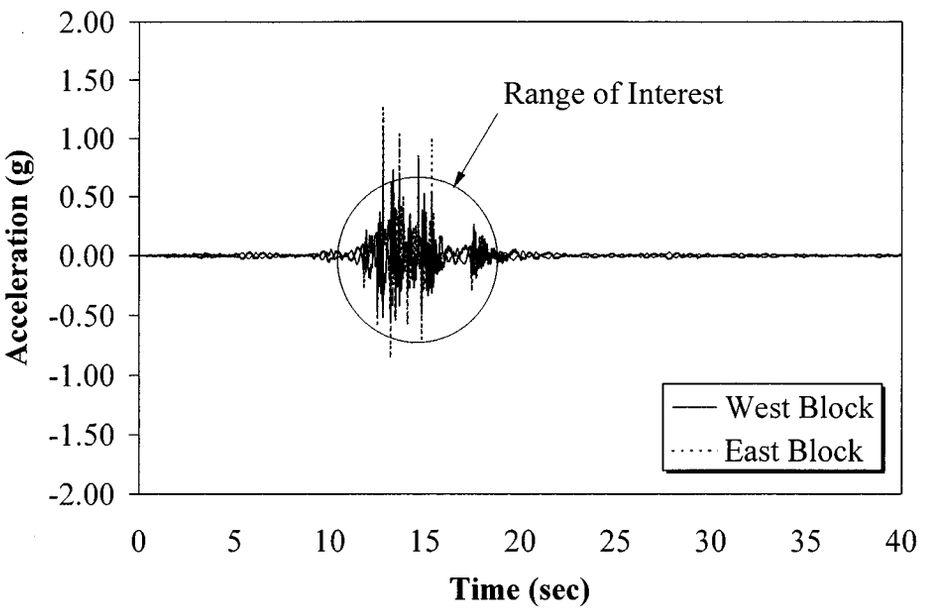

FIGURE 4-62 Block Accelerations History for Run V1

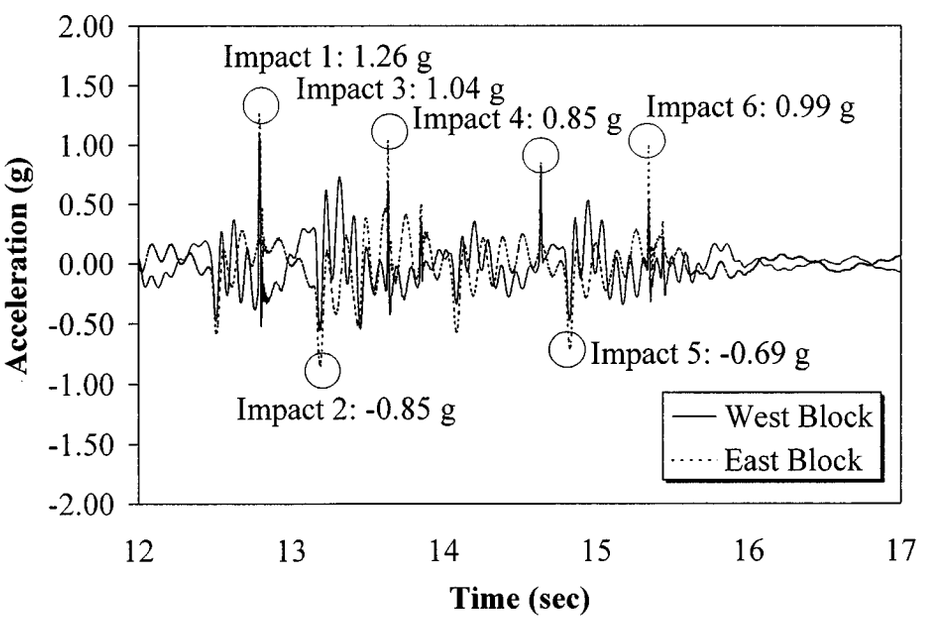

FIGURE 4-63 Block Accelerations History for Run V1

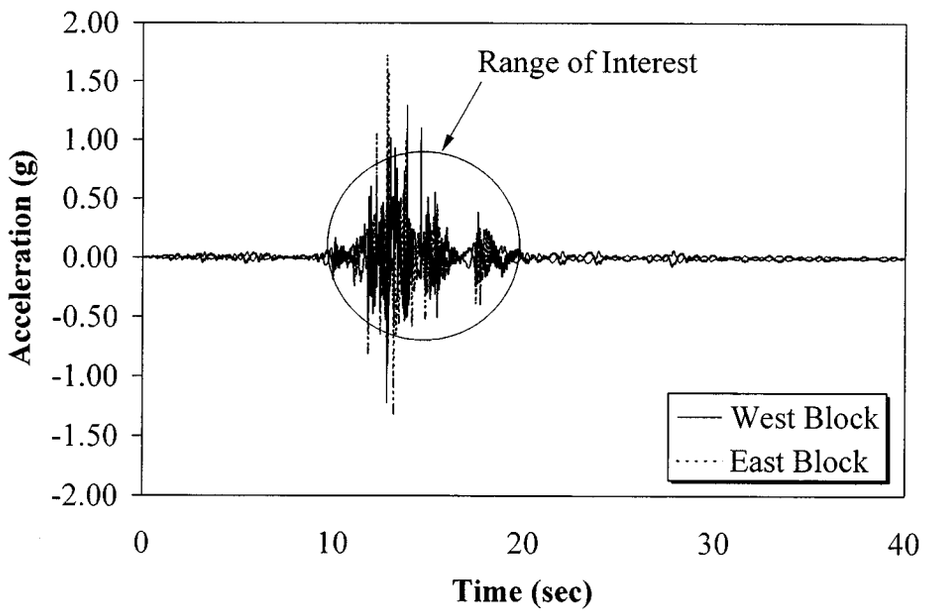

FIGURE 4-64 Block Accelerations History for Run V3

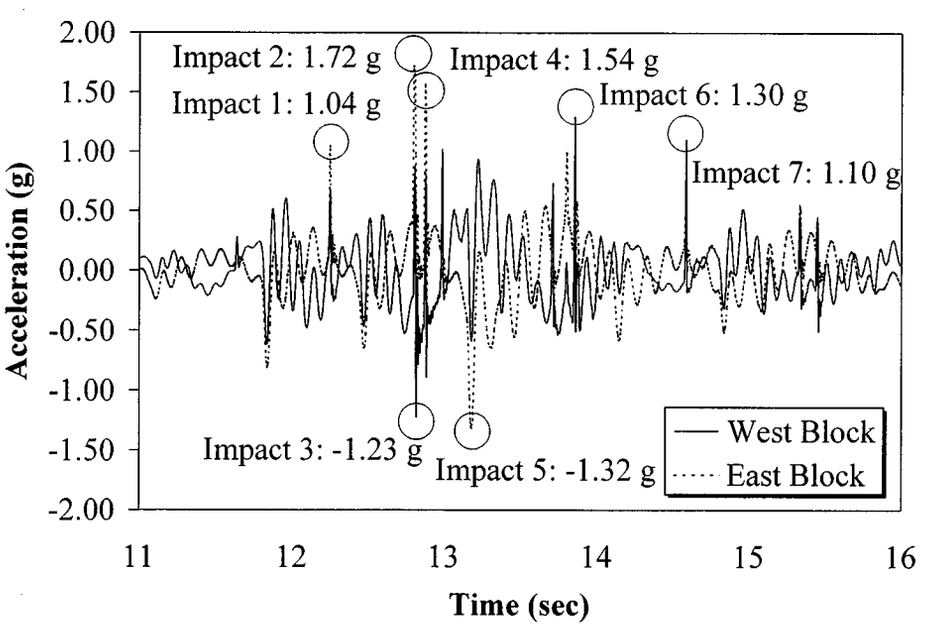

FIGURE 4-65 Block Accelerations History for Run V3

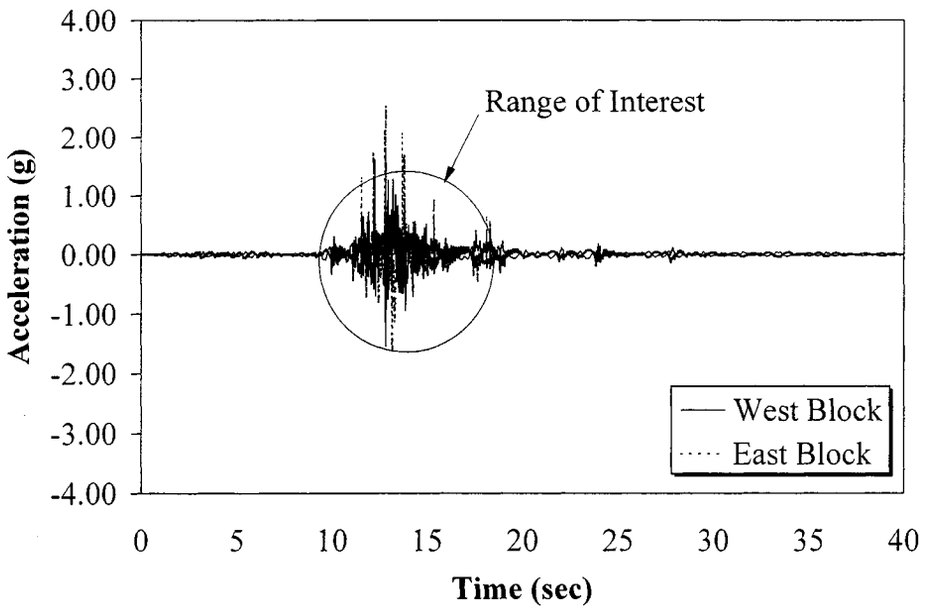

FIGURE 4-66 Block Accelerations History for Run V5

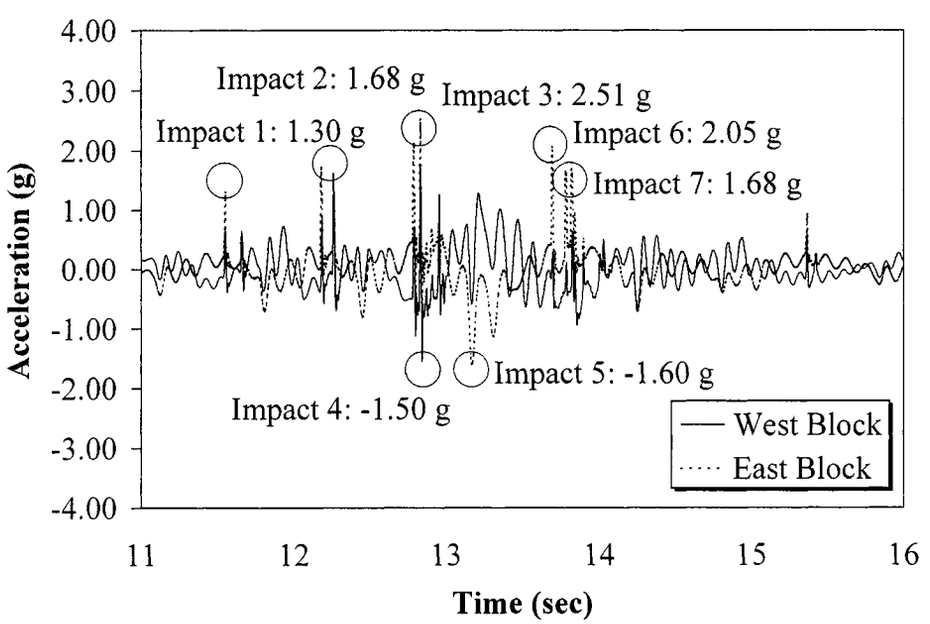

FIGURE 4-67 Block Accelerations History for Run V5

4.4.2 Relative Displacements

The hinge relative displacement histories for the range of time during which impacts occurred are plotted in figures 4-68 to 4-70. The maximum hinge displacement approximately 8.9 mm (0.35 in) for the 0.50×Loma Prieta motion and increased to 9.7 mm (0.38 in) and 10.4 mm (0.41 in) when the specimen was subjected to the 1.00×Loma Prieta and 1.50×Loma Prieta excitations, respectively. One can see the trend for small increase of the peak displacement with increasing input acceleration, which was also observed in the previous test series. It can be also observed that the maximum hinge displacements proved to be almost insensitive to the number of restrainers when the restrainer gap was adjusted to zero. Furthermore, even in the most critical case, the segments did not become unseated.

Figures 4-71 to 4-73 show the displacement histories of the two blocks relative to the shake table. It is important to note that, even two restrainer cables were capable of preventing notable out-of-phase motion of the two blocks. Regarding the magnitudes of the displacements undergone by the blocks, the case of the two restrainer cables showed similar trends with the case of six restrainer cables. The east block experienced slightly higher relative displacements due to its flexible supports. The displacements for both blocks ranged from 38 mm (1.5 in) to 140 mm (5.5 in) and their magnitude increased with the magnitude of the input accelerations.

4.4.3 Restrainer Elongation and Forces

The restrainer elongation histories are presented in figures 4-74 to 4-76. It should be noted that, as indicated by equation (2-10), the restrainer yield displacement is independent of the number of

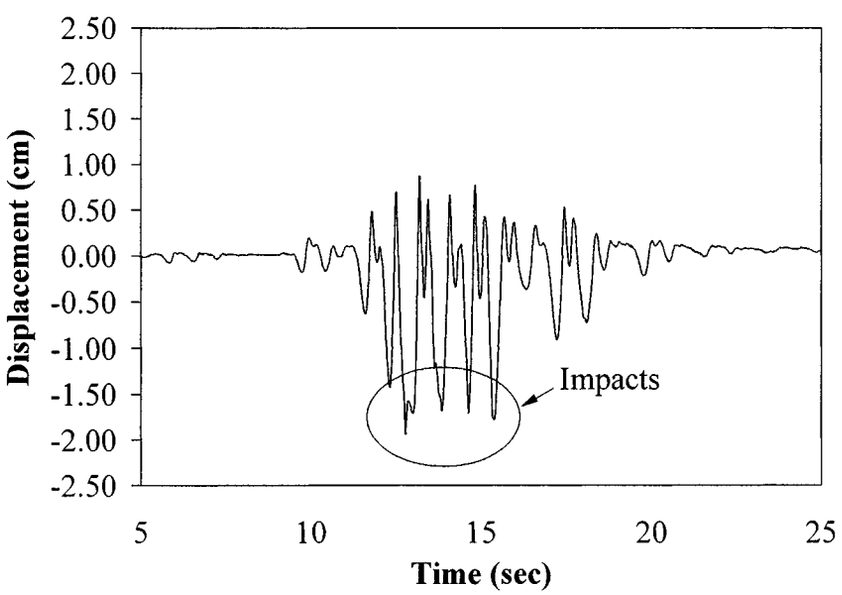

FIGURE 4-68 Hinge Relative Displacement History for Run V1

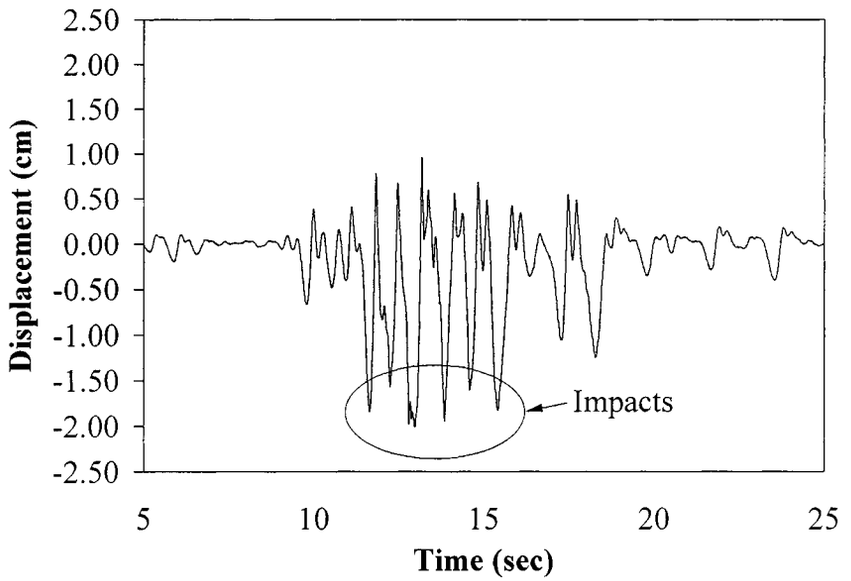

FIGURE 4-69 Hinge Relative Displacement History for Run V3

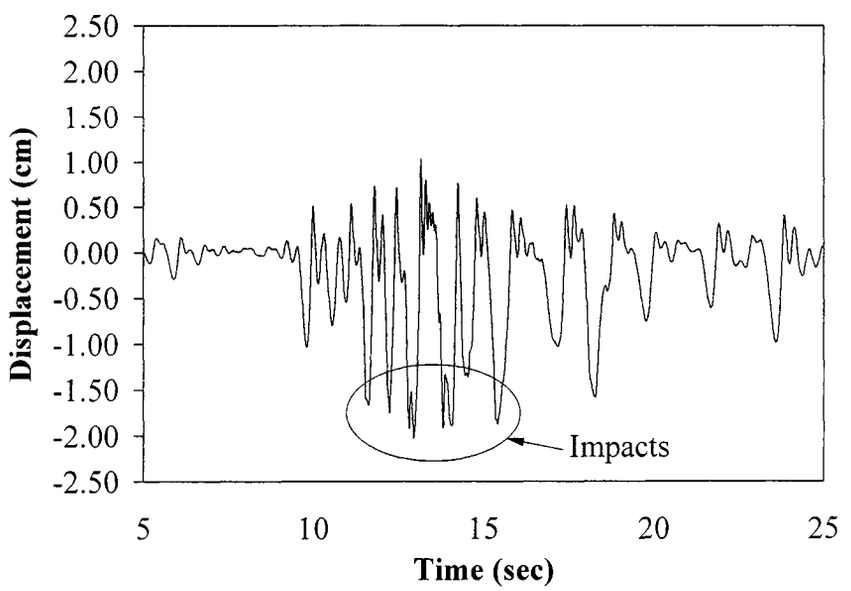

FIGURE 4-70 Hinge Relative Displacement History for Run V5

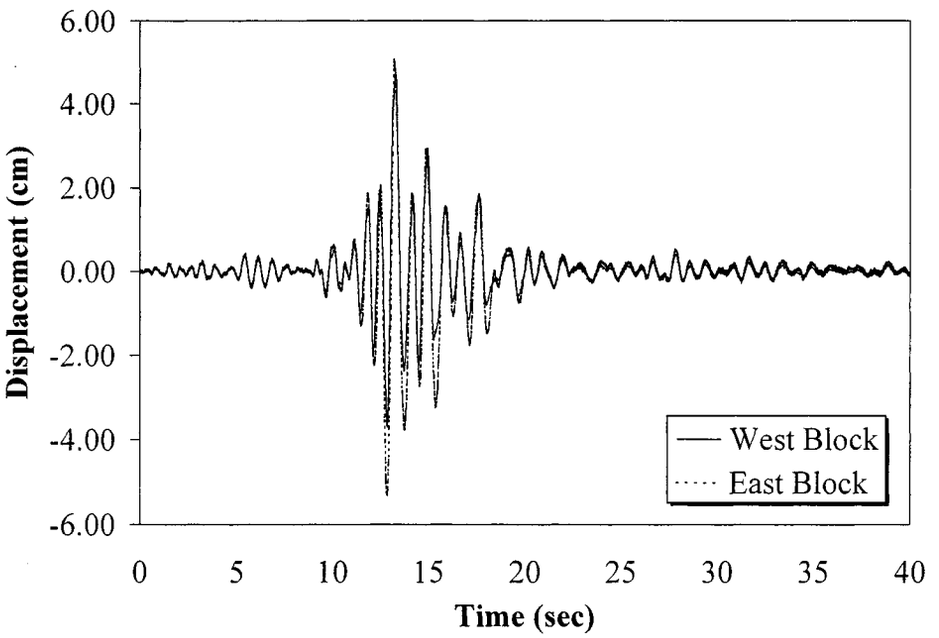

FIGURE 4-71 Block Displacements Relative to the Shake Table History for Run V1

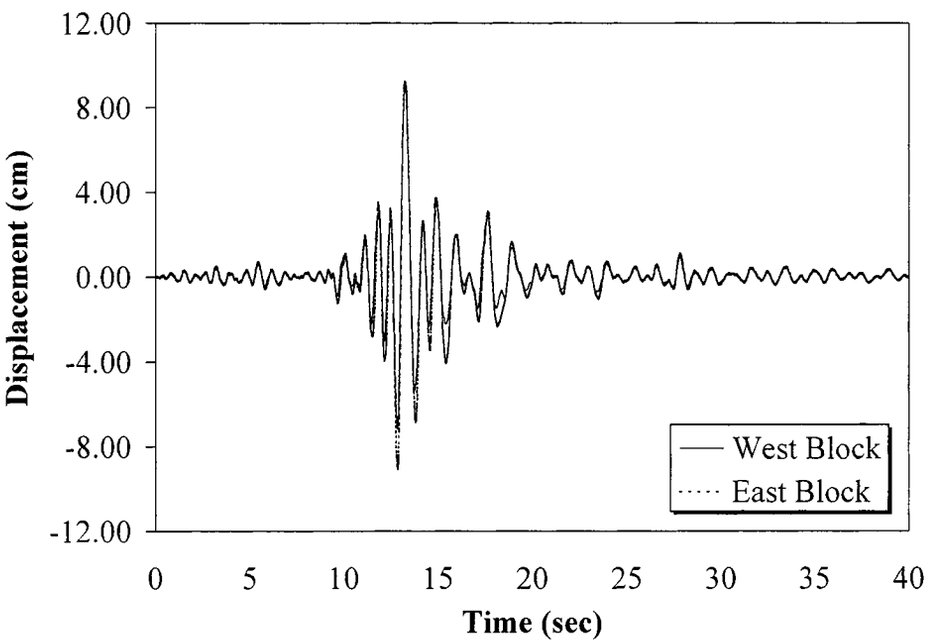

FIGURE 4-72 Block Displacements Relative to the Shake Table History for Run V3

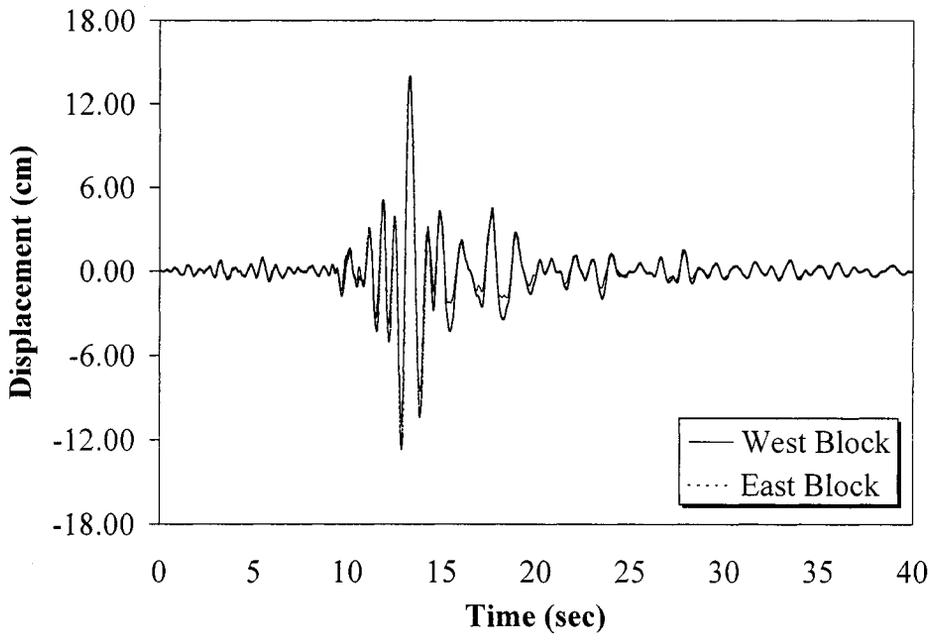

FIGURE 4-73 Block Displacements Relative to the Shake Table History for Run V5

restrainers used. Therefore, similarly to the case of six restrainer cables, the restrainers were considered to yield as soon as they reached the scaled yield deformation value of 8.8 mm (0.35 in). Restrainers almost yielded during the 0.50×Loma Prieta excitation, while they well passed the yield point during both the 1.00×Loma Prieta and the 1.50×Loma Prieta motions. According to equation (4-2), the scaled restrainer yield force, F_y, is directly proportional to the number of restrainers. Therefore, F_y is 87.0 KN (19.6 kips), which is equal to 1/3 of the yield force for six restrainers. Figures 4-77 to 4-79 show the restrainer force histories. Since the restrainer slack was set to zero, the restrainers were engaged as soon as they were stretched. The maximum restrainer force exceeded the scaled yield force by 9 percent in the 1.00×Loma Prieta motion and by 18 percent in the 1.50×Loma Prieta motion. It should be noted that, because restrainers were not scaled, they did not actually yield and, therefore, they continued to take forces even after they reached the scaled yield point. If the restrainers had actually yielded, the force build up would have been less. Furthermore, restrainer failure could have occurred.

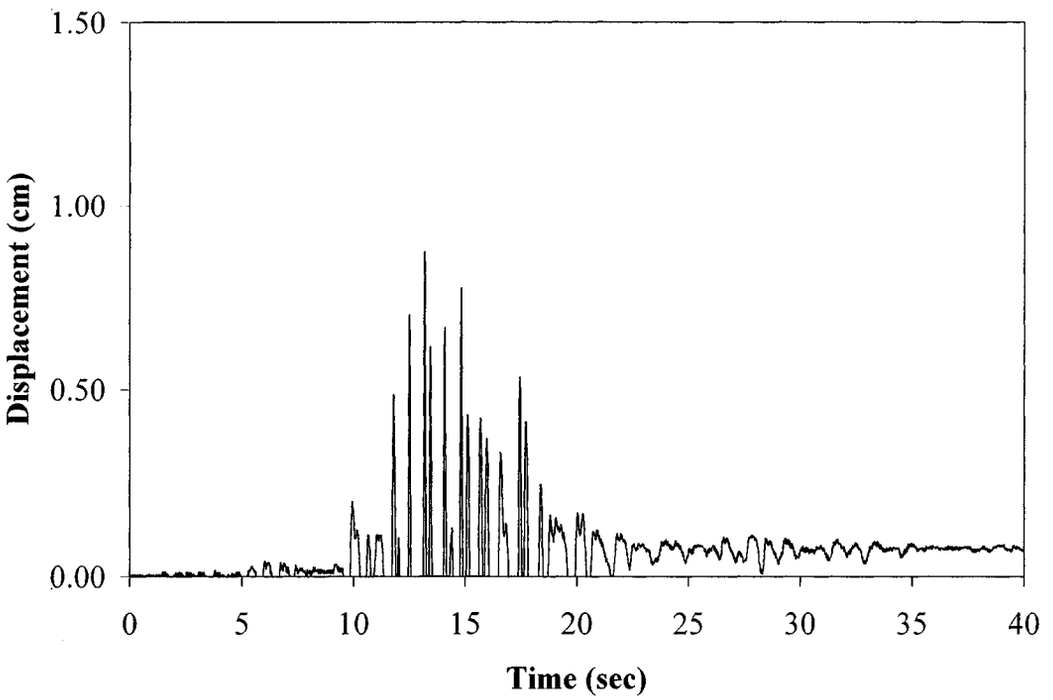

FIGURE 4-74 Restrainer Cable Elongation History for Run V1

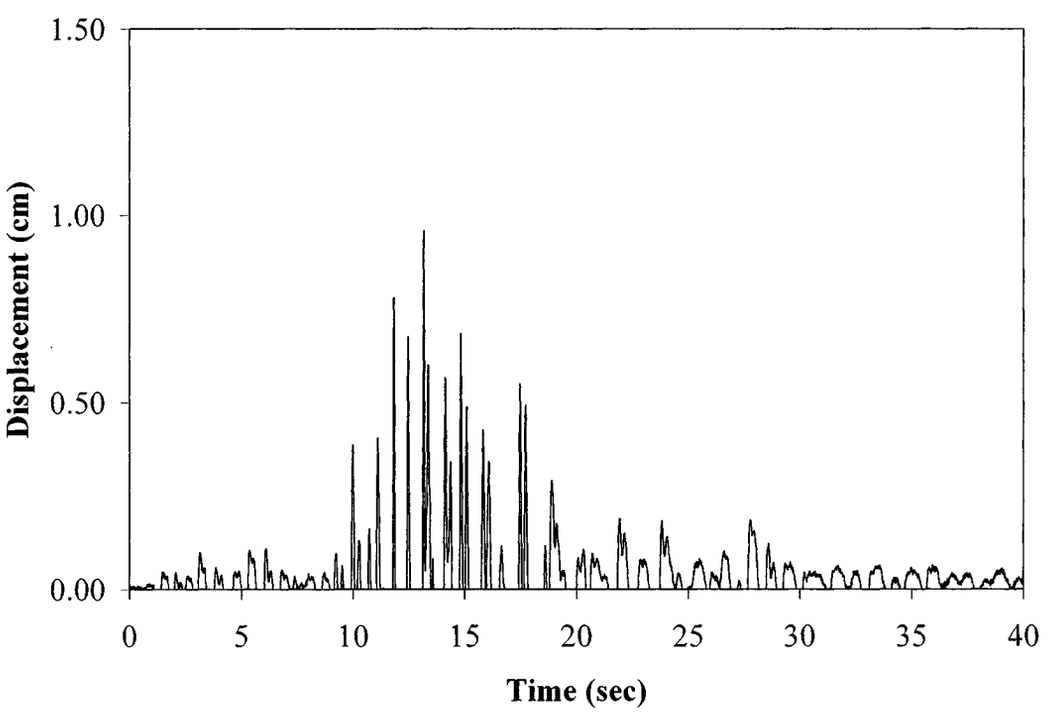

FIGURE 4-75 Restrainer Cable Elongation History for Run V3

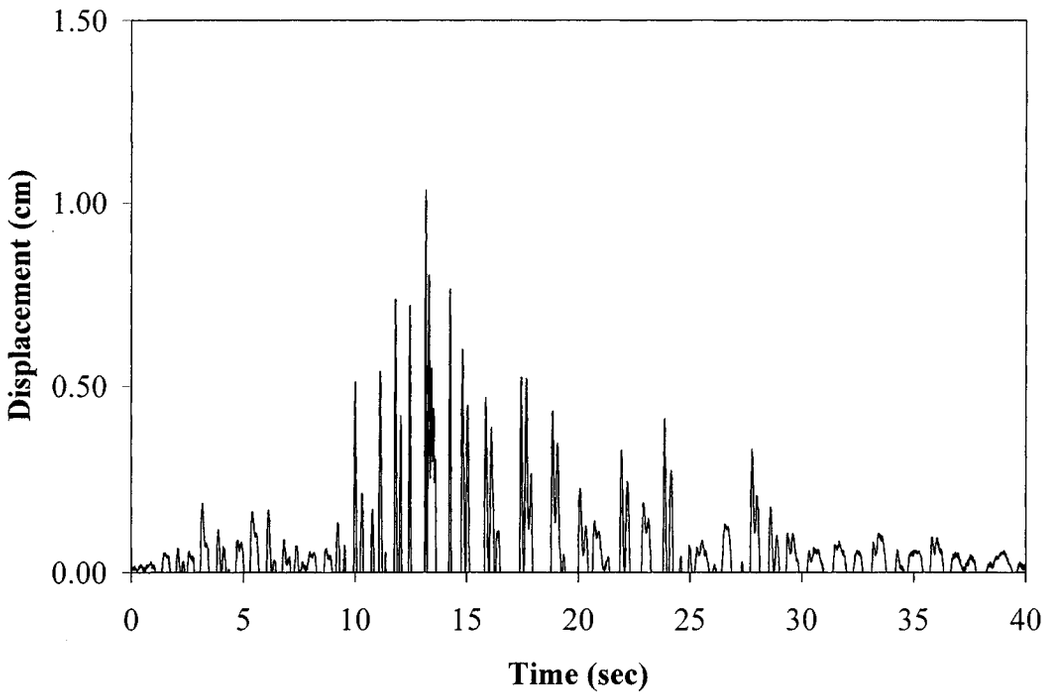

FIGURE 4-76 Restrainer Cable Elongation History for Run V5

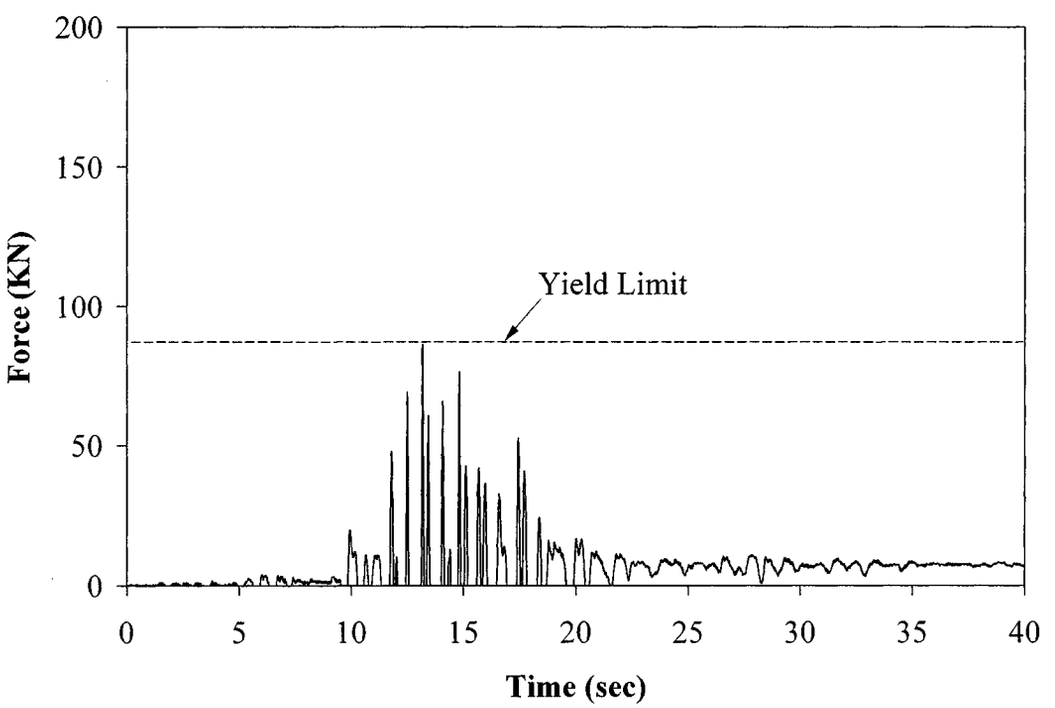

FIGURE 4-77 Restrainer Cable Force History for Run V1

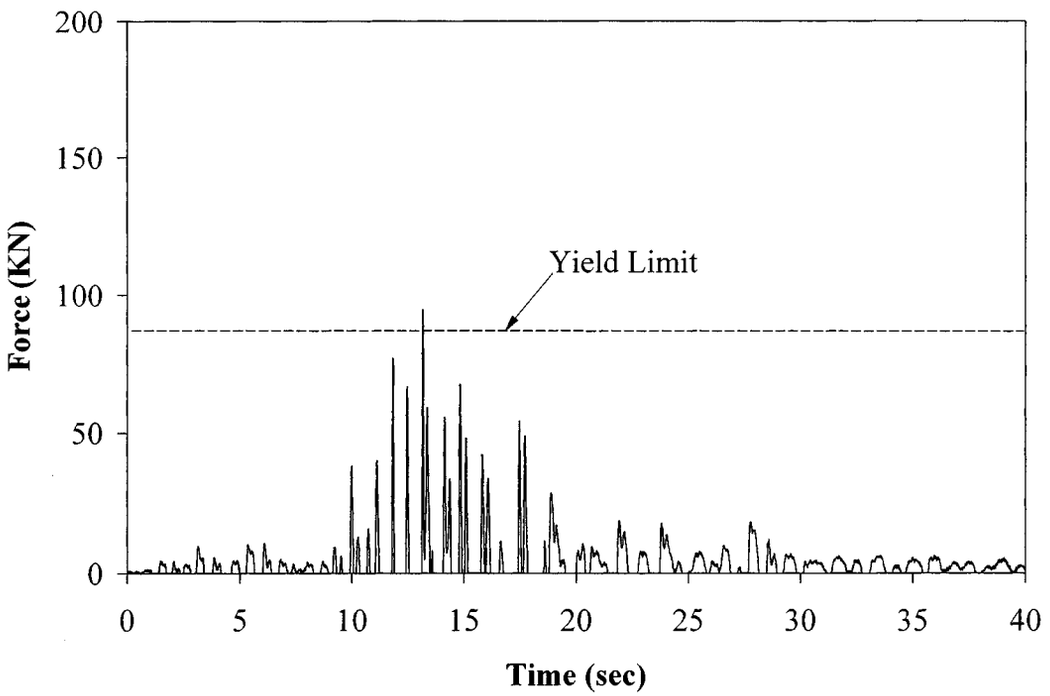

FIGURE 4-78 Restrainer Cable Force History for Run V3

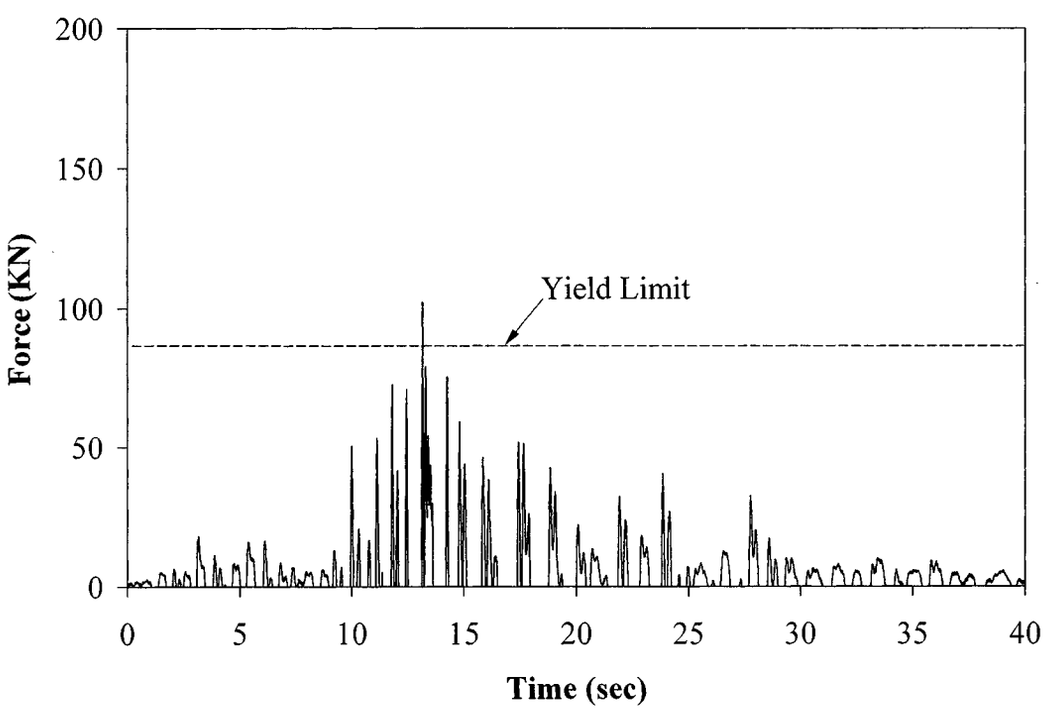

FIGURE 4-79 Restrainer Cable Force History for Run V5

4.5 Test Series VI

In test series VI the behavior of the unrestrained system was examined.

4.5.1 Absolute Accelerations

Figures 4-80 to 4-83 show the recorded acceleration histories of the two box girder segments when no restrainers were present. As indicated by the acceleration values generated during impact, the collisions between the blocks were noticeably more intense compared to the cases that had restrainers. As shown in table 4-4, even at lower amplitude motion, the two blocks experienced very high accelerations that reached 5.61 g and 5.23 g for the west and the east block, respectively. These accelerations were significantly higher than the corresponding accelerations when the two blocks were tied with restrainers. Unlike the cases with restrainers, in which the peak accelerations occurred in the east block, the peak accelerations were recorded on the west block for both the 0.50×Loma Prieta and the 0.75×Loma Prieta excitations. Furthermore, the occurrence of impacts is limited to a shorter range of time, which varies from 13 s to 14 s. Figures 4-80 to 4-83 also imply that the impacts can be divided into two main groups. Each group roughly includes three major impacts; however, the accelerations during the collisions of the second group were of higher amplitude compared to the accelerations in the first group. The time interval between the two groups is approximately 1 s. Another conclusion that can be drawn is that impact altered the characteristics of motion of the two blocks. As shown in figures 4-81 and 4-83, prior to the collisions, the two blocks were vibrating out-of-phase due to their individual dynamic properties. After the impacts, the blocks were still moving out-of-phase but higher frequencies were now dominating the response.

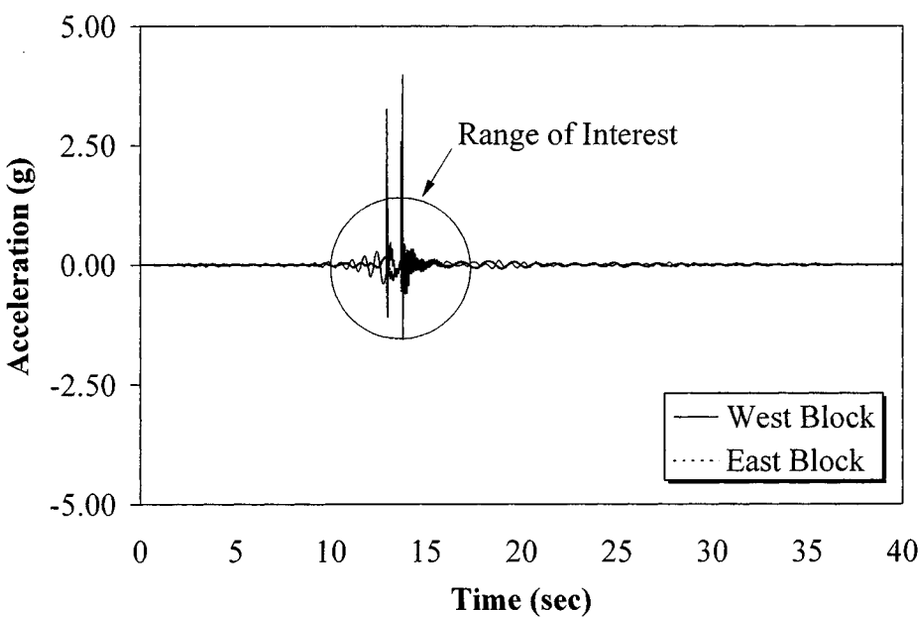

FIGURE 4-80 Block Accelerations History for Run VI1

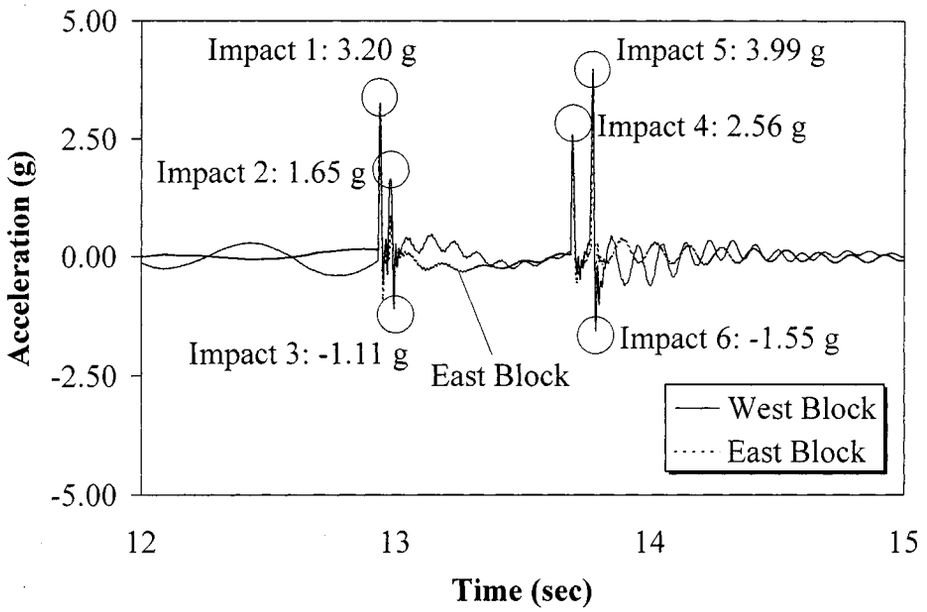

FIGURE 4-81 Block Accelerations History for Run VI1

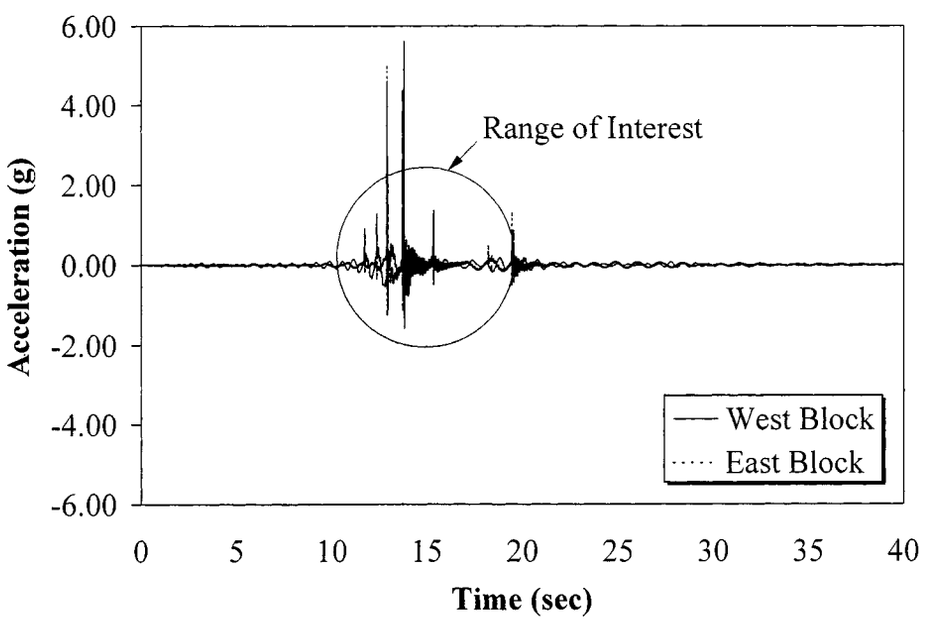

FIGURE 4-82 Block Accelerations History for Run VI2

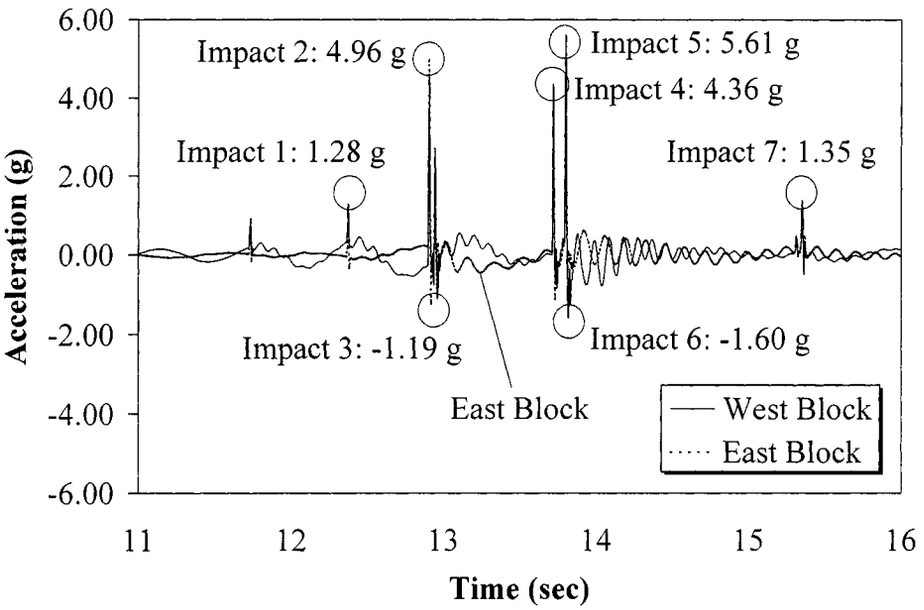

FIGURE 4-83 Block Accelerations History for Run VI2

TABLE 4-4 Maximum Recorded Accelerations for the Cases without Restrainers

Earthquake Motion	Maximum Acceleration (g)	
	West Block	East Block
0.50×Loma Prieta	3.99	3.56
0.75×Loma Prieta	5.61	5.23

4.5.2 Relative Displacements

The hinge relative displacement response for the two tests without restrainers is plotted in figures 4-84 and 4-85 and tabulated in table 4-5. In both cases, the maximum hinge displacement exceeded the scaled seat width value of 65 mm (2.6 in). Therefore, if the built seat width had been scaled down, the two blocks would have become unseated. The absence of restrainers resulted in a 13 mm (0.5 in) residual displacement after the completion of the 0.50×Loma Prieta run. As a consequence, the minimum recorded hinge displacement in the 0.75×Loma Prieta motion was 42 mm (1.64 in), higher than the assumed expansion joint gap of 25.4 mm (1 in).

TABLE 4-5 Recorded Hinge Displacements for the Cases without Restrainers

Earthquake Motion	Hinge Displacement (mm)	
	Maximum	Minimum
0.50×Loma Prieta	108.8	-27.9
0.75×Loma Prieta	116.2	-41.7

Figures 4-86 and 4-87 show the two block displacement histories relative to the shake table. Note that, unlike the cases with restrainers, the two blocks experienced notable out-of-phase motion prior to collision due to their different dynamic properties and the lack of restrainers. However, as was also indicated by the acceleration records, the features of the out-of-phase motion changed after the impact. This observation is more obvious for the east block, which underwent significantly higher displacements after its collisions with the west block. Generally, the two blocks experienced much higher relative displacements when they were unrestrained. As shown in table 4-6, the maximum displacements ranged from 61 mm (2.4 in) to 84 mm (3.3 in) and from 95 mm (3.7 in) to 132 mm (5.2 in) for the west and the east block, respectively. The corresponding values for the restrained cases were: 46 mm (1.8 in) to 69 mm (2.7 in) and 50 mm (1.9 in) to 71 mm (2.8 in), for six restrainers with zero restrainer gap, and, 48 mm (1.9 in) to 70 mm (2.8 in) and 53 mm (2.1 in) to 74 mm (2.9 in), for two restrainers and zero restrainer gap.

TABLE 4-6 Displacements of the Blocks Relative to the Shake Table for the Cases without Restrainers

Earthquake Motion	Maximum Displacement (mm)	
	West Block	East Block
0.50×Loma Prieta	61.4	95.4
0.75×Loma Prieta	83.5	131.9

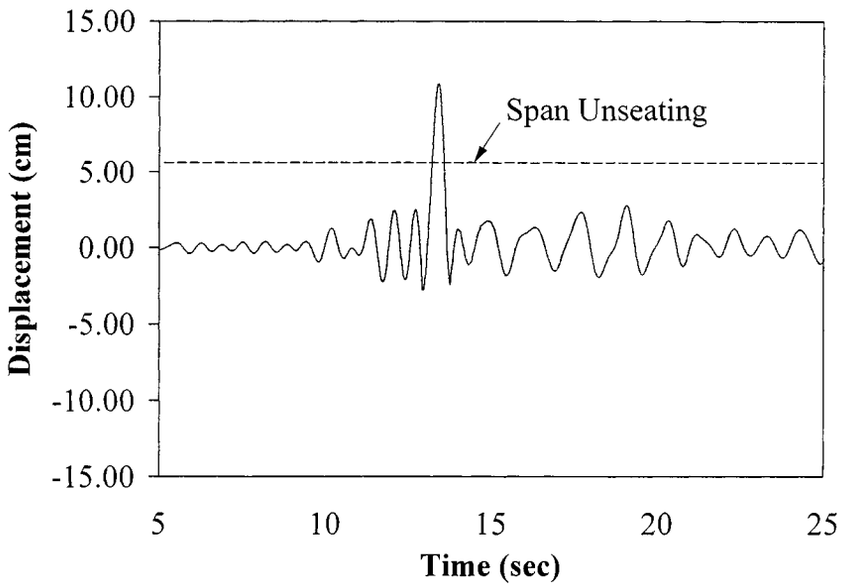

FIGURE 4-84 Hinge Relative Displacement History for Run VI1

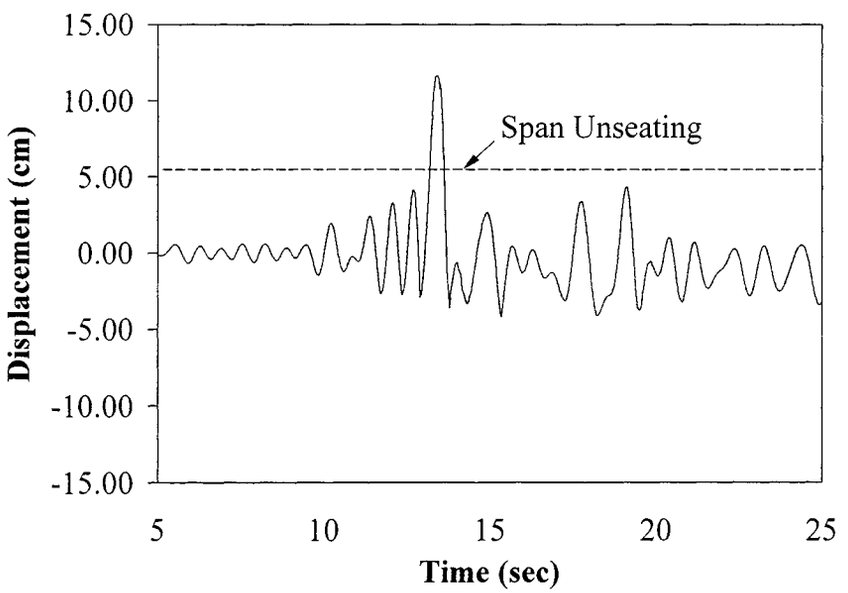

FIGURE 4-85 Hinge Relative Displacement History for Run VI2

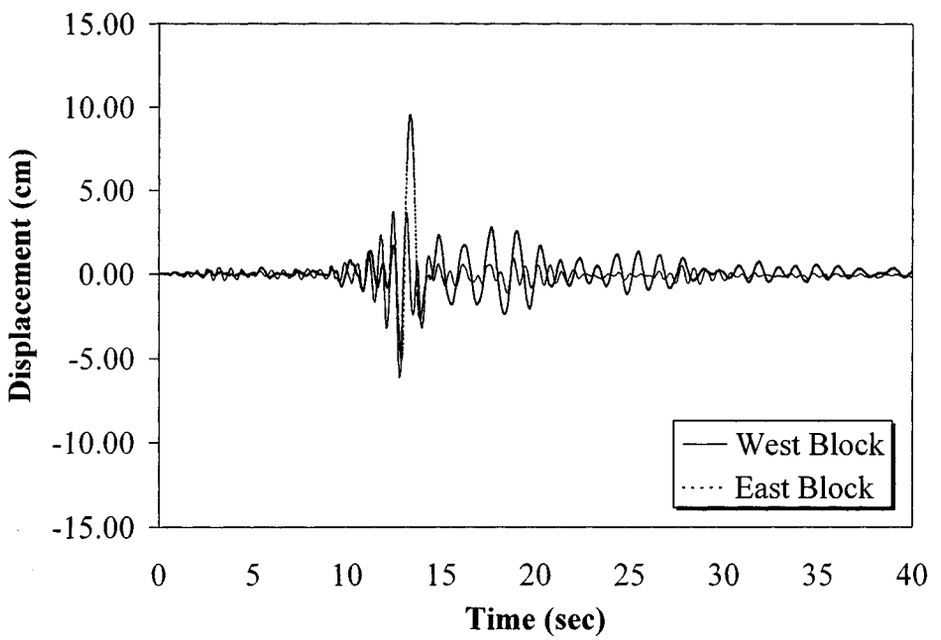

FIGURE 4-86 Block Displacements Relative to the Shake Table History for Run VI1

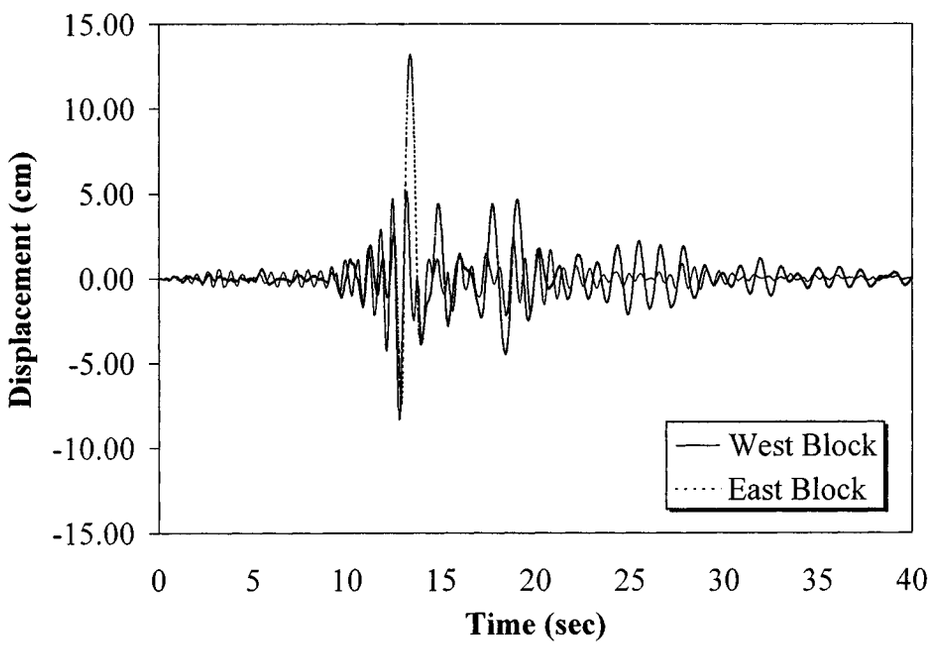

FIGURE 4-87 Block Displacements Relative to the Shake Table History for Run VI2

4.6 Comparison between the Results of All Test Series

4.6.1 Maximum Accelerations

The maximum recorded accelerations of the two blocks as a function of the input peak ground acceleration for six restrainers and the three values of the restrainer gap are given in figures 4-88 and 4-89. In all the cases the maximum acceleration values were recorded during impact. The main trend, which is observed in both plots, is that increasing the input acceleration resulted in increasing the block acceleration. However, when the restrainer gap was not zero, the block accelerations were reduced for input accelerations greater than 0.30 g. It can be also seen that the rate of increase of the block acceleration with the input acceleration is more significant for higher values of restrainer gap. This can be mainly attributed to the fact that, for zero or very small values of initial restrainer slack, the restrainers are activated almost immediately after the two adjacent bridge spans start moving away from each other, and, therefore, provide a better restraint to the system. As a result, the two frames are forced to vibrate in-phase and the intensity of the impacts between the segments is mitigated. Of course, this phenomenon, which is relatively easy to understand in the case of two frames only, becomes more complex for multi-span bridges because several spans can collide to each other. Furthermore, in the latter case the abutments are also involved. The involvement of abutments can further complicate the sequence of impacts that can take, since they add to the longitudinal stiffness and strength of the system.

Figures 4-90 and 4-91 show the maximum impact accelerations for the three different cases with variable number of restrainers examined in this study. As it can be observed in figure 4-90, the recorded maximum accelerations, which occurred in the unrestrained system, were roughly three times higher than the impact accelerations when restrainers were used. According to figure 4-91, the effect of the number of restrainers on the impact acceleration is not significant. However, the two blocks generally experienced higher accelerations when they were restrained with six cables.

4.6.2 Maximum Displacements

The maximum displacements of the two blocks relative to the shake table versus the input acceleration for six restrainer cables and varying restrainer gaps are plotted in figures 4-92 and 4-93. It can be seen that the relationship between the input peak ground acceleration and the block displacement is linear. It should be noted that, since the two blocks were practically rigid, the deformations were exclusively undergone by the elastomeric pads. Since the bearings were not equipped with any device for energy dissipation and the rubber damping ratio was relatively small, it was presumed that they would behave in a linear elastic manner. Based on figures 4-92 and 4-93, this assumption was verified. It can be also observed that, unlike the output

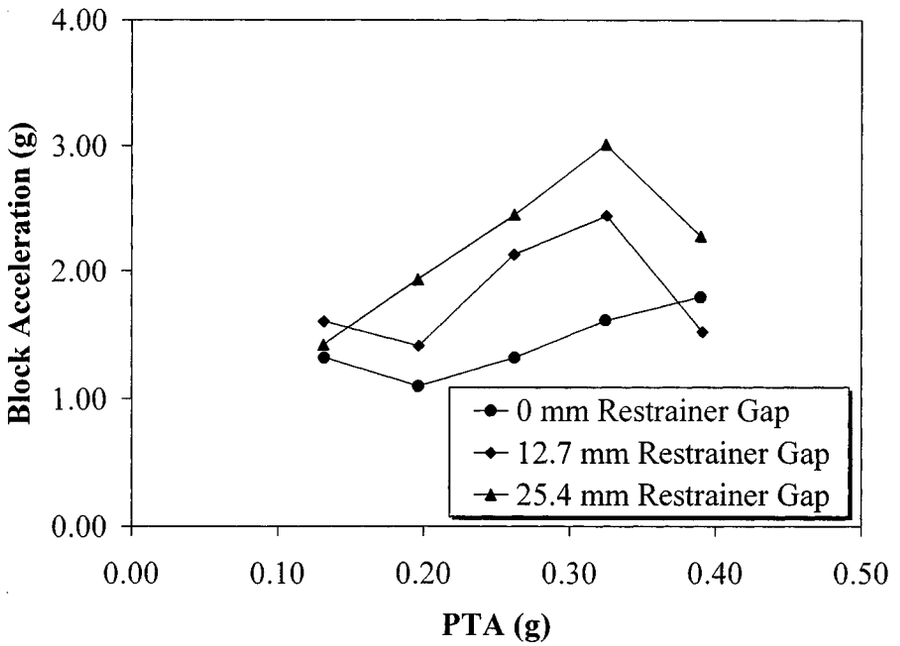

FIGURE 4-88 West Block Maximum Acceleration vs. Input Acceleration (6 Restrainer Cables)

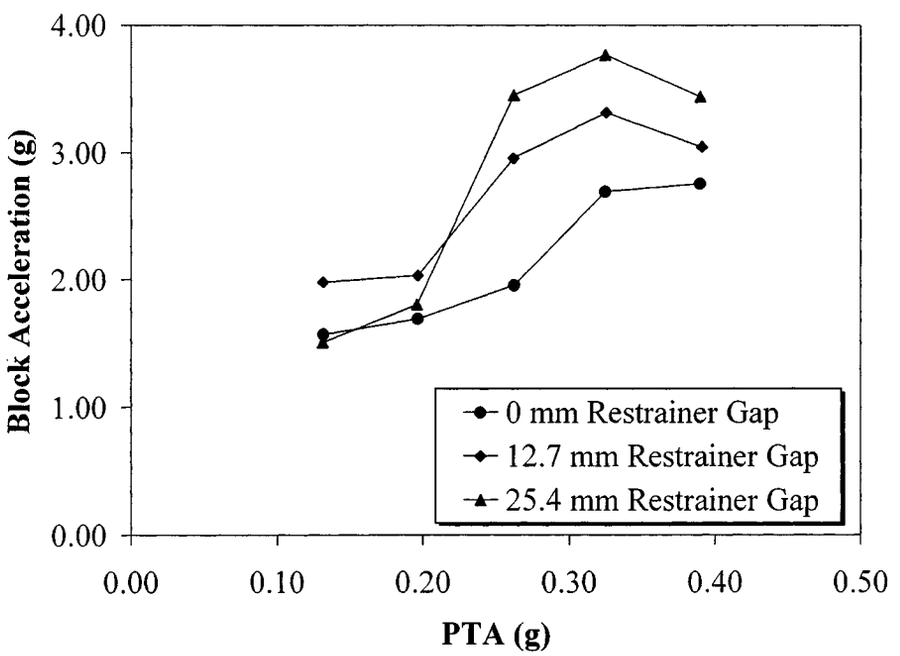

FIGURE 4-89 East Block Maximum Acceleration vs. Input Acceleration (6 Restrainer Cables)

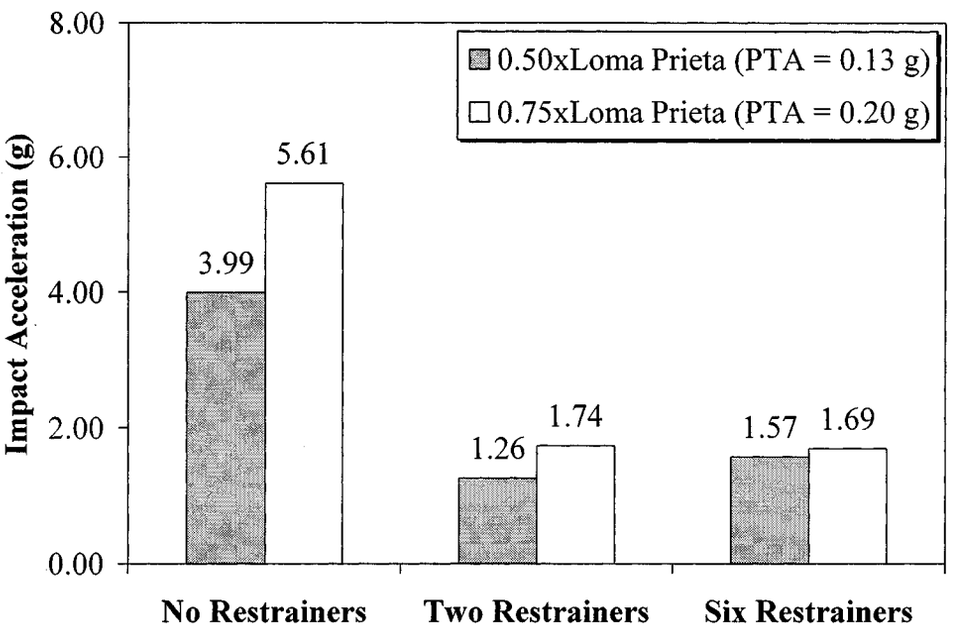

FIGURE 4-90 Envelope of Maximum Impact Acceleration vs. Number of Restrainers – All Cases (0 mm Restrainer Gap)

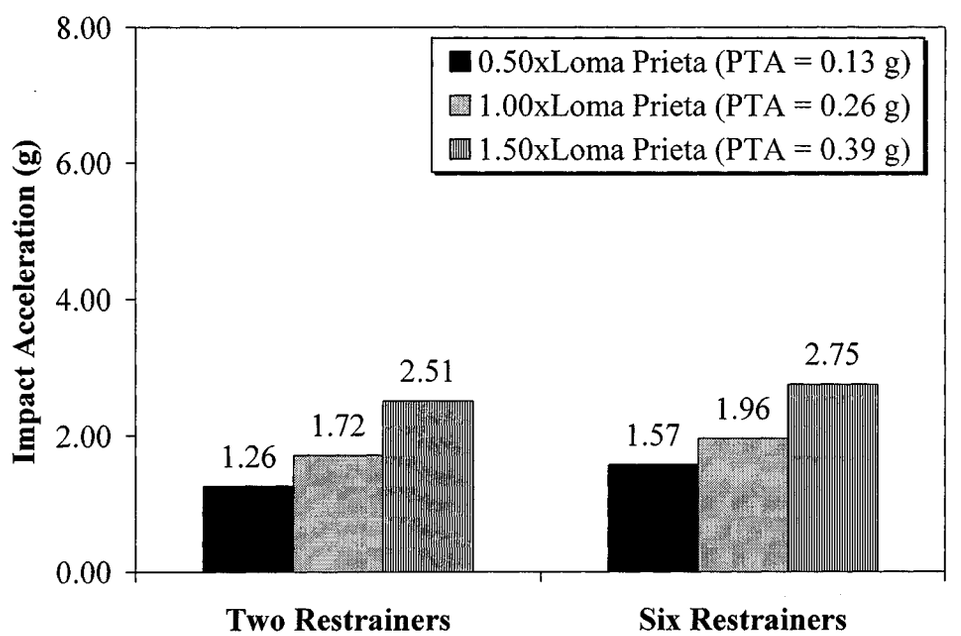

FIGURE 4-91 Envelope of Maximum Impact Acceleration vs. Number of Restrainers – Cases with Restrainers (0 mm Restrainer Gap)

accelerations, the block displacements were practically unaffected by the variations in the restrainer gap. In addition to figures 4-92 and 4-93, figures 4-94 and 4-95 show the force-displacement relationships of the west and the east block, respectively, for the first five seconds of run IV1. It can be easily seen that there was not any apparent loop formation and, therefore, the assumption of not significant energy dissipation was further confirmed. Based on these figures, the effective stiffness of the elastomeric bearings was calculated to be approximately 969 KN/m (5.5 kips/in) and 1039 KN/m (5.9 kips/in) for the west and the east block, respectively. These stiffness values are higher than the expected values based on the design bearing stiffness. However, this can be mainly attributed to the fact that the presented stiffness calculation was made at very small displacements, while the design stiffness was based on large displacements, in which some stiffness degradation was presumed.

In figures 4-96 and 4-97, the maximum relative displacements at the hinge are plotted as a function of the number of restrainers. The unrestrained system experienced much higher hinge relative displacements compared to the two restrained cases. As shown in figure 4-96, for both earthquake motions, the recorded displacements of the unrestrained system were twice as much as the scaled seat width value. This implies that in the case of a real bridge, the available seat width would have been inadequate and the bridge spans would have become unseated. On the contrary, when restrainers were used, the hinge displacements were relatively small and span unseating did not occur. Finally, the effect of the number of restrainers on the hinge relative displacement was rather insignificant.

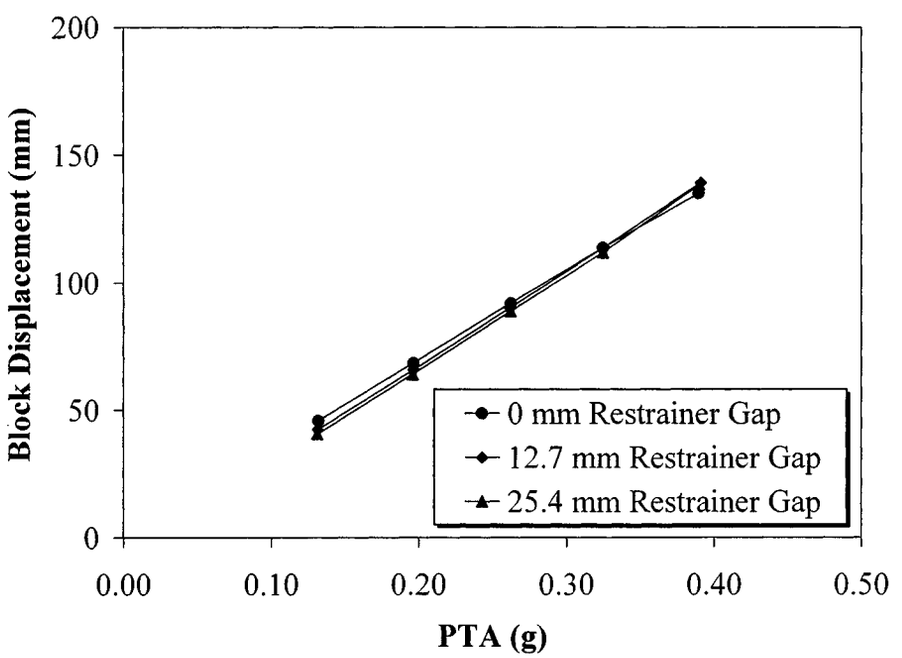

FIGURE 4-92 West Block Maximum Displacement Relative to the Shake Table vs. Input Acceleration (6 Restrainer Cables)

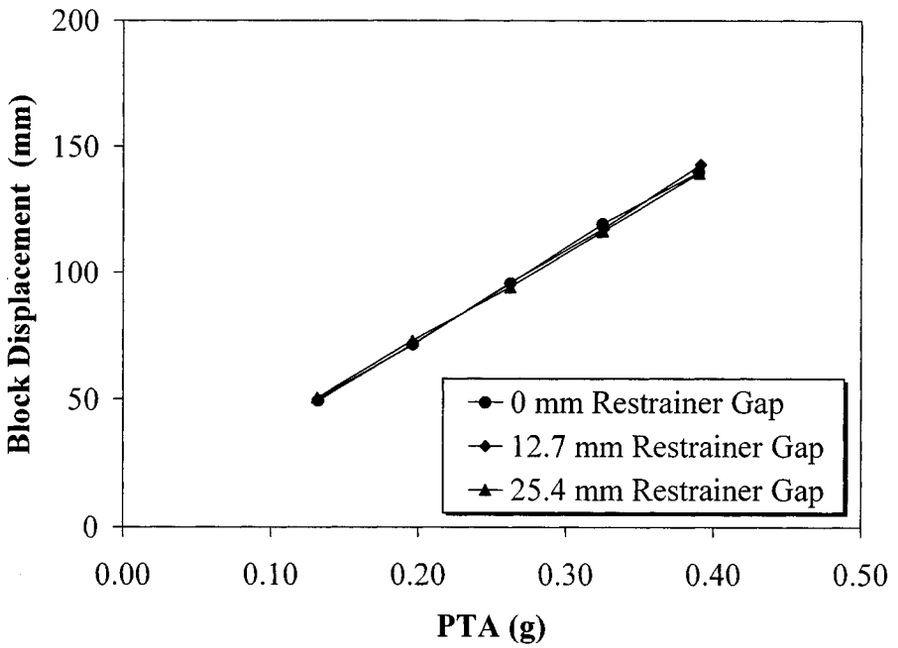

FIGURE 4-93 East Block Maximum Displacement Relative to the Shake Table vs. Input Acceleration (6 Restrainer Cables)

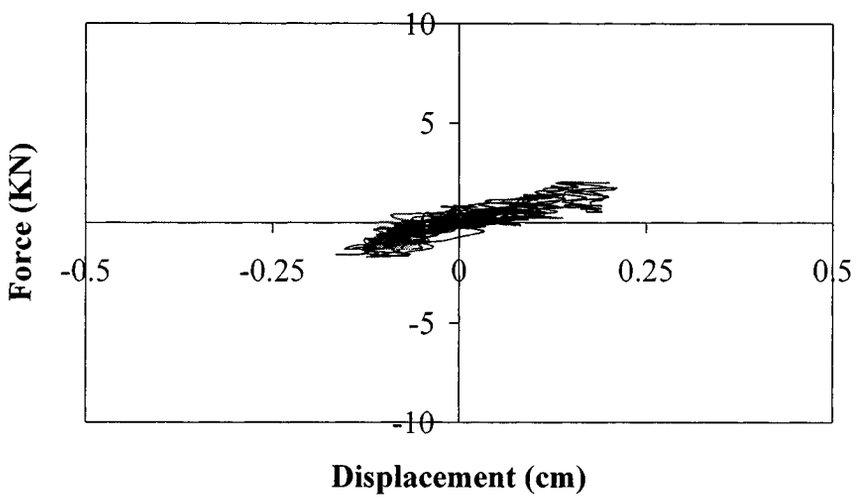

FIGURE 4-94 West Block Force-Displacement Relationship (0-5 s, Run IV1)

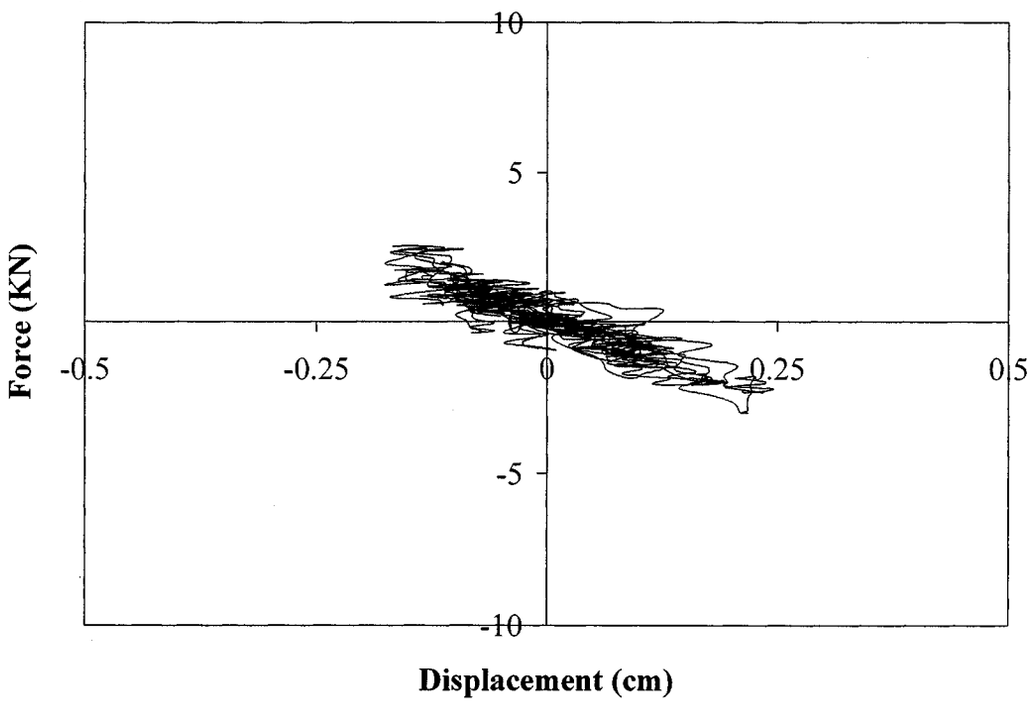

FIGURE 4-95 East Block Force-Displacement Relationship (0-5 s, Run IV1)

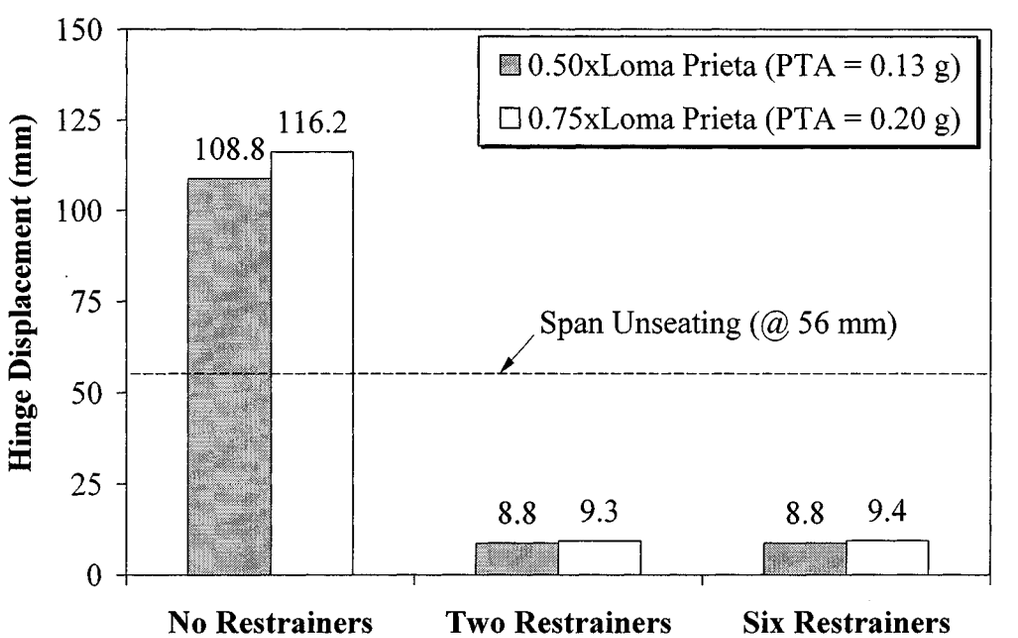

FIGURE 4-96 Envelope of Maximum Relative Displacement at Hinge vs. Number of Restrainers – All Cases (0 mm Restrainer Gap)

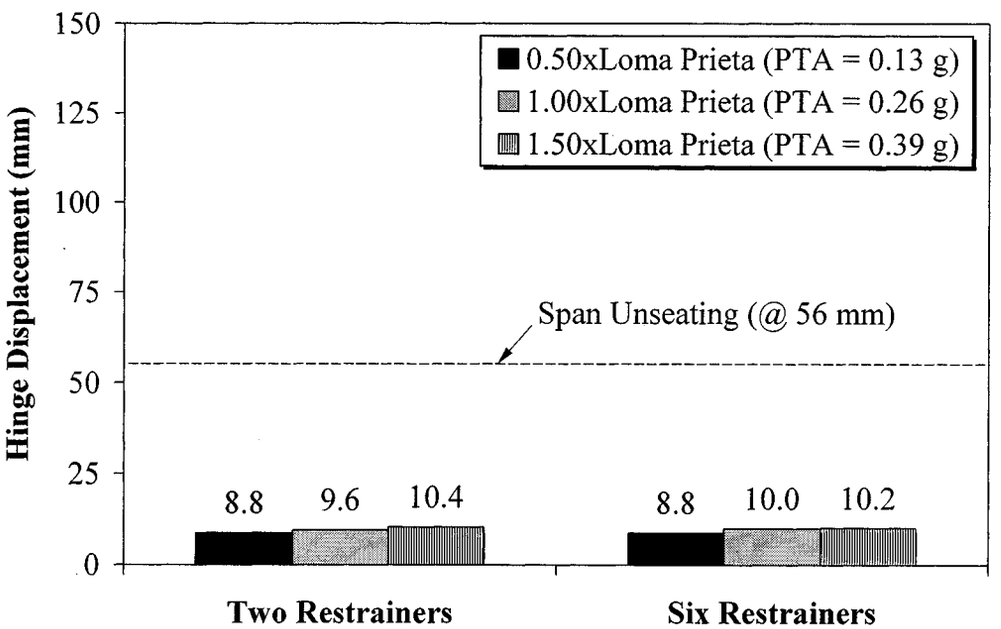

FIGURE 4-97 Envelope of Maximum Relative Displacement at Hinge vs. Number of Restrainers – Cases with Restrainers (0 mm Restrainer Gap)

4.6.3 Maximum Restrainer Forces and Ductilities

Figure 4-98 shows the maximum calculated restrainer force versus the input acceleration for three restrainer gap values and six restrainers. The yield force is based on scaled values. The restrainers did not actually yield during the tests. It can be observed that restrainer yielding is inversely proportional to the restrainer gap It can be observed that restrainer yielding is inversely proportional to the restrainer gap. Restrainers yielded for peak ground accelerations equal to approximately 0.15 g, 0.25 g, and 0.35 g, corresponding to 0 in (0 mm), 0.5 in (12.7 mm), and 1 in (25.4 mm) restrainer gaps, respectively.

The envelopes of the total maximum restrainer force as a function of the number of restrainers are given in figure 4-99. Based on figure 4-99, it can be seen that, for all the input motions, the ratio of the maximum force corresponding to six cables over the maximum force corresponding to two cables was approximately equal to three, which is also the ratio of the number of restrainers utilized in each case. This observation can lead to the conclusion that the problem under consideration is linear in terms of the number of restrainers used, and, that the cable stress levels in the case with two restrainers were close to those in the case with six restrainers.

The maximum restrainer ductility is defined as the ratio of the maximum restrainer displacement over the restrainer displacement at yield. Because the restrainers did not actually yield during the tests, the ductilities discussed in this section were lower than the values expected in a system with yielding cables. The peak restrainer ductilities for all the cases with six restrainers are

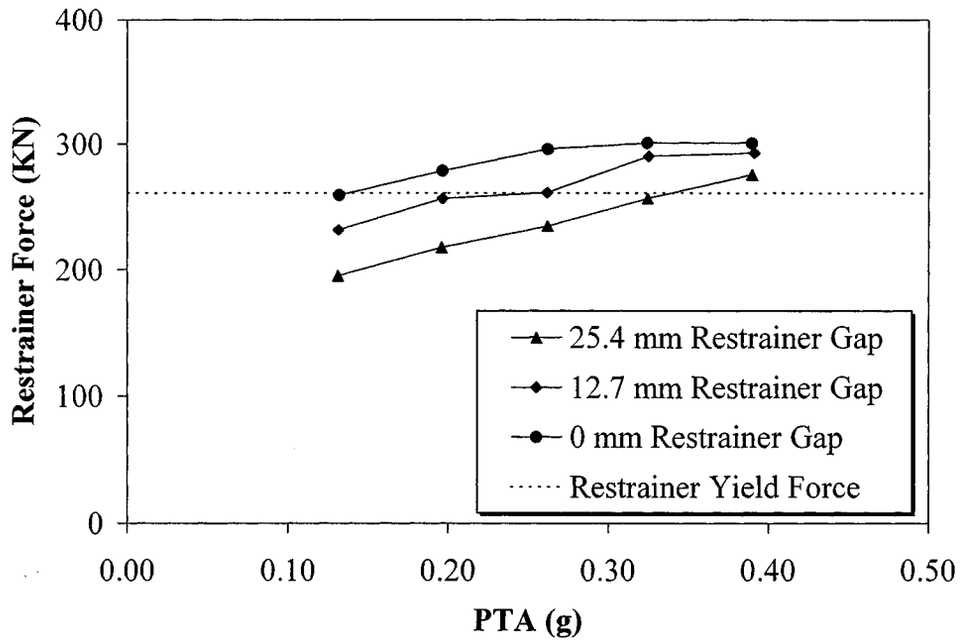

FIGURE 4-98 Maximum Restrainer Force vs. Input Acceleration (6 Restrainer Cables)

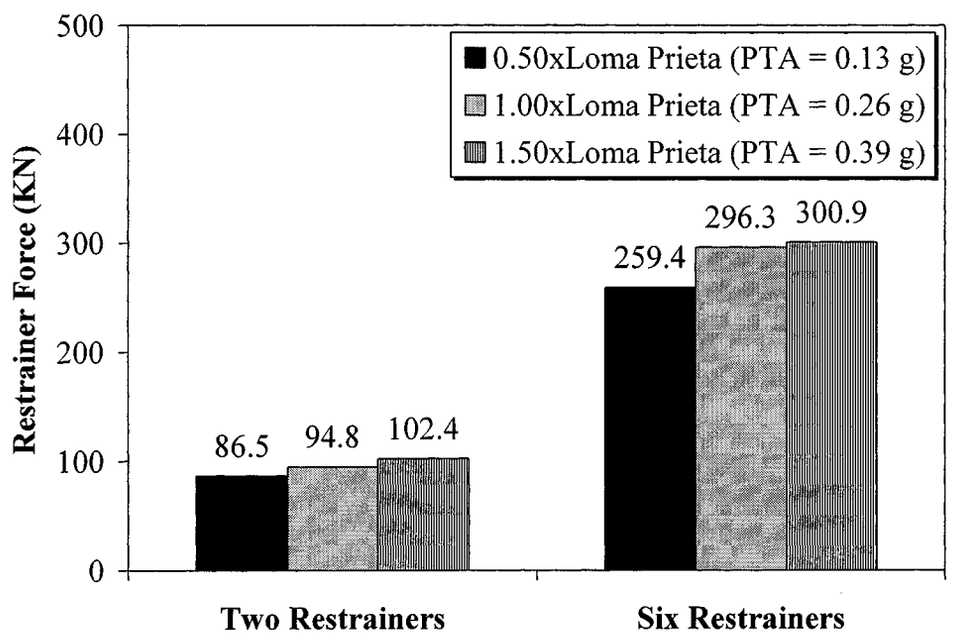

FIGURE 4-99 Envelope of Maximum Restrainer Force vs. Number of Restrainers (0 mm Restrainer Gap)

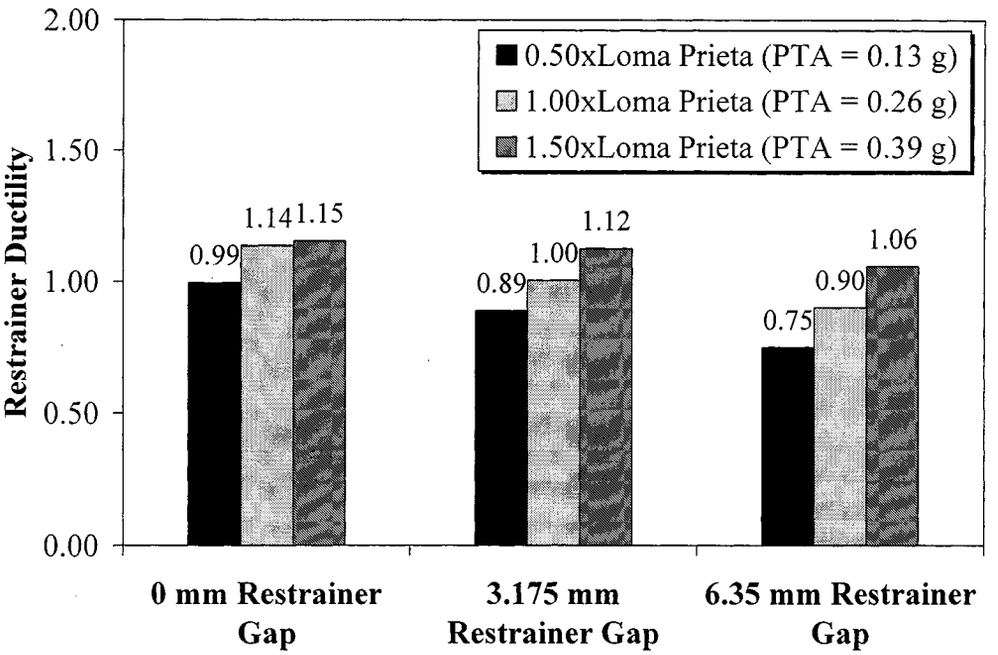

FIGURE 4-100 Envelope of Maximum Restrainer Ductility vs. Restrainer Gap (6 Restrainer Cables)

shown in figure 4-100. It can be seen that the design procedure aim at keeping the restrainers elastic, which means that the ductility of restrainers should be less than one, was not accomplished. However, only when the restrainer gap was set to zero, the restrainers experienced significant yielding. In the other two cases, yielding occurred only during the high-amplitude earthquake motions.

4.6.4 In-plane Rotations

The in-plane rotations of the two blocks are given in figures 4-101 to 4-104. The in-plane rotations were calculated using the data recorded by the four Temposonic displacement transducers, which were used to measure the absolute displacements of the two blocks. If $\Delta_{i,l}$ and $\Delta_{i,r}$ are the absolute displacements measured by the two Temposonics mounted on the left and the right web of each block, respectively, at any time step i, the in-plane rotation angle, ϕ_i, can be calculated as follows:

$$\phi_i = (\Delta_{i,l}-\Delta_{i,r})/L \qquad (4\text{-}3)$$

where L is the distance between the two transducers. Since the total width of each block and the web thickness were equal to 2.0 m (78.74 ft) and 20 cm (7.87 in), respectively, L was taken equal to 1.8 m (70.87 ft). It should be noted that the equation (4-3) assumes small in-plane rotation angles, for which $\tan\phi \cong \phi$. Furthermore, the adopted sign convention results in positive angles for counterclockwise rotations and negative angles for clockwise rotations.

Figures 4-101 and 4-102 show the in-plane rotations of the west and the east block, respectively, which occurred during the 0.75×Loma Prieta motion, for the three different cases with variable number of restrainers examined in this study. As it can be observed in both plots, the in-plane rotations experienced by the unrestrained system were significantly higher compared to the in-plane rotations of the two restrained systems. Furthermore, there is not any apparent effect of the number of restrainers on the in-plane rotations of the two blocks. It can be also seen that the east block generally underwent higher in-plane rotations than the west block.

The in-plane rotations that occurred in the two blocks during the 1.50×Loma Prieta excitation are presented in figures 4-103 and 4-104. Although the two blocks experienced higher in-plane rotations than during the 0.75×Loma Prieta motion, the in-plane rotations were still considerably smaller compared to the in-plane rotations underwent by the unrestrained system during the 0.75×Loma Prieta motion. Therefore, it can be concluded that restrainers can significantly reduce the in-plane rotations, which may occur at the in-span hinges between adjacent bridge segments due to construction imperfections or random direction of the ground motion.

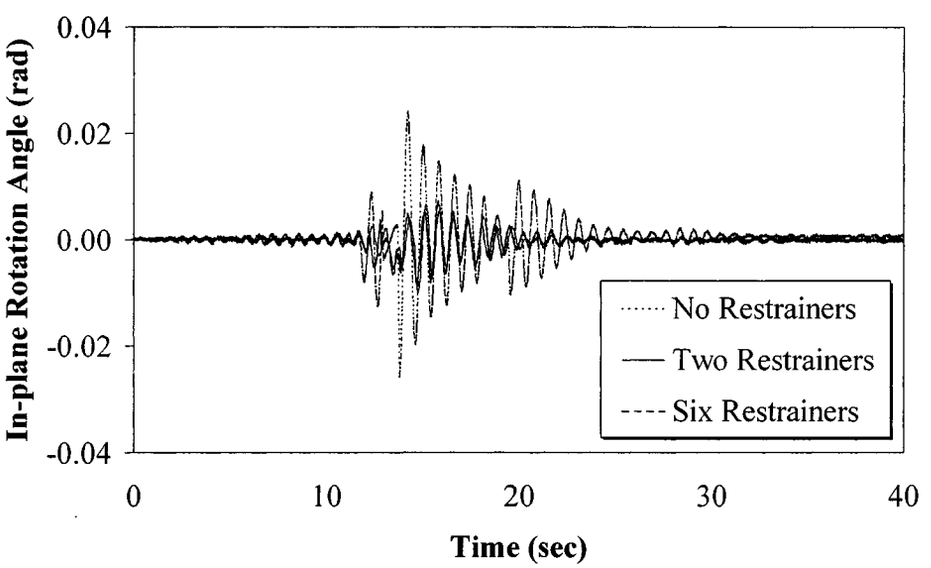

FIGURE 4-101 West Block In-plane Rotations during the 0.75×Loma Prieta Motion – All Cases (0 mm Restrainer Gap)

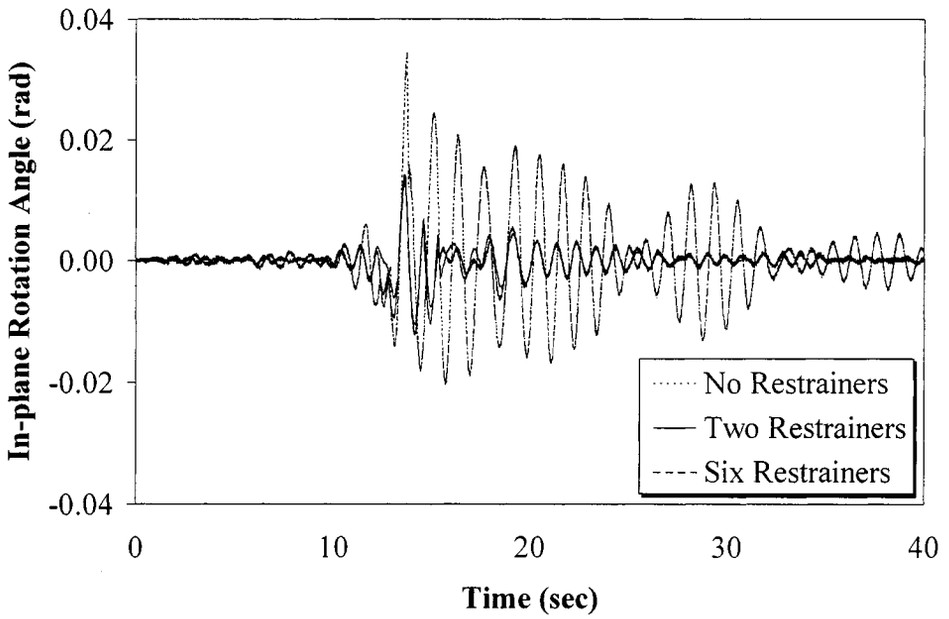

FIGURE 4-102 East Block In-plane Rotations during the 0.75×Loma Prieta Motion – All Cases (0 mm Restrainer Gap)

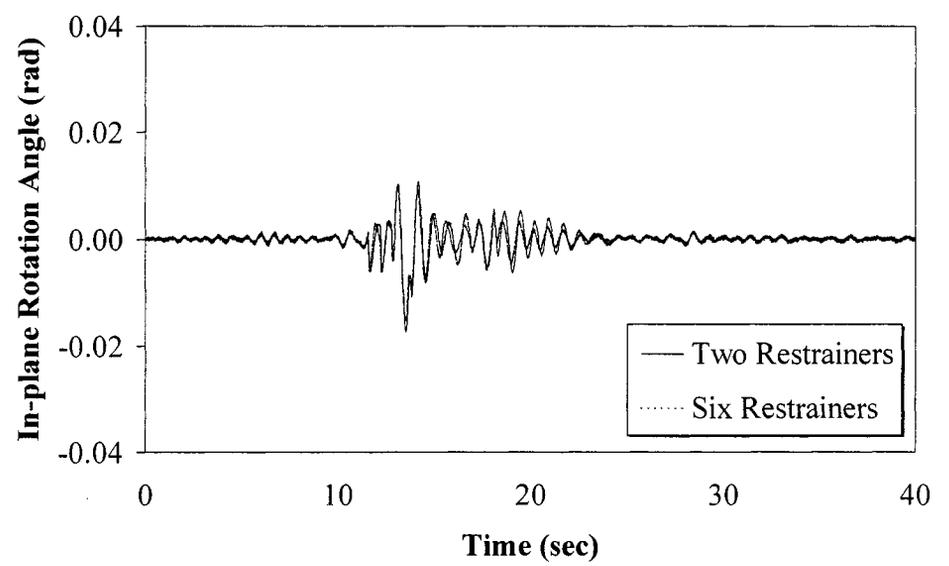

FIGURE 4-103 West Block In-plane Rotations during the 1.50×Loma Prieta Motion – Cases with Restrainers (0 mm Restrainer Gap)

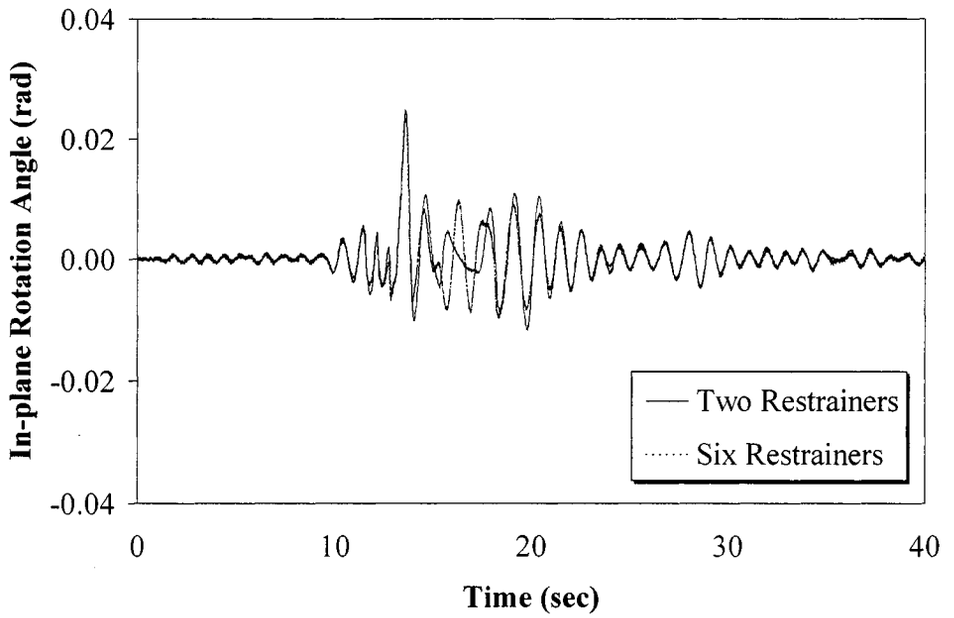

FIGURE 4-104 East Block In-plane Rotations during the 1.50×Loma Prieta Motion – Cases with Restrainers (0 mm Restrainer Gap)

SECTION 5
SUMMARY, CONCLUSIONS AND RECOMMENDATIONS

5.1 Summary

One of the most predominant bridge failure modes during the 1971 San Fernando Earthquake in California was the collapse of bridge spans due to excessive longitudinal movements, which were beyond the available seat width at expansion joints and abutments. CALTRANS has since installed seismic restrainers at narrow hinges that reduce the relative displacements across the joints and transfer longitudinal seismic forces between adjacent bridge frames. The most common type of restrainer for multi-span bridges with in-span hinges in the U.S. is the cable restrainer that uses high-strength steel cables anchored to the diaphragms or webs of concrete box girder segments.

Currently, AASHTO specifications contain a simple restrainer design method, while CALTRANS provides a more elaborate equivalent static procedure to determine the required number of restrainers for bridges with the potential to become unseated during an earthquake. Both methods have been evaluated for different types of bridges in a series of analytical studies. These studies indicated that the current methods are conservative in some cases and unconservative in others, mainly because they do not account for several parameters, which were found to significantly affect the seismic response of the restrained system. The most important of these parameters include the restrainer stiffness, the restrainer gap and the frame period ratio. As far as experimental studies are concerned, the only experimental study reported was on quasi-static cyclic behavior of in-span hinges. However, neither the dynamic response nor the response of restrainers were addressed.

The main objectives of this study were to investigate the pounding between adjacent bridge spans at in-span hinges, to evaluate the performance and efficacy of seismic restrainers in inhibiting relative displacements across the hinges, and, to assess the effects of the restrainer gap, the number of restrainers and the variations in the peak ground acceleration on the response of the hinge-restrainer system.

A portion of a reinforced concrete box girder bridge, with realistic hinge dimensions, was constructed based on a database of six representative bridges in California. Since the dynamic response in the longitudinal direction was examined and skewness effects were neglected, a longitudinal slice corresponding to 1/8 of the bridge was considered as the reference bridge to be used in this experiment. Furthermore, a scale factor of 1/4 was applied to the mass and stiffness of the two spans of the reference bridge. The specimen consisted of two concrete blocks representing the bridge spans on either side of the hinge. The blocks were supported by elastomeric bearings, simulating the stiffness of the substructure, and were placed on one shake table. Cable restrainers were used to tie the two blocks. The design of the restrainers was done according to the current CALTRANS restrainer design procedure. The number of restrainers required was multiplied by the scale factor of 1/4 to obtain the scaled restrainer stiffness, resulting in six cables. Various acceleration records were considered for being used as input excitation. Considering their peak acceleration level and frequency content, as well as the

periods of the blocks, the 1989 Loma Prieta Earthquake Record was chosen to be the record used in this experiment.

The experiments presented in this study were performed at the Large Scale Structures Laboratory at the University of Nevada, Reno. The parameters that were varied during the tests were the number of restrainer cables and the initial restrainer gap. The specimen was subjected to incrementally increasing shake table acceleration, corresponding to different multiples of the chosen reference record. The specimen was instrumented with direct current displacement transducers and variable measurement range accelerometers. The relative displacements at the hinge, the absolute displacements of the two blocks and the accelerations on the top of the specimen were measured. The restrainer forces were calculated based on the recorded restrainer displacements and the specified restrainer stiffness. The impacts between the two blocks, which occurred during the experiments, were thoroughly examined. Furthermore, restrainer yielding and span unseating were identified.

5.2 Limitations, Experimental Observations and Conclusions

The experimental study described in this report has the following limitations:

1. The actual un-scaled dimensions for the hinge width and gap as well as the restrainer properties were used in this study. Therefore, neither restrainer yielding nor span unseating were visually observed during the test. Restrainer yielding and span unseating were calculated by comparing the test results to the scaled values of restrainer yield deformation and seat width respectively. It should be noted that, in a field case, the system behavior could be substantially different after the restrainer yield, especially if the ultimate restrainer displacement is also reached. Cable failure would convert the restrainer system to unrestrained and span unseating would probably occur.
2. In order to avoid compression of the frequent content, which would significantly reduce the intensity of the impact between the two blocks as well as the chances of restrainer yielding and span unseating, it was decided to use the original un-scaled earthquake record. Therefore, the response of the system was evaluated under a worst possible scenario ground motion rather than a realistic earthquake excitation.
3. The response of in-span hinges and restrainers are influenced not only by pounding at the hinge location, but by pounding elsewhere in the superstructure, as well as the response behavior of the substructure elements. This requires a more careful consideration of the boundary conditions at the end of the tested configuration and a more accurate modeling of the substructure elements. In this test, no boundary conditions were included at the ends of the two blocks, while the whole substructure was represented by the stiffness of the elastomeric pads on which the blocks were supported. Therefore, the test specimen used in this study cannot simulate the actual response of the in-span restrainer system, but can only be used to provide information about some of its overall response characteristics and trends under a worst-case scenario excitation.

The main observations that were drawn based on the response of the specimen used in this experimental study are listed below:

1. The impact accelerations of the two blocks increased with increasing peak ground acceleration. Furthermore, the number of collisions was proportional to the levels of input acceleration.
2. The rate of increase of the impact acceleration with the peak ground acceleration was more significant for higher values of restrainer gap. However, for non-zero restrainer gaps, the measured accelerations during pounding between the adjacent bridge segments diminished after the input acceleration reached a certain level. The value of this level depends on specific dynamic characteristics of the system and the frequency content of the earthquake excitation, as well as the increased level of in-plane rotations that further complicated the response of the two blocks.
3. The impact acceleration levels experienced by the unrestrained system were considerably higher compared to the impact accelerations of the restrained systems.
4. The two segments vibrated mainly in-phase even for restrainer stiffness three times smaller than the stiffness calculated based on the CALTRANS restrainer design method. On the contrary, out-of-phase motion was predominant in the unrestrained system.
5. When the system was unrestrained, collisions between the two adjacent bridge spans significantly altered the characteristics of their vibration by shifting the frequency content of the undergone motion to a higher range. Prior to impacts, the two blocks were vibrating out-of-phase due to their different fundamental periods, but, after the collisions were terminated, the blocks were still moving out-of-phase, however, higher frequencies were dominating the response.
6. All the unrestrained systems considered in this study underwent much higher hinge relative displacements and, therefore, they were more susceptible to span unseating compared to the restrained system, even for low-amplitude earthquake motions. It should be noted that, for both earthquake motions used in this study, the two spans became unseated when restrainers were not used. However, in all the restrained system cases, the hinge displacements were relatively small and span unseating did not occur.
7. The hinge relative displacement increased slightly with the level of the input acceleration. Furthermore, higher values of restrainer gap produced higher levels of hinge relative displacement. Finally, the hinge relative displacement was practically unaffected by the restrainer stiffness.
8. For linear elastic behavior of the elastomeric bearings and essentially rigid superstructure, which was the case in this experiment, the displacements of the two blocks increased linearly with the input peak ground acceleration. In addition, the block supported on the more flexible bearings underwent higher displacements than the block supported on stiffer pads.
9. The extent of restrainer yielding increased with increasing earthquake motion but decreased with increasing restrainer gap. The restrainers used in this study yielded for peak ground accelerations equal to approximately 0.15 g, 0.25 g, and 0.35 g, corresponding to 0 in (0 mm), 0.5 in (12.7 mm), and 1 in (25.4 mm) restrainer gap, respectively.
10. The most critical case for restrainer design corresponded to zero restrainer gap because the restrainers were engaged immediately after the initiation of the out-of-phase motion

of the two adjacent segments. The restrainer forces, which were developed in this case, were significantly higher compared to the cases with non-zero slack. However, the intensity of the impacts between the two blocks was mitigated.

Based on the observations listed above, the following general trends regarding the hinge-restrainer system behavior, which can be considered in bridge design, can be drawn:

- The amplitudes of the impact accelerations, which occur between the two adjacent bridge frames after the closure of the expansion joint gap, tend to increase with increasing amplitudes of the input motion. Therefore, when the system is subjected to high-amplitude earthquake motions, the actual frame ductility demands can be significantly different compared to the specified target ductility, which was calculated without considering the impact phenomenon. Typically, the more flexible frame will pound against the stiff frame, increasing the ductility demands on the stiff frame beyond the design demand. However, beyond certain levels of ground acceleration, there is a chance that the impact accelerations will decrease. This depends on the particular dynamic characteristics of the two frames, the frequency content of the input motion and the in-plane rotations of the two spans. This is consistent with results of analytical studies (Maragakis, 1984).
- The restrainers are generally capable of reducing the intensity of the collisions between the adjacent bridge segments, inhibiting the relative hinge displacements at the in-span hinge and preventing span unseating. This is mainly because the restrainers provide a stiff link between the two frames and, therefore, contribute to the reduction of significant out-of-phase motion between the adjacent frames, even if the frame natural periods are significantly different. The in-phase motion is more apparent when the stiffness of the two segments under consideration is comparable to the total restrainer stiffness.
- The restrainers result in reduction of the impact accelerations and relative hinge displacements. At the same time, the restrainer forces and, therefore, the restrainer ductility demands, increase with the level of input acceleration. Especially when the restrainer gap is set to zero, which in actual bridges corresponds to low ambient temperatures, the restrainers may experience significant yielding even under moderate earthquake excitations. Considering that cable restrainers do not have straight alignment and high concentrated stresses are expected to develop at the locations where the cables pass around the two 90^{o} bends on the drum, restrainer failure may occur at these locations. Such a failure could change the dynamic properties of the hinge-restrainer system and increase the possibility of span unseating. (Selna et al., 1998)

5.3 Recommendations for Further Research

This experimental study focused primarily on the evaluation of the efficiency of seismic restrainers in reducing relative displacements at in-span hinges. Among the several parameters, which could affect the response of multiple-frame bridges tied with seismic restrainers at intermediate hinges, the effects of the restrainer stiffness and the restrainer gap were thoroughly investigated. Furthermore, this was the first experiment of this type and many details and issues for performing such a test were identified and addressed. Therefore, the results of the current

experimental study can serve as a useful reference for future studies on hinge restrainers. In the process, several needs for future research have been identified and listed below:

- The current study accounts only for a certain period ratio of the two adjacent bridge frames. However, the experiments performed in this study, as well as results from a variety of analytical studies in the past, showed that variations in the frame period ratio can have significant effects on the dynamic response of the hinge-restrainer system. The behavior of a wide variety of existing bridges that have been retrofitted with cable restrainers, can be examined by varying the period ratio and useful conclusions can be drawn, which can serve as a general guidance to bridge designers. Different periods of the two segments can be obtained by changing the stiffness and/or the weight of the blocks as necessary to achieve a certain period ratio between the two adjacent spans.
- The earthquake ground motion used in the current study was based on the specific dynamic properties of the two spans of the reference bridge under consideration and it was selected in order to maximize the relative movement of the two blocks. However, variable frame period ratios would allow for a larger set of earthquake motions to be used. This will allow a more conclusive investigation of the effects of the ground accelerations.
- Since only one shake table was used for the testing of the specimen in this study, the effects of non-uniform input motions due to different soil conditions across the bridge foundation were not taken into account. Furthermore, only two spans were considered because of the limitations imposed by the shake table geometry and dead load capacity. Future experimental studies that can utilize more than one shake table, could incorporate multiple frames and investigate the effects of incoherent ground motions and abutments on the overall restrained system response.
- The current study accounts for longitudinal earthquake response of straight bridges with in-span hinges subjected to longitudinal ground motion. Further studies are needed to examine the response of skewed bridges under longitudinal and transverse excitations, as well as the response of simply supported spans.

SECTION 6
REFERENCES

AASHTO (1996). "Standard Specifications for Highway Bridges," American Association of State Highway and Transportation Officials, Sixteenth Edition.

ASTM (1986). "Standard Test Method for Compressive Strength of Cylindrical Concrete Specimens," ASTM C39-86, American Society for Testing and Materials.

ASTM (1987). "Standard Practice for Capping Cylindrical Concrete Specimens," ASTM C617-87, American Society for Testing and Materials.

Bjornsson, S., Stanton, J., and Eberhard, M. (1997). "Seismic Behavior of Skewed Bridges," Report No. SGEM 97-1, University of Washington, Seattle, WA, June.

CALTRANS (1989). "Bridge Design Aids," California Department of Transportation, October.

CALTRANS (1993). "Bridge Design Specifications," California Department of Transportation, January.

CALTRANS (1994). "Memo to Designers," California Department of Transportation, May.

CALTRANS (1996). "Memo to Designers," California Department of Transportation, December.

Carter, M., and Bentley, S. P. (1991). "Correlations of Soil Properties," Pentech Press, London, 1991.

Clough, R. W., and Penzien, J. (1993). Dynamics of Structures, Second Edition, McGraw-Hill, Inc., 1993.

Comartin, C., Green, M., and Tubbesing, S. (1995). "The Hyogo-Ken Nanbu Earthquake," Preliminary Reconnaissance Report, Earthquake Engineering Research Institute, Oakland, CA, February.

Fenves, G., and Desroches, R. (1994)."Response of the Northwest Connector in the Landers and Big Bear Earthquakes," Report No. UCB/EERC-94-12, Earthquake Engineering Research Center, University of California, Berkeley, CA, December.

Fenves, G., and Desroches, R. (1997)."New Design and Analysis Procedures for Intermediate Hinges in Multiple Frame Bridges," National Seismic Conference on Bridges and Highways, Sacramento, CA, July, pp. 667 – 681.

FHWA (1986). "Seismic Design of Highway Bridge Foundations, Volume II: Design Procedures and Guidelines," Publication No. FHWA-RD-86-102, Federal Highway Administration, U.S. Department of Transportation Research and Development, Turner-Fairbank Highway Research Center, June.

Hudgings, T., Eberhard, M. O., and Stanton, J. F. (1997). "Design of Seismic Bridge Restrainers Considering Spatial Variation of Ground Motions," Report No. SGEM 97-2, Civil Engineering Department, University of Washington, Seattle, WA, July.

Jennings, P. C. (1971). "Engineering Features of the San Fernando Earthquake of February 9, 1971," Report No. EERL-71-2, Earthquake Engineering Research Laboratory, California Institute of Technology, Pasadena, CA, December.

Maragakis, E. (1984). "A Model for Rigid Body Motions of Skewed Bridges," Report No. EERL 85-2, Earthquake Engineering Research Laboratory, California Institute of Technology, Pasadena, CA, December

Moehle, J. P. (1995). "Northridge Earthquake of January 17, 1994: Reconnaissance Report, Volume 1, Highway Bridges and Traffic Management," Earthquake Spectra, Vol. 11 (No. 3), pp. 287-372.

OPTIM Corporation (1993). "Technical Manual for the Megadac Series 3100," BL 1152 Release 1.0, July.

Prakash, V., Powell, G. H., and Fillipou, F. C. (1993). "DRAIN 3DX: Base Program User Guide," Structural Engineering, Mechanics and Material, Department of Civil Engineering, University of California, Berkeley, CA, November.

Priestley, M. J. N., Seible, F., and MacRae, G. (1992). "Design Guidelines for Assessment Retrofit and Repair of Bridges for Seismic Performance," Structural Systems Research Project, Report No. SSRP-92-1, University of California, San Diego, La Jolla, CA, August, pp. 266.

Randall, M. J., Saiidi, M., Maragakis, E., and Isakovic, T. (1998). "Restrainer Design Procedures for Multi-Span Simply Supported Bridges," Report No. NCEER-98-4, Civil Engineering Department, University of Nevada, Reno, NV, April.

Saiidi, M., Maragakis, E., Abdel-Ghaffar, S., Feng, S., and O'Connor, D. N. (1993). "Response of Bridge Hinge Restrainers During Earthquakes-Field Performance, Analysis, and Design," Report No. CCEER-93-6, Civil Engineering Department, University of Nevada, Reno, NV, May.

Saiidi, M., Maragakis, E., and Feng, S. (1992). "An Evaluation of the Current CALTRANS Seismic Restrainer Design Method," Report No. CCEER-92-8, Civil

Engineering Department, University of Nevada, Reno, NV, October.

Selna, L. G., Malvar, L., and Zelinski, R. (1989). "Bridge Retrofit Testing: Hinge Cable Restrainers," Journal of Structural Engineering, ASCE, Vol. 115 (No. 4), pp. 920-933.

Singh, S. and Fenves, G. L. (1994). "Earthquake Analysis and Response of Two – level Viaducts," Report No. UCB/EERC-94-11, Earthquake Engineering Research Center, University of California, Berkeley, CA, November.

Trochalakis, P., Eberhard, M. O., and Stanton, J. F. (1995). "Evaluation and Design of Seismic Restrainers for In-Span Hinges," Report No. WA-RD 387.1, Washington State Transportation Center, Seattle, WA, August.

Trochalakis, P., Eberhard, M. O., and Stanton, J. F. (1996). "Unseating of Simply Supported Spans During Earthquakes," Report No. WA-RD 387.2, Washington State Transportation Center, Seattle, WA, May.

Yang, Y. S., Priestley, M. J. N., and Ricles, J. (1994). "Longitudinal Seismic Response of Bridge Frames Connected By Restrainers," Report No. UCSD/SSRP-94-9, Structural Systems Research Project, University of California, San Diego, La Jolla, CA, September.

Yashinsky, M., Hipley, P., and Nguyen, Q., (1995). "The Performance of Bridge Seismic Retrofits During the Northridge Earthquake," Caltrans Office of Earthquake Engineering, June.

APPENDIX A
PLACEMENT OF THE TEST SPECIMEN ON THE SHAKE TABLE AND INSTALLATION OF THE RESTRAINER CABLE UNIT

The 14.5 ft x 14.0 ft shake table area consists of $1''-8$ UNC threaded inserts on a 12 in grid spacing. There are two different insert configurations on the grid. The first configuration is defined as the 'strong holes' with an allowable capacity of 54 kips (240.2 KN). These inserts pass through the table deck into the deck ribs. The rest of the holes are termed the 'weak holes'. These inserts are embedded in the 1 in thick deck and have a design capacity of 39 kips (173.5 KN). Three strong and one weak holes were used to connect each bearing pad to the shake table (figure A-1). The procedure of placing and securing the specimen on the table was as follows:

- Eight 16 in (40.64 cm) x 16 in (40.64 cm) steel plates were bolted to the shake table utilizing $1''-8$ UNC all-thread rods. Each plate had four 1 ½-in (3.81 cm) diameter holes located at the four corners to allow the rods to pass through to the table. It should be noted that the height difference between the two types of bearing pads used in this study was approximately 1.5 in (3.81 cm). Hence, in order to maintain the same height on the top of the bearings, the four plates at the bottom of the slenderer pads had a thickness of 1 in (2.54 cm), while the other four plates supporting the shorter pads were 2 ½ in (6.35 cm) thick (figure A-2).
- Eight 9 in (22.86 cm) x 9 in (22.86 cm) x ¾ in (1.91 cm) steel plates were then welded to the previous wider plates. As shown in figure A-3, four ½-in (1.27 cm) diameter flat head bolts were sticking out from each of the thinner plates. These bolts were passed through the four holes drilled on the bottom 8 in (20.32 cm) x 8 in (20.32 cm) mounting plate of the bearing pads in order to connect the pads to the steel plates.
- Similarly, eight 16 in (40.64 cm) x 16 in (40.64 cm) x 1 in (2.54 cm) steel plates with four ½-in (1.27 cm) diameter flat head bolts protruding (figure A-4) were bolted to the top 14 in (35.56 cm) x 14 in (35.56 cm) mounting plate of the bearings. These plates were then bonded to the bottom concrete surface of the two box girder segments using a multi-purpose construction epoxy. REZI-WELD 1000 epoxy was utilized because of its high shear strength (28 MPa-2 days, 24 MPa-14 days) and long pot life. Furthermore, four ½-in (1.27 cm) diameter dowels were bolted to the top mounting plate of each of the bearing pads and, subsequently, passing through the top steel plates, anchored to the specimen (figure A-5). The same type of epoxy was used to secure the dowels in the concrete.

The new installation procedure, mandated by CALTRANS for all new and retrofitted bridges with C-1 type restrainers (CALTRANS, 1996), uses disc springs (figure A-6) to 'pre-tension' the restrainer cables prior to setting the cables with the correct initial slack to allow for thermal movements. The Cable Yield Indicator (CYI), a new device contrived by CALTRANS engineers to demonstrate the possible yielding of the restrainers after a strong earthquake, was placed on every cable end. As shown in figure A-7, the CYI is a large crush sleeve that is placed on the cable stud ends. The CYI is set to crush at the yield strength of the 3/4-in-diameter restrainer cable. When the cable receives a load large enough to possibly yield it, the Cable Yield Indicator will deform. The deformation will give the field engineer a definite indication that the cable has yielded and that the hinge seat or diaphragm may have been damaged.

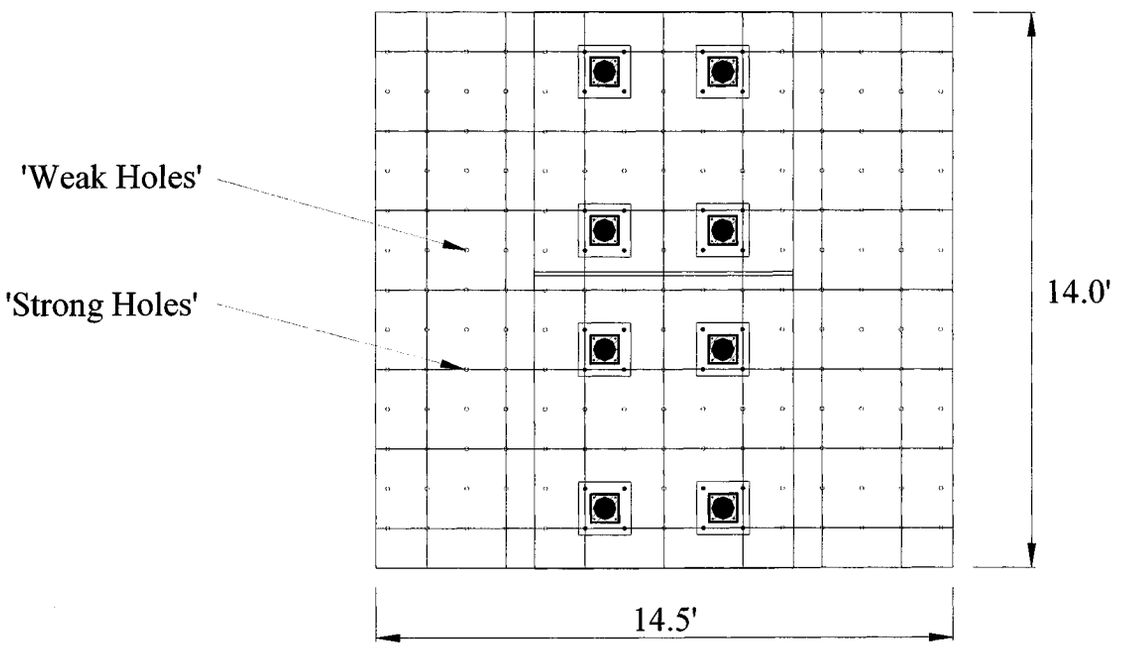

FIGURE A-1 Connection of the Bearing Pads to the Shake Table

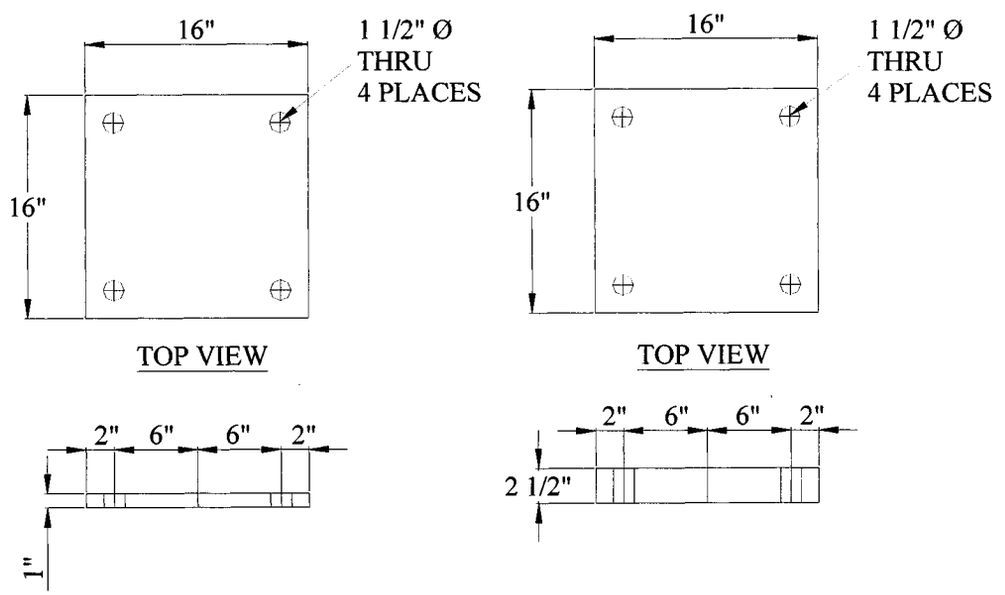

FIGURE A-2 (a) 16 in x 16 in x 1 in plates, (b) 16 in x 16 in x 2 1/2 in plates

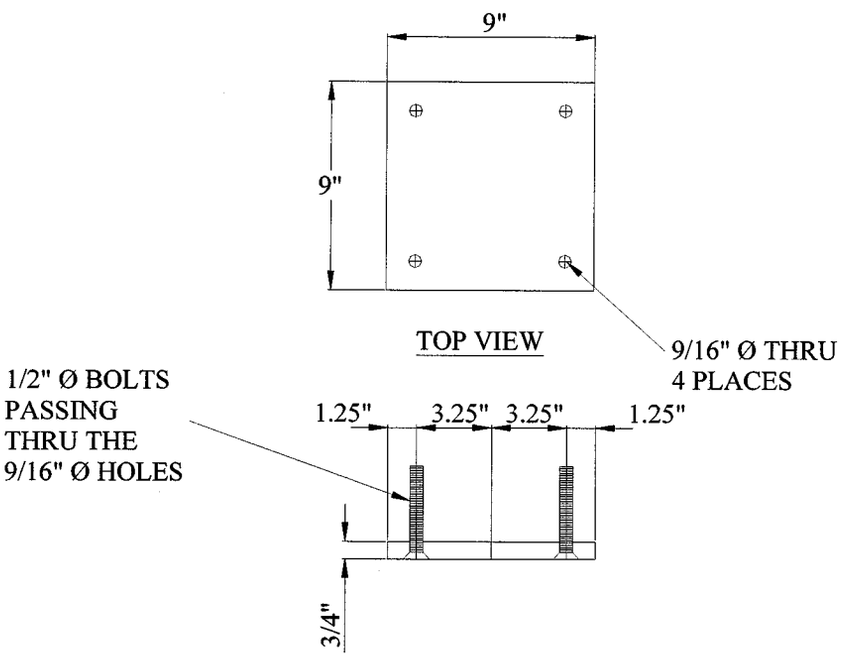

FIGURE A-3 9 in x 9 in x 3/4 in plates

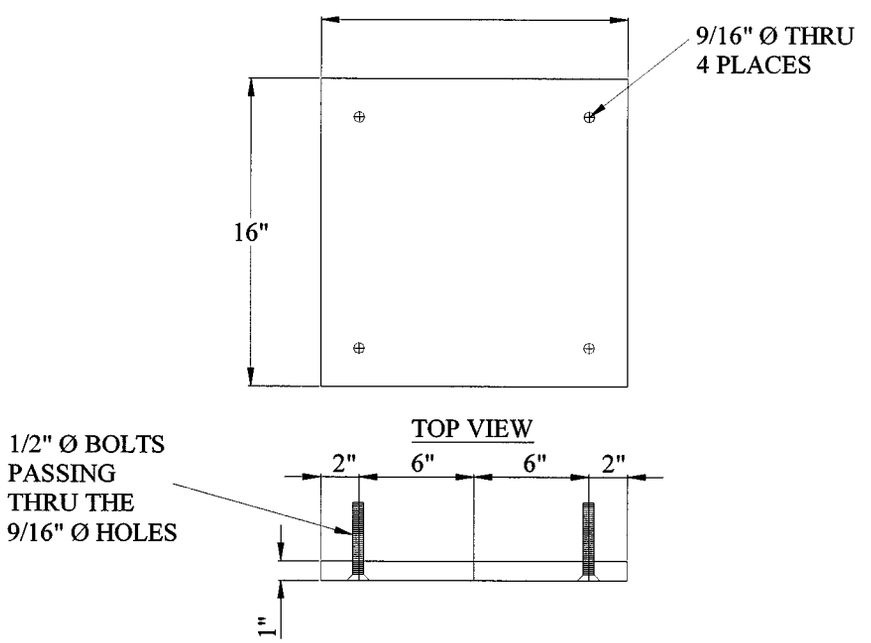

FIGURE A-4 16 in x 16 in x 1 in plates

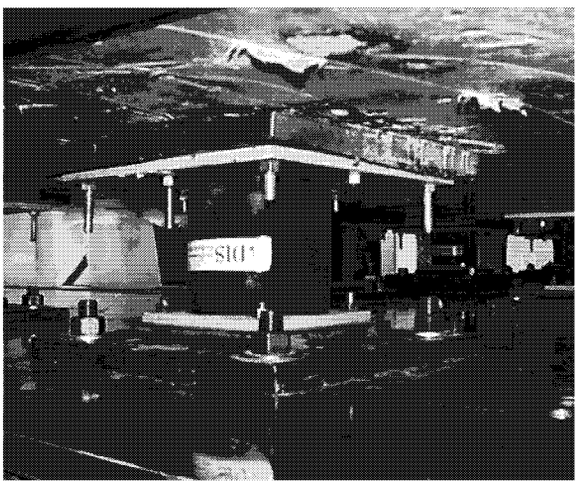

FIGURE A-5 Elastomeric Bearing Detail

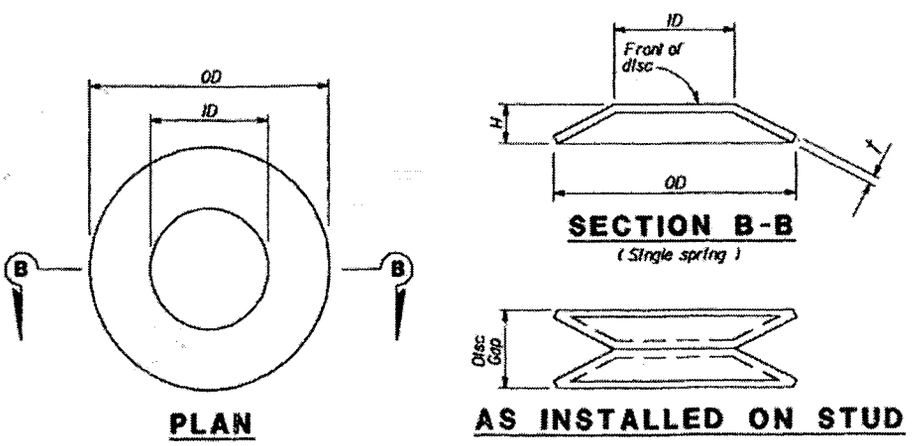

FIGURE A-6 Disc Springs (CALTRANS, 1996)

The restrainer unit installation procedure included the following steps:

- Cable Yield Indicator, spherical washers and disc springs were installed on one anchorage, while only spherical washers and disc springs were placed on the other anchorage (figure A-8). It should be noted that CALTRANS requires the placement of a thread locking system on disc spring stud before setting the nut. However, since this was an experimental study rather than a permanent retrofit work, the cable manufacturers were consulted and it was decided to double-nut the cable end instead of using the adhesive in order to secure the fixity of the system. The disc springs were installed front-to-front as shown in figure A-6.
- The cables were tightened until the disc spring collapsed and there was no disc gap remaining between the discs. Both anchorages of the restrainer cable unit were adjusted simultaneously.

- The aforementioned restrainer configuration corresponds to zero restrainer gap. In order to increase the restrainer slack, the nuts were backed off a distance equal to the target restrainer gap value.

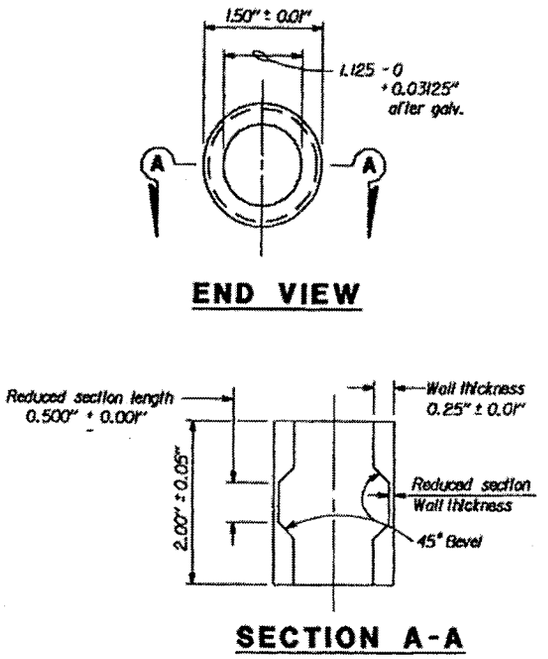

FIGURE A-7 Cable Yield Indicator (CYI) (CALTRANS, 1996)

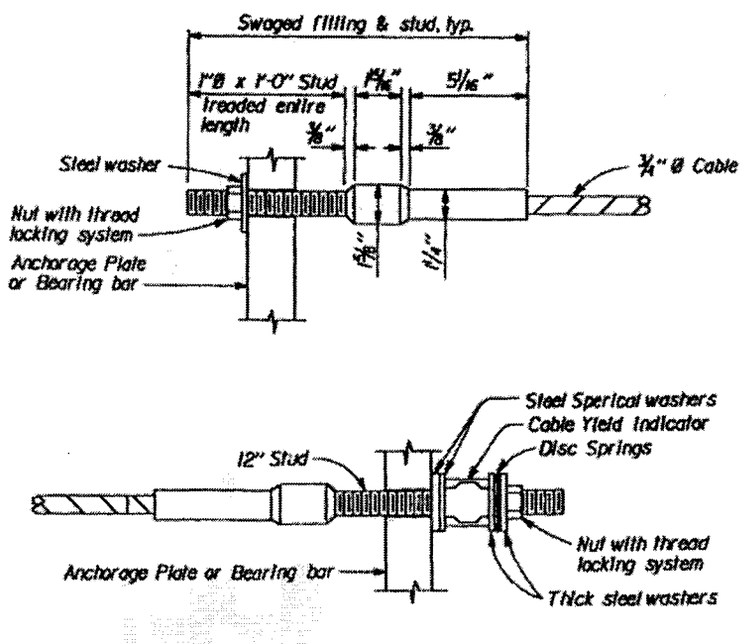

FIGURE A-8 Cable End Anchorage Details (a) Fixed End, (b) Adjustment End (CALTRANS, 1996)

Two different types of lead bricks were utilized in this study in order to provide the supplementary mass. The first type consisted of 12 in (30.48 cm) x 12 in (30.48 cm) x 4 in (10.16 cm) square bricks with a total weight of 0.256 kips (1.14 KN) each, while the second type had the same plan dimensions but half thickness. Sixty bricks of the first type and twenty bricks of the second type were used. Table A-1 shows the number of lead bricks provided for each block and the resulting supplementary mass. The lead was arranged in layers consisting of 20 bricks each. Three layers were placed inside the east block, while one layer was sufficient for the west block. (figure A-9).

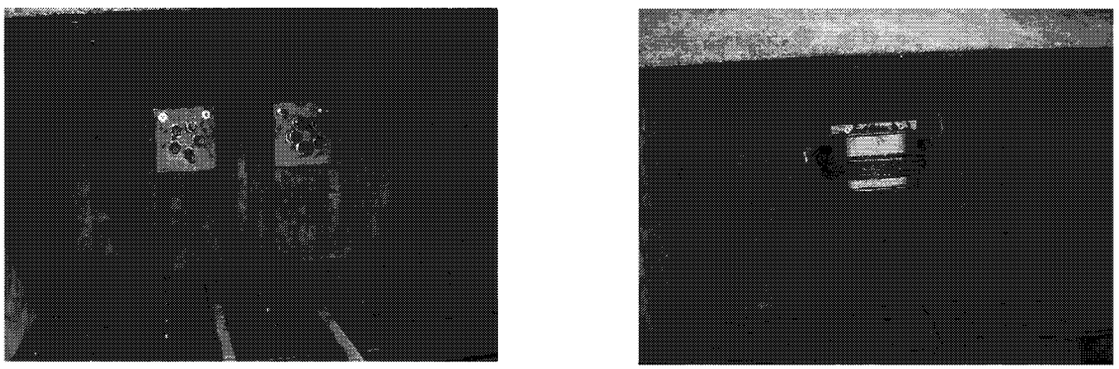

FIGURE A-9 Supplementary Weight Detail

TABLE A-1 Supplementary Weight Properties

Lead Brick Type	Dimensions (cm)	Weight (KN)
A	30.5 x 30.5 x 10.2	1.112
B	30.5 x 30.5 x 5.1	0.556

East Block		
Lead Brick Type	**No. of Bricks**	**Total Weight (KN)**
A	40	44.48
B	20	11.12
Σ	60	55.6

West Block		
Lead Brick Type	**No. of Bricks**	**Total Weight (KN)**
A	20	22.24
B	-	-
Σ	20	22.24

To prevent the blocks from falling off the box girder during the test, two steel plates were used. The plates had six 1 1/16-in (2.70 cm) diameter holes drilled along the bottom and side edges to attach to the concrete blocks (figure A-10). Each plate was mounted on six 1-in (2.54 cm)

diameter threaded rods anchored to the webs and the bottom slab of the corresponding box girder segment. High-strength epoxy was utilized to secure the rods in the concrete.

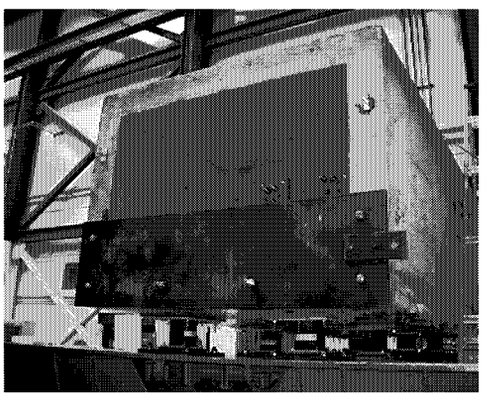

EAST BLOCK

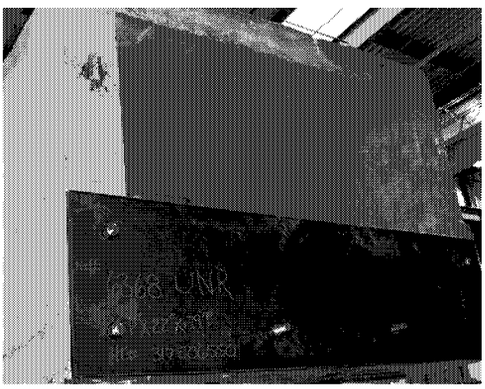

WEST BLOCK

FIGURE A-10 Cover Plate Detail

MULTIDISCIPLINARY CENTER FOR EARTHQUAKE ENGINEERING RESEARCH

A National Center of Excellence in Advanced Technology Applications

University at Buffalo, State University of New York
Red Jacket Quadrangle ▪ Buffalo, New York 14261-0025
Phone: 716/645-3391 ▪ Fax: 716/645-3399
E-mail: mceer@acsu.buffalo.edu ▪ WWW Site: http://mceer.buffalo.edu

University at Buffalo *The State University of New York*

ISSN 1520-295X